PANI: A Novel Algorithm for Fast Discovery of Putative Target Nodes in Signaling Networks

Huey-Eng Chua[§] Sourav S Bhowmick[§] Lisa Tucker-Kellogg[‡]
Qing Zhao[§] C F Dewey, Jr[†] Hanry Yu[¶]

[§]School of Computer Engineering, Nanyang Technological University, Singapore
[‡]Mechanobiology Institute, National University of Singapore, Singapore
[¶]Department of Physiology, National University of Singapore, Singapore
[†]Division of Biological Engineering, Massachusetts Institute of Technology, USA
chua0530|assourav|zhaoqing@ntu.edu.sg, LisaTK|nmiyuh@nus.edu.sg, cfdewey@mit.edu

ABSTRACT

Biological network analysis often aims at the *target identification problem*, which is to predict which molecule to inhibit (or activate) for a disease treatment to achieve optimum efficacy and safety. A related goal, arising from the increasing availability of semi-automated assays and moderately parallel experiments, is to suggest many molecules as potential targets. The *target prioritization problem* is to predict a subset of molecules in a given disease-associated network which contains successful drug targets with highest probability. Sensitivity analysis prioritizes targets in a dynamic network model according to principled criteria, but fails to penalize off-target effects, and does not scale for large networks. We describe PANI (**P**utative T**A**rget **N**odes Pr**I**oritization), a novel method that prunes and ranks the possible target nodes by exploiting concentration-time profiles and network structure (topological) information. PANI and two sensitivity analysis methods were applied to three signaling networks, MAPK-PI3K; myosin light chain (MLC) phosphorylation and sea urchin endomesoderm gene regulatory network which are implicated in ovarian cancer; atrial fibrillation and embryonic deformity. Predicted targets were compared against a reference set: the molecules known to be targeted by drugs in clinical use for the respective diseases. PANI is orders of magnitude faster and prioritizes the majority of known targets higher than sensitivity analysis. This highlights a potential disagreement between absolute mathematical sensitivity and our intuition of influence. We conclude that empirical, structural methods like PANI, which demand almost no run time, offer benefits not available from quantitative simulation and sensitivity analysis.

1. INTRODUCTION

Drug discovery research has gradually shifted from observation-based approaches with phenotypic screening, toward target-based research aimed at molecular mechanisms of disease [26]. Observation-based approaches screen drug compounds *in vitro*, *ex vivo*, or *in vivo*; and measure empirical outcome for determining which drugs are "active" against the disease. In contrast, target-based approaches identify a particular molecule (e.g., enzyme, receptor) that functions prominently in a validated mechanism of the disease, and then synthesize a drug compound to interact specifically with that target molecule. One key expectation in target-based drug development is that specificity for one disease-causing molecule and lack of binding to other molecules will minimize toxicity. Another emerging research area is the network-based drug discovery approaches which exploit knowledge of disease mechanism at a systems level [226].

There is an ongoing debate on the value of observation-based, target-based, and network-based approaches in drug development [39, 107, 97]. As the debate continues, innovations in experimental methods are chipping away at the previous distinctions between these approaches. Hybrid strategies are increasingly accessible, in part because of cost-effective methods for parallelizing experiments on tissues and living cells. Technologies, such as microfluidic cell culture arrays, and high-content imaging [220, 45, 40], facilitate investigations that bridge between screening empirical outcomes, targeted study of disease mechanisms, and/or network-based systems biology [155]. The specific methods are diverse and rapidly changing, but one clear trend is an increase in customized [155] designs for high-throughput experiments, meaning that individual investigators decide not only the treatments and controls for the input samples, but they also decide which measurements to perform on the samples (e.g., which genes to measure, which behaviors to quantify). This level of design is particularly challenging when experiments have enough "high throughput" coverage to exceed the biological expertise of any single investigator, but not enough coverage to skip the decision-making step and simply measure every variable.

Experimental innovation often creates novel computational problems, including immature research topics where simple algorithms might be effective. Experimental trends in drug discovery research are now creating demand for computational automation to assist in the selection of molecule sets for multiplex assays. *This paper addresses molecule selection in a manner that deliberately spans the gap from network-based and target-based computation to observation-*

based goals for final outcome. The first step of this work is to formalize "target prioritization", the problem of choosing a set of *putative target* molecules for further study. Next, we present a fast and novel algorithm called PANI (**P**utative T**A**rget **N**odes Pr**I**oritization), which uses network information and simple empirical scores to prioritize and rank biologically relevant target molecules in signaling networks.

A *putative target* node in a signaling network is a protein that when perturbed is able to achieve desirable efficacy and safety in terms of regulation of a particular *output node*. Informally, an *output node* is a protein that is either involved in some biological processes (e.g., proliferation) which may be deregulated, resulting in manifestation of a disease (e.g., cancer) or be of interest due to its physiological role in the disease. An example of an output node for the application of cancer drug design might be `Akt` (a node of interest in the `MAPK-PI3K` network [93]). Constitutive activation of `Akt` was shown to be oncogenic and may be targeted to disrupt ovarian tumor cell growth [8]. Regulation of the output node provides a means to restore normalcy to the diseased network [106].

PANI is a generic algorithm applicable to any biological signaling network. The algorithm PANI starts with a preprocessing step that prunes the *candidate nodes* (nodes being considered for analysis) based on a *reachability rule* to reduce computation cost. Then, in its main phase, PANI prioritizes nodes using a score based on a kinetic property called *profile shape similarity distance* (PSSD) and two network structural properties, namely *target downstream effect* (TDE) and *bridging centrality* (BC) [111]. Putative target nodes are nodes with high ranking score.

Profile shape similarity distance measures the similarity between concentration-time series profiles (plot of a node's concentration against time) using a customized distance measure that, for example, permits delays and inversions. PSSD is a distance measure which identifies the most relevant upstream regulators. *Target downstream effect* measures the potential impact on the network when a node is perturbed. The impact is determined by the number of nodes downstream of the target and the likelihood that these nodes are associated to off-target effects. *Bridging centrality* identifies nodes that are located at a connecting bridge between modular subregions in a network [111]. Note that structural properties (TDE and BC) are used to identify important nodes that the kinetic property (PSSD) fails to identify (e.g., `Raf` in the `MAPK-PI3K` network).

In Section 5, we evaluate the performance of PANI by comparing it against two state-of-the-art global sensitivity analysis (GSA)-based techniques [296, 238] run on three signaling networks, namely `MAPK-PI3K` [93], myosin light chain (`MLC`) phosphorylation [160], and endomesoderm [138], which are implicated in ovarian cancer, atrial fibrillation, and embryonic deformity, respectively. Instead of defining success according to the internal logic of the original network, the goal is to agree with empirical outcome: namely, to *predict* the set of molecules that is actually targeted by drugs given to human patients. Our study shows that PANI can identify a majority of targets in these networks and many of these targets are ignored by the two GSA-based approaches (multiparametric sensitivity analysis (MPSA) [296] and SOBOL [238]). Further, it is orders of magnitude faster than MPSA [296] and SOBOL [238]. Finally, extrapolating trends from the results suggests some insights and possible reasons why empirical outcome of disease is not addressed well by sensitivity analysis.

2. RELATED WORK

Sensitivity analysis [296, 193, 108] is a family of closely related methods that is frequently proposed for target identification. Sensitivity analysis measures the effect of a parameter perturbation (e.g., a kinetic rate constant change) on the output node and assigns sensitivity values to a node based on the extent of output node perturbation. The parameters are ranked according to the sensitivity value and *sensitive parameters* (parameters with high sensitivity values) are then selected as potential targets [108]. The parameter values of a real biological network vary depending on genetics, cellular environment and cell type. Thus, no single "true" nominal parameter value exists. Hence, more appropriate are GSA-based methods [296], such as SOBOL [238] and MPSA [296], which measure the effect on the output node when all parameters are varied simultaneously.

Although GSA-based methods can identify sensitive parameters of the system, they have several limitations. First, they require simulating the network behavior for a combinatorial number of different parameter combinations, making it computationally expensive, especially for larger networks. SOBOL analysis takes about 21 hours for the `MLC` phosphorylation network [160] with 105 nodes. For larger network (e.g., the endomesoderm network [138] with 622 nodes), it fails to complete the analysis due to memory problem. Second, these methods generally identify parameters resulting in maximum output node perturbation without considering off-target effects. Third, these methods may miss "insensitive" nodes that may be important drug targets, since they only consider one property (sensitivity) in their ranking. For instance, MPSA [296] and SOBOL [238] ignore `Akt` as a target node although active `Akt` can inhibit activation of `ERK` in differentiated myotubes via `Raf-Akt` interaction [214]. PANI is designed to address these limitations. The key differences between PANI and these GSA-based approaches are as follows. The latter approaches typically create many sets of simulation data using some random samplers and then use some statistical measures on the simulation results to determine which parameters should be ranked higher. In contrast, PANI filters out "irrelevant" nodes to reduce unnecessary computational cost, then ranks the nodes by computing an *aggregate score* that is based on certain structural *and* kinetic properties of the network, instead of using sensitivity and focussing *solely* on the kinetic aspect of the network.

3. TARGET PRIORITIZATION PROBLEM

In this section, we first describe the graph model for representing signaling networks and then briefly describe our running example, the `MAPK-PI3K` network [93]. Next, we introduce the notions of *profile shape similarity*, *target downstream effect* and *bridging centrality*[111]. Finally, we define the *putative targets* prioritization problem that we address in this paper. Henceforth, we use the notations shown in Table 1.

In order to validate the accuracy of our proposed technique for prioritizing suitable target nodes, it is important to choose signaling networks that have been well-studied for the roles their nodes play when targeted with relevant drugs for a specific disease. Hence, we chose `MAPK-PI3K` [93], `MLC` phosphorylation [160], and endomesoderm [138] networks,

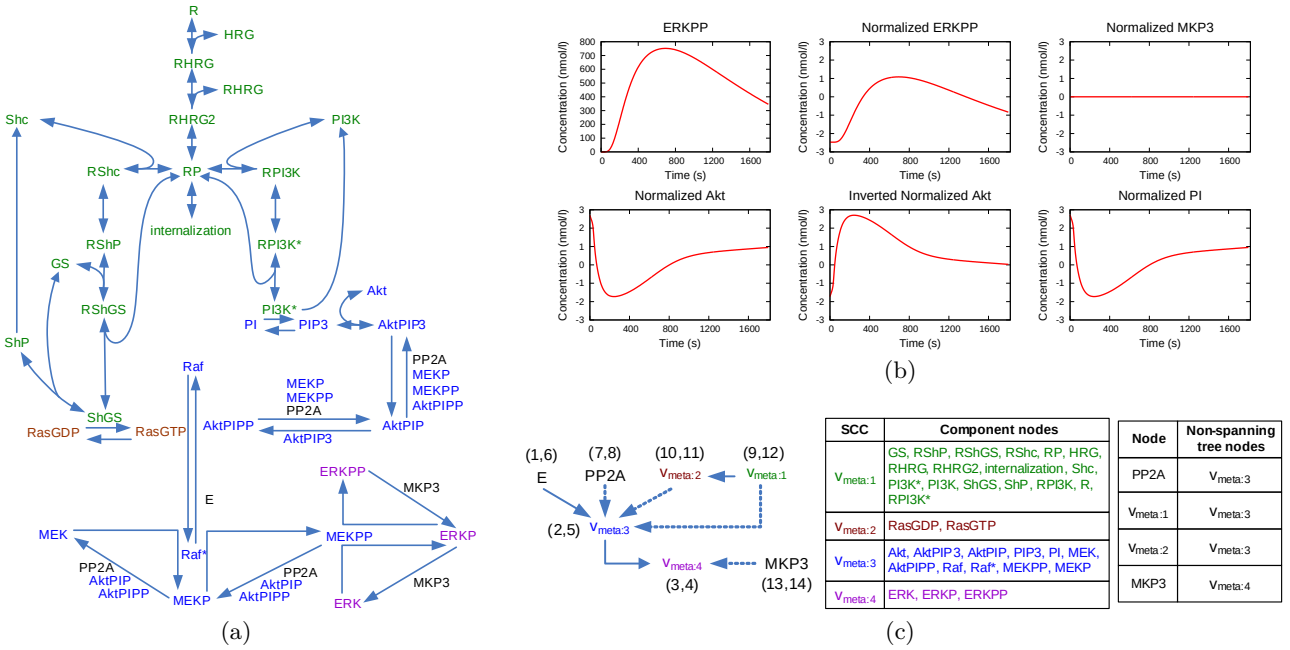

SCC	Component nodes
$V_{meta:1}$	GS, RShP, RShGS, RShc, RP, HRG, RHRG, RHRG2, internalization, Shc, PI3K*, PI3K, ShGS, ShP , RPI3K, R, RPI3K*
$V_{meta:2}$	RasGDP, RasGTP
$V_{meta:3}$	Akt, AktPIP3, AktPIP, PIP3, PI, MEK, AktPIPP, Raf, Raf*, MEKPP, MEKP
$V_{meta:4}$	ERK, ERKP, ERKPP

Node	Non-spanning tree nodes
PP2A	$V_{meta:3}$
$V_{meta:1}$	$V_{meta:3}$
$V_{meta:2}$	$V_{meta:3}$
MKP3	$V_{meta:4}$

Figure 1: (a) MAPK-PI3K signaling cascade adapted from [93], (b) concentration-time profiles, (c) indexed directed acyclic graph representation of Fig. 1a with strongly connected component and non-spanning tree edge table. Solid and dotted arrows correspond to edges in the spanning and non-spanning tree, respectively.

Symbols	Description
V_{meta}	Set of meta nodes $\{v_{meta:1}, v_{meta:2}, \cdots, v_{meta:i}\}$ where $v_{meta:i}$ is the i^{th} strongly connected component (SCC).
ζ_u	Concentration-time profile $\{\varsigma_{u[1]}, \varsigma_{u[2]}, \cdots, \varsigma_{u[i]}\}$ of node u where $\varsigma_{u[i]}$ is the value at time point i.
DTW(ζ_u, ζ_v)	Dynamic time warping (DTW) distance between ζ_u and ζ_v.
$\rho_{u,v}$	Probability of perturbing node v when node u is perturbed.
θ_u	Degree of node u.
Φ_v	Set of profile shape similarity distances (PSSD) $\{\Phi_{(u_1,v)}, \Phi_{(u_2,v)}, \cdots, \Phi_{(u_i,v)}\}$ with respect to v where $\Phi_{(u_i,v)}$ is the PSSD value between ζ_{u_i} and ζ_v.
Υ	Set of target downstream effect (TDE) $\{\Upsilon_{u_1}, \Upsilon_{u_2}, \cdots, \Upsilon_{u_i}\}$ where Υ_{u_i} is the TDE value of node u_i.
Λ	Set of bridging centrality (BC) $\{\Lambda_{u_1}, \Lambda_{u_2}, \cdots, \Lambda_{u_i}\}$ where Λ_{u_i} is the BC value of node u_i.
Ψ_X	Ranked list $\{\psi_{X:u_1}, \psi_{X:u_2}, \cdots, \psi_{X:u_i}\}$ based on property X where $\psi_{X:u_i}$ is the rank of node u_i. Node u_1 will be assigned a higher rank than u_2 ($\psi_{X:u_1} < \psi_{X:u_2}$) if $X_{u_1} > X_{u_2}$.
ω_X	Scalar weight factor associated to property X.
T	Set of nodes $\{t_1, t_2, \cdots, t_i\}$ such that there exists a path from each node $t_i \in T$ to the output node.

Table 1: Notations.

which are implicated in ovarian cancer, atrial fibrillation, and gastrulation phase of embryonic development, respectively. In the sequel, we shall use the MAPK-PI3K network as running example. Specifically, we use the **heregulin** (HRG)-induced **ErbB** receptor signaling network in Chinese hamster ovary cells proposed in [93] and select phosphorylated ERK (ERKPP) as the output node since ERKPP has been found to be upregulated in ovarian cancer and silencing of ERK1/2 protein expression using siRNA inhibits tumor cell proliferation [244]. Fig. 1a illustrates this network and is derived from the ordinary differential equation (ODE) model described in [93]. The exact parameters and initial concentrations of this model (BIOMD0000000146) can be found in Biomodels.net [144].

3.1 Graph Model of Signaling Networks

A signaling network can be represented as a directed hypergraph $H = (V_H, E_H)$[128] where the nodes V_H represent molecules (e.g., proteins) and the hyperedges E_H represent interactions. The hyperedge $(U, W) \in E_H$ connects a set of source nodes ($U \subset V_H$) to a set of target nodes ($W \subset V_H$). The complex formation of AktPIP3 from Akt and PIP3 is an example of a hyperedge (Fig. 1a). Analysis of directed hypergraphs is generally more complex than graphs and many graph algorithms cannot be used directly on hypergraphs [128]. Hence, they are often transformed into an equivalent bipartite or substrate digraph for analysis [128]. We use the bipartite digraph representation since it retains the original information of the hypergraph [128]. A bipartite digraph is denoted as $B = (P \bigcup Q, E_B)$ where P and Q are disjoint node sets and there is no edge connecting nodes in the same set. Signaling networks generally contain strongly connected components (SCC). In a given SCC containing nodes $u, v \in V_H$, there exists a path from u to v and vice versa. The existence of SCC is a result of feedback loops that are common in complex regulatory control [140]. An example of feedback loop in Fig. 1a is the double phosphorylation-dephosphorylation cycle involving ERK, ERKP and ERKPP where MKP3 acts as the phosphatase and MEKPP acts as the kinase.

3.2 MAPK-PI3K Network

The coupled MAPK-PI3K network (Fig. 1a) is involved in up to 30% of human cancers [157] due to its roles in cell survival signaling. Here, we briefly describe the MAPK-PI3K network as depicted in Fig. 1a. This model describes the **heregulin** (HRG)-induced **ErbB** receptor signaling network in Chinese hamster ovary cells. Extracellular signals such as HRG can result in dimerization of receptor tyrosine kinases on the cell surface. This causes the intracellular portions of

the receptors to be phosphorylated, which then binds to an adaptor protein known as growth factor receptor-bound protein 2 (Grb2). This complex binds son of sevenless (SOS), thereby activating SOS which facilitates exchange of membrane-bound Ras-GDP to Ras-GTP [239]. The activated Ras-GTP in turn binds Raf leading to activation and phosphorylation of Raf (p-Raf) [15]. p-Raf then phosphorylates and activates MEK which in turn phosphorylates ERK. Phosphorylated ERK is translocated from the cytoplasm to the nucleus where it activates various transcription factors (e.g., c-Myc) [154]. Parallel to this cascade is the PI3K-Akt pathway, which is activated when HRG-stimulated receptor (RP) binds to and activates PI3K. The activated PI3K phosphorylates phosphoinositol lipids which recruit and activate Akt. The MAPK and PI3K-AKT cascades interacts at the level of Raf and PP2A [108].

3.3 Profile Shape Similarity Distance (PSSD)

In signaling networks, signal responses to perturbation are typically measured in terms of phosphoprotein concentrations dynamics [136] represented as concentration-time profiles (Fig. 1b). Time profile comparison is frequently used to identify node regulatory relationships for gene regulatory [271] and metabolic networks [211] for purpose such as elucidating network conductivities. There are certain considerations in comparing these phosphoprotein concentration-time profiles. In signaling networks, reactions occur at different and non-uniform rates [1] resulting in profiles with variable time delays. Hence, a distance measure based on one-to-one alignment on a time axis (Euclidean) is ineffective at detecting similarity in these profiles. A non-linear measure, such as *dynamic time warping* (DTW) distance, allows a more intuitive alignment between profiles [121] and is more suitable for biological time series data such as gene and protein expression [1]. Specifically, DTW distance identifies the profiles of Akt and ERKPP (Fig. 1b) as similar whereas Euclidean distance did not (Section 5). Although DTW has been used in many different applications ranging from speech processing to biomarkers identification [121], to the best of our knowledge, it has not been used in the context of drug discovery.

DEFINITION 1. *Given two discrete time series ζ_u and ζ_v, the **dynamic time warping distance** between them is defined recursively as:*

$$\text{DTW}(\zeta_u, \zeta_v) = \xi(First(\zeta_u), First(\zeta_v)) + Min \begin{cases} \text{DTW}(\zeta_u, Rest(\zeta_v)) \\ \text{DTW}(Rest(\zeta_u), \zeta_v) \\ \text{DTW}(Rest(\zeta_u), Rest(\zeta_v)) \end{cases}$$

where $First(\zeta_u) = \{\varsigma_{u[1]}\}$, $Rest(\zeta_u) = \{\varsigma_{u[2]}, \varsigma_{u[3]}, \cdots, \varsigma_{u[n]}\}$, $\xi(\varsigma_{u[i]}, \varsigma_{v[j]}) = (\varsigma_{u[i]} - \varsigma_{v[j]})^2$ and $\varsigma_{u[i]}$ is the value of ζ_u at time point i [121].

Although DTW distance is robust to time warping, it can miss similar profiles that have undergone y-axis warping [121] and inversely similar profiles. These profiles are common in signaling networks where signals may be amplified or attenuated as they pass through the signaling cascade, partly due to the relative levels of activators and inhibitors within the cascade [13]. Moreover, profiles of nodes tend to be similar to their activators and inversely similar to their inhibitors [243]. Hence, we extend DTW distance to address these limitations. The profiles are Z-normalized using $ZNormalize(\zeta_u) = \frac{\varsigma_{u[i]} - \overline{\zeta_u}}{\sigma(\zeta_u)}$, $\forall \varsigma_{u[i]} \in \zeta_u$ where $\sigma(\zeta_u)$ and $\overline{\zeta_u}$ are the variance and mean of ζ_u, respectively, to minimize the effects of y-axis warping. For inversely similar profiles (ζ'_u), $\text{DTW}(\zeta'_u, \zeta_v)$ will yield a lesser value than $\text{DTW}(\zeta_u, \zeta_v)$. Hence, both DTW distances will be computed and the lesser distance selected as the PSSD ($\Phi_{(u,v)}$). We note that the profiles have to be non-stationary for meaningful DTW distance comparison. Since signaling networks pass along biological signals by modifying concentration of phosphoproteins [136], we expect most of these profiles to be non-stationary.

DEFINITION 2. *Given a concentration-time profile ζ_u having n time points, denoted as $\zeta_u = \{\varsigma_{u[0]}, \cdots, \varsigma_{u[n]}\}$, let m be the median value of ζ_u. The corresponding **inverted profile** is denoted as $\zeta'_u = \{\varsigma'_{u[0]}, \cdots, \varsigma'_{u[n]}\}$ where $\varsigma'_{u[i]} = 2 \times m - \varsigma_{u[i]}$.*

DEFINITION 3. *Given a signaling network $H = (V_H, E_H)$, let ζ_u, ζ_v be the Z-normalized concentration-time profiles of $u, v \in V_H$. The **profile shape similarity distance** of u with respect to v is defined as:*

$$\Phi_{(u,v)} = Min(\text{DTW}(\zeta_u, \zeta_v), \text{DTW}(\zeta'_u, \zeta_v))$$

For example, to calculate $\Phi_{(\text{Akt,ERKPP})}$, ζ_{ERKPP} and ζ_{Akt} are Z-normalized using $ZNormalize(\zeta)$ (Fig. 1b). Then, ζ'_{Akt} is obtained by inverting ζ_{Akt}. Finally, $\text{DTW}(\zeta_{\text{Akt}}, \zeta_{\text{ERKPP}})$ and $\text{DTW}(\zeta'_{\text{Akt}}, \zeta_{\text{ERKPP}})$ are calculated and the smaller value is assigned as $\Phi_{(\text{Akt,ERKPP})}$.

3.4 Target Downstream Effect (TDE)

Perturbations of nodes *downstream* of the target node is one of the contributing factors of off-target effects for drugs such as cerivastatin which was subsequently withdrawn from the market [150]. The *target downstream effect* of a node v assesses this risk based on the probability of perturbing a *downstream node* w and the likelihood of w causing off-target effects. Node w is *downstream* of v if there exists a path from v to w. The probability of perturbing a downstream node depends on the likelihood of the existence of a path from v to w (path probability). Hence, it can be calculated by assigning suitable edge weights using edge confidence score in protein-protein interaction (PPI) databases [247] and then multiplying the weights of all edges in the path. If there are multiple paths from v to w, the overall probability can be computed as the maximum of all paths' probabilities. The likelihood of a *downstream node* causing off-target effect is dependent on the degree of the node since high degree nodes are more likely to be involved in essential PPIs [96].

DEFINITION 4. *Given a signaling network $H = (V_H, E_H)$, let W be the set of downstream nodes of $v \in V_H \setminus W$. Let $\rho_{v,w}$ be the probability of perturbing $w \in W$ when target node v is perturbed and θ_w be the degree of w. The **target downstream effect** of v is defined as $\Upsilon_v = \sum_{w \in W} (\rho_{v,w} \times \theta_w)$.*

For example, $\Upsilon_{\text{ERK}} = 7$ since $W = \{\text{ERKP}, \text{ERKPP}\}$, $\theta_{\text{ERKP}} = 4$, $\theta_{\text{ERKPP}} = 3$, and $\rho_{\text{ERK,ERKP}} = \rho_{\text{ERK,ERKPP}} = 1$.

3.5 Bridging Centrality (BC)

The *bridging centrality* identifies *bridging nodes* (nodes with high *bridging centrality* value) which are located between functional modules in the signaling network and mediate signal flow between the modules [111]. Compared to hub nodes (nodes with high degree), bridging nodes are more effective drug targets with fewer off-target effects [111].

The *bridging centrality* of a node is the product of two ranks, namely, the inverses of *betweenness centrality* [37] and *bridging coefficient* [111], since bridging nodes have higher *betweenness centrality* and *bridging coefficient* than other nodes [111] and the ranking function used in this paper assigns higher rank to larger value. The *betweenness centrality* of a node v, denoted as Ω_v, is the fraction of shortest paths counted over all pairs of vertices that pass through that node [37]. Hence, $\Omega_v = \sum_{s \neq v \neq t \in V} \frac{\sigma_{st}(v)}{\sigma_{st}}$ where σ_{st} is the number of shortest paths from node s to node t and $\sigma_{st}(v)$ is the number of shortest paths from s to t passing through v [37]. The *bridging coefficient* of a node v, denoted as Γ_v, is the average probability of leaving its neighborhood and is computed as $\Gamma_v = \frac{1}{\theta_v} \sum_{i \in N_v, \theta_i > 1} \frac{\eta_i}{\theta_i - 1}$ where θ_v is the degree of v, N_v is the set of neighbors of v, and η_i is the number of outgoing edges of node $i \in N_v$ [111].

DEFINITION 5. *Given inverse betweenness centrality rank $\Psi_{\frac{1}{\Gamma:v}}$ and inverse bridging coefficient rank $\Psi_{\frac{1}{\Omega:v}}$ of node v, the **bridging centrality** of v is defined as $\Lambda_v = \Psi_{\frac{1}{\Gamma:v}} \times \Psi_{\frac{1}{\Omega:v}}$.*

3.6 Putative Target Prioritization

The above three properties are used to determine if a node is a *putative target node*. A *putative target node* must promise better output node regulation (better efficacy) and reduced off-target effects than other nodes, which means smaller PSSD, smaller TDE, and larger BC values. Hence, *putative targets* prioritization is equivalent to a rank aggregation problem [161] with nodes ranked based on each property and the rankings aggregated into a combined score (*putative target score*). Nodes having top scores are called *putative target nodes* and prioritized over other nodes. We use the weighted-sum approach to aggregate the rank. This allows poor performance in one criterion to be compensated by good performance in other criteria, resulting in approximate ranking and hence, approximate prioritization. The approximate prioritization is good enough if it can prioritize majority of the known drug targets over other nodes. In Section 5, validations on the `MAPK-PI3K` and `MLC` phosphorylation networks revealed that PANI requires less minimum number of top ranking targets to identify all relevant known drug targets in [184] compared to SOBOL and MPSA. For the endomesoderm network (largest network available on Biomodels.net [144]), MPSA and SOBOL analysis fail due to memory issue; and [184] contains no relevant drugs. Hence, we assess the biological relevance in terms of the percentage of top-10% ranked targets implicated in the regulation of `endo16`, a gene found to be essential for gastrulation [213], a phase early in embryonic development. We find that in the top-10% PANI-ranked targets, 72.13% of them are implicated in the regulation of `endo16`. Hence, majority of targets prioritized by PANI are biologically relevant.

DEFINITION 6. *Given a signaling network $H = (V_H, E_H)$ and an output node $v_o \in V_H$, let Φ_{v_o} be the PSSD property evaluated with respect to v_o, Υ and Λ be the TDE and BC properties, respectively. Let ω_c be the weight associated with property $c \in C = \{\Phi_{v_o}, \Upsilon, \frac{1}{\Lambda}\}$ and $\Psi_{c:v}$ be the rank of node $v \in V_H$, based on property c and normalized to a range of [0 1]. Then, the **putative target score** of a node v is defined as $score_{v,C} = \sum_{c \in C} (\omega_c \times \Psi_{c:v})$ where $\sum_{c \in C} \omega_c = 1$.*

Algorithm 1 Algorithm PANI.

Input: H, ζ, v_o
Output: Ψ_{score}
1: $(T, B, G) \leftarrow PruneNodes(H, v_o)$// Phase 1
2: **return** $PrioritizeNodes(\zeta, v_o, T, B, G)$// Phase 2

Algorithm 2 The *PruneNodes* procedure (Phase 1).

Input: $H = (V_H, E_H), v_o \in V_H$
Output: $T, B = (V_B, E_B), G = (V_{\text{DAG}}, E_{\text{DAG}})$
1: $B \leftarrow$ Compute bipartite graph of H// Phase 1.1
2: $G \leftarrow Convert2\text{DAG}(B)$// Phase 1.2
3: $V_{root} \leftarrow$ Get set of root nodes in V_{DAG}
4: **for all** $u \in V_{root}$ **do**
5: $\quad G \leftarrow Index\text{DAG}(G, u, \phi)$// Phase 1.3
6: **end for**
7: $T \leftarrow$ Get set of nodes in V_{DAG} that can reach v_o// Phase 1.4
8: **return** T, B, G

DEFINITION 7. *Given a signaling network $H = (V_H, E_H)$ and an output node $v_o \in V_H$, the goal of the **putative targets prioritization problem** is to rank the nodes using the putative target score (Ψ_{score}) and top ranking nodes are prioritized as putative targets.*

The weights $\omega_{\Phi_{v_o}}$, ω_Υ and $\omega_{\frac{1}{\Lambda}}$ affect the putative target score and hence the decision of whether a node is a putative target. Interestingly, we observe that among the entire range of weights we tested, the minimum number of top ranking targets (*MinNode*) required to identify at least 75% of the relevant known drug targets in [184] is 19 and 72 for the `MAPK-PI3K` and `MLC` phosphorylation networks, respectively. The size of the networks are 36 and 105, respectively. Further, when the weights vary in the range [0.1 – 0.9], the impact of the weights on the ranking result reduce with increasing network size. For instance, the Spearman's ranking coefficient ranges between ~ 0.45 to 1 for the `MAPK-PI3K` network while it ranges between ~ 0.8 to 1 for the endomesoderm network having 622 nodes. The effects of using different weights are described in Section 5. In the sequel, we assign $\omega_{\Phi_{v_o}} = 0.4$, $\omega_\Upsilon = 0.3$ and $\omega_{\frac{1}{\Lambda}} = 0.3$.

4. THE ALGORITHM PANI

PANI (Algorithm 1) consists of two phases, namely, *target pruning* (line 1) and *target prioritization* (line 2), which we shall elaborate in turn.

Phase 1: Target Pruning. The target pruning process (Algorithm 2) consists of four subphases, namely the *bipartite graph conversion* phase (line 1), the *directed acyclic graph* (DAG) *conversion* phase (line 2), the DAG *indexing* phase (line 5) and the *reachability-based pruning* phase (line 7). Conceptually, nodes positioned along a parallel path or downstream of the output node do not influence it and can be pruned. Note that retroactivity phenomenon in *reduced signaling network models* (*reduced models*) may result in a downstream node influencing an upstream node [125]. The *reduced models* are formed by further lumping of reactions in original models which are constructed from experimental data fitting. In this work, we use published models constructed directly from experimental data fitting and do not perform further network reduction on these models prior to analysis using PANI.

The first two subphases preprocess the input hypergraph into a DAG which has a consistent topological ordering, making indexing of the DAG easier subsequently. In the bipartite

Ψ_P	Node	$\Psi_{\Phi_{v_o}}$	Ψ_Υ	$\Psi_{\frac{1}{\Delta}}$	$\Psi_{\frac{1}{\Delta}}$	Ψ_M	Ψ_S
Kinase							
1	ERKPP$^\flat$	34	16	21	1	32	32
2	AktPIP†$^\flat$	28	13	24	3	35	35
4	ERKP$^\flat$	21	17	19	1	33	33
5	RP†$^\flat$	33	5	26	6	27	27
6	RHRG2$^\flat$	32	4	27	6	25	25
8	AktPIP3†$^\flat$	16	12	28	3	36	36
9	AktPIPP†$^\flat$	27	13	9	3	34	34
10	Raf*†$^\flat$	13	11	30	3	19	19
11	MEKPP†$^\flat$	17	14	16	3	30	30
12	PI3K*†$^\flat$	22	3	29	6	29	29
13	MEK$^\flat$	20	10	18	3	3	3
14	MEKP$^\flat$	19	13	10	3	31	31
15	ERK$^\flat$	18	16	5	1	1	1
16	Raf†$^\flat$	14	9	22	3	9	9
17	PI3K$^\flat$	25	2	21	6	13	12
18	RPI3K$^{\star\flat}$	31	3	11	6	23	23
19	Akt	29	9	2	3	14	11
20	RHRG	26	3	17	6	26	26
23	RPI3K	24	3	8	6	24	24
27	E	12	8	3	4	7	6
35	R	3	1	2	6	11	5

Ψ_P	Node	$\Psi_{\Phi_{v_o}}$	Ψ_Υ	$\Psi_{\frac{1}{\Delta}}$	$\Psi_{\frac{1}{\Delta}}$	Ψ_M	Ψ_S
Phospholipid							
3	PIP3$^\flat$	23	11	31	3	28	28
7	PI$^\flat$	30	9	20	3	6	14
GTPase							
21	RasGTP	5	7	32	5	18	18
25	RasGDP	6	6	15	5	8	13
Phosphastase							
22	MKP3	12	15	4	2	10	8
29	PP2A	12	8	1	4	12	7
Adaptor molecule							
24	ShGS	7	4	25	6	17	17
28	Shc	4	2	23	6	2	2
32	GS	9	3	7	6	4	4
34	ShP	1	2	12	6	16	16
Tyrosine kinase receptor:adaptor molecule complex							
26	RShGS	11	3	14	6	22	22
30	RShc	8	3	13	6	20	20
31	RShP	10	3	6	6	21	21
Others							
33	internalization	15	1	3	6	15	15
36	HRG	2	1	2	6	5	10

Table 2: Prioritization result with ERKPP as output node (v_o). Nodes marked with †and $^\flat$ are known ovarian cancer drug targets and Pani-identified putative target nodes, respectively. Ψ_P, Ψ_M, Ψ_S and $\Psi_{\frac{1}{\Delta}}$ denote the rankings based on PANI, MPSA, SOBOL and distance to output node, respectively.

Algorithm 3 The *Convert*2DAG procedure (Phase 1.2).

Input: $B = (V_B, E_B)$
Output: $G = (V_{\text{DAG}}, E_{\text{DAG}})$
1: B.SCC $\leftarrow$ Get set of B's SCC
2: **for all** $B.\text{SCC}_i \in B.\text{SCC}$ **do**
3: add $v_{meta:i}$ to V_B
4: **for all** $v \in B.\text{SCC}_i$ where $u \notin B.\text{SCC}_i$ **do**
5: Replace all (u, v) with $(u, v_{meta:i})$
6: Replace all (v, u) with $(v_{meta:i}, u)$
7: Remove v from V_B
8: **end for**
9: **end for**
10: **return** B

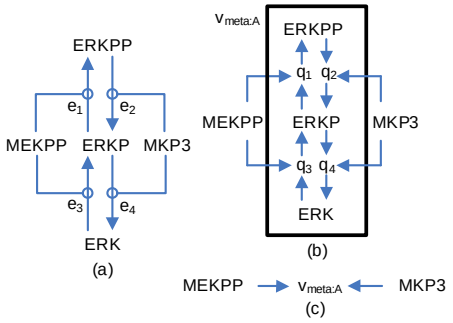

Figure 2: (a) Hypergraph (adapted from Fig. 1a), (b) Bipartite graph representation of Fig. 2a, and (c) DAG representation of Fig. 2b.

graph ($B = (V_B, E_B)$) conversion phase (line 1), we use the method in [72] which converts a hyperedge $(U, W) \in E_H$ to a set of bipartite edges $\{(u_i, q), \ldots, (q, w_j)\} \subset E_B$ where $u_i \in U$, $w_j \in W$, $V_B = P \bigcup Q$, $P = U \bigcup W$ and $q \in Q$ by connecting the incoming node u_i and outgoing node w_j via node q. For example, in Fig. 2a, hyperedge e_1 is converted to its bipartite form by adding a virtual node q_1 and connecting all its incoming and outgoing nodes to q_1 (See Fig. 2b). In the DAG conversion phase (Algorithm 3), we use the approach in [256] which identifies SCCs in the graph using [251] (line 1) and replaces each SCC with a meta node

Algorithm 4 The *Index*DAG procedure (Phase 1.3).

Input: $G = (V_{\text{DAG}}, E_{\text{DAG}}), u, v$
Output: G
1: **if** $v.preorder = \phi$ **then**
2: Set $v.preorder$ to next index
3: **for all** $w \in V_{\text{DAG}}$ where $(v, w) \in E_{\text{DAG}}$ **do**
4: $G \leftarrow Index\text{DAG}(G, w, v)$
5: Add w to $v.descendants$
6: $v.descendants \leftarrow v.descendants \bigcup w.descendants$
7: $v.\text{NST}Nodes \leftarrow v.\text{NST}Nodes \bigcup w.\text{NST}Nodes$
8: **end for**
9: Set $v.postorder$ to next index
10: **else if** $v.preorder \neq \phi$ and $u \neq \phi$ **then**
11: Add v to $u.descendants$
12: Add v to $u.\text{NST}Nodes$
13: **end if**
14: **if** $u \neq \phi$ **then**
15: $u.descendants \leftarrow u.descendants \bigcup v.descendants$
16: $u.\text{NST}Nodes \leftarrow u.\text{NST}Nodes \bigcup v.\text{NST}Nodes$
17: **end if**
18: **return** G

$v_{meta:i}$ (lines 2- 9). For example, Fig. 2c is the DAG form of Fig. 2b where SCC=$\{$ERKPP,ERKP,ERK$\}$ is replaced with $v_{meta:A}$ and the edges are reconfigured as (MEKPP,$v_{meta:A}$) and (MKP3,$v_{meta:A}$).

The DAG indexing phase (Algorithm 4) facilitates efficient assessment of node reachability and is used for node pruning to reduce target search space. We adopt the indexing approach of [49] which performs depth-first traversal on the DAG $G = (V_{\text{DAG}}, E_{\text{DAG}})$. During the traversal, the preorder index of v is assigned (line 2), and v's descendants (lines 5-6) and non-spanning tree children (line 7) are also stored for use later in the *reachability-based pruning* phase. Finally, the postorder index v is assigned (line 9) when all of v's descendants are visited. For example, in Fig. 1c, the root nodes (E, PP2A, $v_{meta:1}$ and MKP3) are first identified and DAG indexing is performed on each of them, starting from E. The preorder and postorder values of E are set to 1 and 6, respectively while the non-spanning tree children and descendants are ϕ and $\{v_{meta:1}, v_{meta:4}\}$, respectively. Repeating the DAG indexing process on each root node re-

Algorithm 5 The *PrioritizeNodes* procedure (Phase 2).

Input: ζ, v_o, T, B, G
Output: Ψ_{score}
1: $\Psi_{\Phi_{v_o}} \leftarrow Rank$PSSD$(\zeta, v_o, T)$// Phase 2.1
2: $\Psi_{\Upsilon} \leftarrow RankTDE(B, T, G)$// Phase 2.2
3: $\Psi_{\frac{1}{\Lambda}} \leftarrow RankBC(B, T)$// Phase 2.3
4: $score \leftarrow$ Compute putative target score
5: **return** $Rank(score)$

Algorithm 6 The *Rank*PSSD procedure (Phase 2.1).

Input: ζ, v, T
Output: Ψ_{Φ_v}
1: **for all** $\zeta_u \in \zeta$ and $u \in T$ **do**
2: $\quad \zeta_u \leftarrow ZNormalize(\zeta_u)$
3: $\quad \zeta'_u \leftarrow$ Compute inverted profile of ζ_u
4: $\quad \Phi_{u,v} \leftarrow Min(DTW(\zeta_u, \zeta_v),$ DTW$(\zeta'_u, \zeta_v))$
5: **end for**
6: **return** $Rank(\Phi_v)$

sults in an indexed DAG. In the *reachability-based pruning* phase (Phase 1.4), only nodes having a path leading to the output node are added to the set of pruned target nodes. A reachability function with a constant time complexity, checks if a node u can reach the output node v_o and returns TRUE when the following conditions are satisfied: (a) $u.preorder \leq v_o.preorder$ and $u.postorder \geq v_o.postorder$ [49], or (b) $w.preorder \leq v_o.preorder$ and $w.postorder \geq v_o.postorder$ where u is a non-spanning tree ancestor of w. These conditions imply the existence of a path from u to v_o. The node u may be a SCC meta node, in which case, all the component nodes in this SCC will be retrieved and added to the set of pruned targets T. For example, in Fig. 1c, if ERKPP (which belongs to $G.\text{SCC}_4$ represented by $v_{meta:4} \in V_{\text{DAG}}$) is chosen as v_o, then no nodes will be pruned as $v_{meta:4}$ is a leaf node and all nodes will be added to T.

Phase 2: Target Prioritization. In this phase (Algorithm 5), the set of pruned nodes T (obtained from Phase 1) is prioritized based on their PSSD (line 1), TDE (line 2) and BC (line 3) properties.

The concentration-time profiles used to compute the PSSD may be obtained from experiments or *in silico* simulations of biological models. In this example, we use the latter approach. For instance, the MAPK-PI3K ODE model [93] was simulated in *Copasi* using parameters: {*duration*=1800 seconds, *intervals*=6 seconds}[1]. For PSSD computation (Algorithm 6), the DTW distances of Z-normalized profiles DTW(ζ_u, ζ_v) and DTW(ζ'_u, ζ_v) are computed (lines 2 and 3) and the lesser distance is selected as $\Phi_{(u,v)}$ (line 4). For TDE computation (Algorithm 7), the set of descendent nodes for node v ($v.descendents$) (Line 2) is derived from the *Index*DAG procedure and the TDE value for v is computed as described in Section 3.4 (Line 4). For BC computation (Algorithm 8), the betweenness centrality is obtained using [37] (line 1) while the bridging coefficient is found by examining neighboring nodes' degree as described in Section 3.5 (line 3). Table 2 reports the normalized ranks of nodes in Fig. 1a for PSSD, TDE and the inverse of BC, denoted as $\Psi_{\Phi_{\text{ERKPP}}}$, Ψ_{Υ} and $\Psi_{\frac{1}{\Lambda}}$, respectively.

[1]The actual CPU time required for the simulation is about 1 second using a 32-bit operating system with 2GB RAM and a dual core processor at 1.86GHz. The simulation time is unrelated to the duration parameter which intuitively, corresponds to the range of ζ and is related to $|\zeta|$ ($\frac{duration}{interval} = |\zeta|$).

Algorithm 7 The *Rank*TDE procedure (Phase 2.2).

Input: $B = (V_B, E_B), T \subset V_B, G = (V_{\text{DAG}}, E_{\text{DAG}})$
Output: Ψ_{Υ}
1: **for all** $v \in T$ **do**
2: $\quad W \leftarrow v.descendants$
3: $\quad$ **for all** $w \in W$ **do**
4: $\quad\quad \Upsilon_v \leftarrow \Upsilon_v + \theta_w \times \rho_{v,w}$
5: $\quad$ **end for**
6: **end for**
7: **return** $Rank(\Upsilon)$

Algorithm 8 The *Rank*BC procedure (Phase 2.3).

Input: $B = (V_B, E_B), T \subset V_B$
Output: $\Psi_{\frac{1}{\Lambda}}$
1: $B.betweenness \leftarrow$ Get betweenness of V_B
2: $\Psi_{\frac{1}{\Omega}} \leftarrow Rank(\frac{1}{B.betweenness})$
3: $B.bridgeCoeff \leftarrow$ Get bridging coefficient of V_B
4: $\Psi_{\frac{1}{\Gamma}} \leftarrow Rank(\frac{1}{B.bridgeCoeff})$
5: **for all** $v \in T$ **do**
6: $\quad \Lambda_v \leftarrow \Psi_{\frac{1}{\Omega:v}} \times \Psi_{\frac{1}{\Gamma:v}}$
7: **end for**
8: **return** $Rank(\frac{1}{\Lambda})$

Algorithm Analysis. We now analyze the time and space complexities of Algorithm PANI.

THEOREM 1. *Algorithm* PANI *takes* $O(|V_B|^2 + |\zeta||T| + |T|^2 + |V_B||E_B|)$ *time in the worst case.*

PROOF. In Algorithm 2, computing the bipartite graph of H takes $O(|V_H| + |E_H|)$ time. For procedure $Convert2$DAG, finding the set of SCC takes $O(|V_B| + |E_B|)$ time using [251] and conversion to DAG takes $O(\sum_{v_i \in G.\text{SCC}} \theta_{v_i})$ time. In the worst case, the signaling network is a complete directed graph and $Convert2$DAG takes $O(|V_B|^2 + |E_B|)$ time since $|V_B| < |V_B|^2$. For *Index*DAG, the depth-first traversal requires $O(|V_{\text{DAG}}| + |E_{\text{DAG}}|)$ time while computing the set of nodes that can reach v_o takes $O(|V_{\text{DAG}}|)$ time. Algorithm 2 takes $O(|V_B|^2 + |E_B|)$ time since $|V_B| = |V_H| + |E_H|$, $|E_B| = \sum_{(U_e, W_e) \in E_H} (|U_e| + |W_e|)$ and $(|V_B| + |E_B|) \geq (|V_{\text{DAG}}| + |E_{\text{DAG}}|)$. In Algorithm 5, *Rank*PSSD takes $O(|\zeta||T| + |T|log|T|)$ time since Z-normalization, inversion of ζ and computation of DTW distance using *Fast*DTW [223] takes $O(|\zeta||T|)$ time each while heapsort takes $O(|T|log|T|)$ time. Let D_t be the set of downstream nodes of $t \in T$, *Rank*TDE takes $O(\sum_{t \in T} |D_t| + |T|log|T|)$ time to calculate TDE and perform heapsort. In the worst case, the signaling network is a single SCC and *Rank*TDE takes $O(|T|^2 + |T|log|T|)$ time. *Rank*BC takes $O(|V_B||E_B| + \sum_{t \in T} |N_t| + |T| + |T|log|T|)$ time where N_t is the set of neighbours of t. Here, heapsort takes $O(|T|log|T|)$ time, calculating betweenness takes $O(|V_B||E_B|)$ time using [37], calculating bridging coefficient and bridging centrality take $O(\sum_{t \in T} |N_t|)$ and $O(|T|)$ time, respectively. In the worst case, the signaling network is a complete directed graph and *Rank*BC takes $O(|V_B||E_B| + |T|^2 + |T| + |T|log|T|)$ time. In Algorithm 5, computing putative target score and ranking the nodes based on this score take $O(|T| + |T|log|T|)$ time. Since $|T| < |T|^2$ and $|T|log|T| < |T|^2$, Algorithm 5 takes

Node	$\Psi_{\frac{1}{DTW}}$	$\Psi_{\frac{1}{Eucl.}}$	Node	$\Psi_{\frac{1}{DTW}}$	$\Psi_{\frac{1}{Eucl.}}$	Node	$\Psi_{\frac{1}{DTW}}$	$\Psi_{\frac{1}{Eucl.}}$	Node	$\Psi_{\frac{1}{DTW}}$	$\Psi_{\frac{1}{Eucl.}}$	Node	$\Psi_{\frac{1}{DTW}}$	$\Psi_{\frac{1}{Eucl.}}$	Node	$\Psi_{\frac{1}{DTW}}$	$\Psi_{\frac{1}{Eucl.}}$
ERKPP	1	1	AktPIP	7	3	PIP3	13	5	AktPIP3	19	12	PP2A	23	15	RasGDP	29	22
RP	2	10	AktPIPP	8	13	ERKP	14	17	interna.$^\sharp$	20	32	RShGS	24	29	RasGTP	30	25
RHRG2	3	8	RHRG	9	7	MEK	15	18	Raf*	21	28	RShP	25	31	Shc	31	26
RPI3K*	4	9	PI3K	10	11	MEKP	16	14	Raf	22	20	GS	26	19	HRG	32	24
PI	5	33	RPI3K	11	6	ERK	17	2	E	23	15	RShc	27	30	R	32	23
Akt	6	34	PI3K*	12	4	MEKPP	18	16	MKP3	23	15	ShGS	28	27	ShP	33	21

$^\sharp$ interna. denotes internalization.

Table 3: Ranking based on inverse of the DTW and Euclidean (Eucl.) distances with respect to ERKPP. Table is read from top to bottom and from left to right.

$O(|\zeta||T| + |T|^2 + |V_B||E_B|)$ time in the worst case. Hence, Algorithm 1 takes $O(|V_B|^2 + |\zeta||T| + |T|^2 + |V_B||E_B|)$ time in the worst case. □

THEOREM 2. *Algorithm* PANI *requires* $O(|V_B| + |E_B| + |V_{\text{DAG}}|^2 + |\zeta|)$ *space in the worst case.*

PROOF. Computing $B = (V_B, E_B)$, the bipartite graph of H, requires $O(|V_B| + |E_B|)$ space to store the nodes and edges. *Convert*2DAG requires $O(|V_B| + |E_B|)$ and $O(|V_{\text{DAG}}| + |E_{\text{DAG}}|)$ space for SCC identification using [251] and for DAG conversion, respectively. Let D_v be the set of nodes such that there exists a path from $v \in V_{\text{DAG}}$ to $d \in D_v$ and let $|E_{v(non-tree)}|$ be the number of non-spanning tree edges of v. *Index*DAG uses $O(|V_{\text{DAG}}| + \sum_{v \in V_{\text{DAG}}} |D_v| + \sum_{v \in V_{\text{DAG}}} |E_{v(non-tree)}|)$ space for storing the descendant nodes and non-spanning tree edges. In the worst case, the spanning tree of the DAG is a linear path and for every node $v \in V_{\text{DAG}}$, there is an edge to every descendant node of v so that *Index*DAG requires $O(|V_{\text{DAG}}| + |V_{\text{DAG}}|^2)$ space. Computing the set of nodes that can reach v_o requires $O(|V_H|)$ in the worst case where no nodes are pruned. Since $(|V_B| + |E_B|) \geq (|V_{\text{DAG}}| + |E_{\text{DAG}}|)$, $|V_B| \geq |V_H|$ and $|E_B| \geq |E_H|$, Algorithm 2 requires $O(|V_B| + |E_B| + |V_{\text{DAG}}|^2)$ space in the worst case. In Algorithm 5, supposing only two profiles (ζ_v and ζ_{v_o}) are stored at any time, *Rank*PSSD requires $O(|\zeta| + |T|)$ space for normalization, inversion, DTW distance calculation ($O(|\zeta|)$ [223]) and heap-sort ranking. *Rank*TDE and *Rank*BC require $O(|T|)$ and $O(|V_B| + |E_B| + |T|)$ space, respectively since computing betweenness requires $O(|V_B| + |E_B|)$ space using [37] and the rest of the steps in *Rank*TDE and *Rank*BC require $O(|T|)$ space. Algorithm 5 requires $O(|\zeta| + |V_B| + |E_B|)$ space since $|T| \leq |V_B|$. Thus, Algorithm 1 requires $O(|V_B| + |E_B| + |V_{\text{DAG}}|^2 + |\zeta|)$ space □

5. RESULTS AND DISCUSSION

PANI is implemented in Java JDK 1.6. In this section, we present the experiments conducted to evaluate its performance and report the results obtained. We compare PANI against two state-of-the-art GSA-based methods: MPSA [296] and SOBOL [238]. The SBML-SAT tool [297] is used to perform MPSA and SOBOL analysis[2]. We use three real-world signaling networks as our dataset, namely MAPK-PI3K [93], MLC phosphorylation [160], and endomesoderm [138]. We run all experiments on an Intel 1.86GHz dual core processor machine with 2GB RAM, running Microsoft Windows XP. For MAPK-PI3K and MLC phosphorylation networks, we set $|\zeta| = 300$; for endomesoderm network, we set $|\zeta| = 700$. Recall from Section 3.6, $\omega_{\Phi_{v_o}} = 0.4$, $\omega_\Upsilon = 0.3$ and $\omega_{\frac{1}{\Lambda}} = 0.3$ for all networks. Since the network examples used here are very well-studied and constructed from extensive literature survey, we set $\rho_{v,w} = 1$.

[2] SBML-SAT was obtained from http://sysbio.molgen.mpg.de/SBML-SAT/ and the default number of simulations set to 2000 and 10000 for MPSA and SOBOL, respectively.

5.1 DTW versus Euclidean Distances (MAPK-PI3K network).

In this experiment we analyze the benefit of deploying a non-linear (DTW distance) measure over a linear distance (e.g., Euclidean) measure for computing PSSD on the MAPK-PI3K network. Table 3 reports that $\Psi_{\Phi_{\text{ERKPP}}}$ values based on DTW and Euclidean distances have low correlation (Spearman's coefficient=0.554, P=0.00045). We visually compare the profile of ERKPP with profiles of nodes that are ranked significantly different by DTW and Euclidean distances. A node is considered to have significantly different ranking if it has a rank difference ($|\Psi_{\frac{1}{DTW}} - \Psi_{\frac{1}{Eucl.}}|$) of $\lfloor \frac{|T|}{2} \rfloor$ or more since this ranking difference is large enough to result in a node being assigned a high rank in DTW distance and low rank in Euclidean distance, and vice versa. We use the inverse of the distance for ranking purpose as the ranking function assigns higher rank to larger values and larger distances in this case imply greater dissimilarity. In Table 3, Akt and PI have large ranking differences. Euclidean distance assigned higher rank to MKP3 even though Akt and PI looked visually more similar to ERKPP (Fig. 1b). Hence, DTW distance is a more suitable measure for comparing PSSD for the MAPK-PI3K network whose node profiles exhibit non-linear relationship, a characteristic common among many signaling networks [1].

5.2 Runtime Performance on Large Signaling Networks.

Although most of the currently published signaling networks are small in size (<100 nodes), larger networks are increasingly being created [138]. With advances in metabolomic technology [240], it will not be many years before an ODE network is produced for the entire human metabolome. Table 4 reports the execution times of the three methods on three networks of increasing size. The SBML-SAT tool encounters segmentation violation error for the endomesoderm network whereas PANI takes around 251 sec. Observe that PANI *is at least two orders of magnitude faster than* MPSA *and* SOBOL. More importantly, PANI *is able to handle large networks which could not run under* MPSA *and* SOBOL.

5.3 Quality and Relevance of Result.

A key issue in this paper is validation of the quality of the result of the proposed algorithm. In this subsection, we address this issue by first comparing the correlation between putative target nodes and sensitive nodes (nodes identified by GSA-based approaches). Then, we evaluate the ranking results in terms of the minimum number of top scoring nodes needed for identifying all the relevant known drug targets in [184] (*MinNode*), the top-3 drug target classes (e.g., kinases) in terms of the nodes' average putative target score, and

Network ($H=(V_H,E_H)$)	$\lvert V_H\rvert$	Execution Time			$\frac{\lvert\tau_{\text{MPSA}}\rvert}{\lvert\tau_{\text{PANI}}\rvert}$	$\frac{\lvert\tau_{\text{SOBOL}}\rvert}{\lvert\tau_{\text{PANI}}\rvert}$
		τ_{PANI}	τ_{MPSA}	τ_{SOBOL}		
MAPK-PI3K network [93]	36	∼6sec	∼18min	∼3hrs	180	1800
MLC phosphorylation network [160]	105	∼11sec	∼2hr	∼21hrs	654.55	6872.73
Endomesoderm network [138]	622	∼251sec	-	-	-	-

Table 4: Execution time of various approaches on networks of different size. '-' indicates that the MPSA and SOBOL analysis did not complete for the endomesoderm network.

Ovarian Cancer Drugs in [184]	Mechanism of Action	Drug Effect	Rank		
			PANI	MPSA	SOBOL
Lapatinib (Phase I) [203]	Bind to ATP-binding site of R, preventing its autophosphorylation	↓RP	5	27	27
Sorafenib (Phase II) [276]	Bind to ATP-binding site of Raf, preventing activation of Raf	↓Raf*	10	19	19
ISIS 5132 (Phase II) [61]	Bind to Raf mRNA to downregulate Raf expression	↓Raf	16	9	9
AZD6244 (Phase II) [285]	Bind and lock MEK into inactive conformation	↓MEKPP	11	30	30
XL147 (Phase I) [180]	Bind to ATP-binding site of PI3K, preventing activation of PI3K	↓PI3K*	12	29	29
Perifosine (Phase I) [133]	Bind to lipid-binding PH domain of Akt	↓AktPIP ↓AktPIPP ↓AktPIP3	2 9 8	35 34 36	35 34 36
ECO-4601 (Phase I) (TLN-4601) [180, 42]	Degrade Raf1 through proteasomal-dependent mechanism	↓Raf	16	9	9
PKI-587 (Phase I) [261]	Inhibits PI3K and mTOR kinases	↓PI3K*	12	29	29
PKI-179 (Phase I) [180]	Small-molecule mimetic of ATP that inhibits PI3K and mTOR kinases	↓PI3K*	12	29	29
BKM120 (Phase I) [180]	ATP competitive inhibitor of PI3K kinase	↓PI3K*	12	29	29
% of known drug targets in top-18 rank			100%	12.5%	12.5%

Table 5: Ovarian cancer drugs found in [184] and ranks of corresponding target based on different approaches.

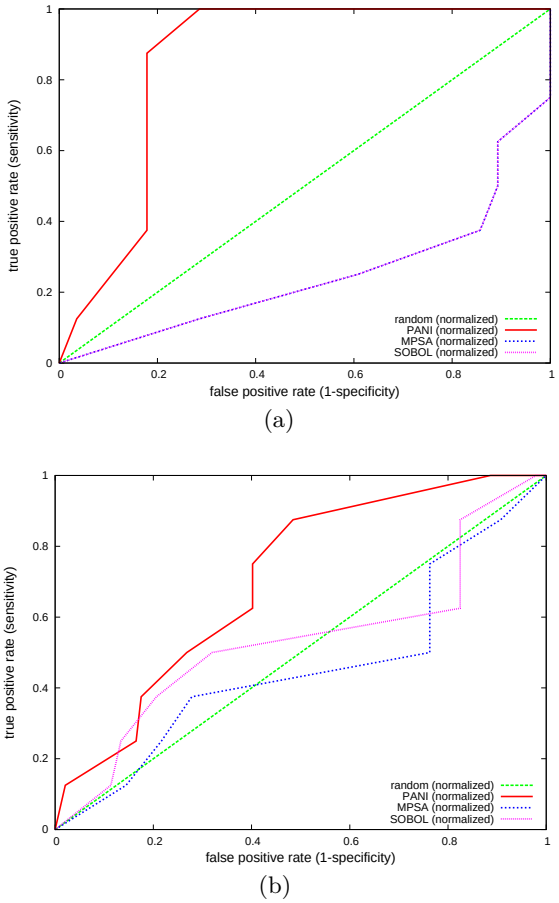

Figure 3: Effect of putative target size on (a) MAPK-PI3K and (b) MLC phosphorylation network results.

biological relevance of potential drug targets identified by PANI and GSA-based approaches.

We compare our result with those obtained from state-of-the-art GSA-based approaches, specifically MPSA [296] and SOBOL[238]. These approaches have been applied to signaling networks [296, 294] to identify potential drug targets which correspond to sensitive parameters of the network. Both MPSA and SOBOL rank kinetic rate constants and initial concentrations of the primary molecular species, which correspond to edges and nodes in the signaling network, respectively. Our approach, PANI, ranks only nodes based on PSSD, TDE and the inverse of BC values. For a meaningful comparison, we will only consider the ranking of nodes. Table 2 shows the rankings of nodes based on MPSA, SOBOL and PANI.

We observe that GSA-based approaches tend to prioritize upstream initiating proteins (such as receptors and ligands) with long signaling distance to the downstream output. This is the opposite of PANI's tendency to choose targets with short pathways to the output. The high sensitivity of downstream protein phosphorylation levels to concentration levels of upstream initiating proteins is mathematically correct due to the amplifying effect of the signal transduction cascade but it is only biologically correct within a controlled experiment when other phenomena remain constant. In a living cell, there are various unknown influences that could perturb some molecule in the pathway and disrupt the information signal from propagating beyond that point [112]. In contrast, PANI may have done well because of its bias towards short signaling distances. The PANI bias is common sense, given the reality that the model is not a complete understanding of influences, whereas the GSA bias towards distant influences relies on a larger number of biochemical/pathway assumptions and creates vulnerability to a larger number of unforeseen effects. Although signaling distance can prioritize known drug targets, its low granularity (assigning multiple nodes to the same rank) limits its usage in networks with large SCC since a large number of nodes may be assigned a low rank which would not yield much insights to the nodes. For example, in Table 2, we observe that the majority (75%) of the known drug targets has small signaling distance ($\Psi_{\frac{1}{\Delta}}$=3). To identify all known drug targets, $\Psi_{\frac{1}{\Delta}}$=6, which essentially covers all the nodes in the network.

MAPK-PI3K network. The Spearman's ranked coefficients for the pairs of methods (MPSA, PANI), (MPSA, SOBOL) and (PANI, SOBOL) are -0.5804, 0.9755, and -0.6162, respectively. Together with Table 2, they show that the putative target nodes PANI prioritizes tend to be less sensitive nodes (ranked low by MPSA and SOBOL). We next examine the biological relevance of the putative target nodes.

Safety, efficacy, and overall quality of predicted targets can be evaluated empirically by comparing the predictions

against the known targets of drugs that have been safe and effective in preclinical trials, and chosen for trials in human. In the MAPK-PI3K signaling network, ERKPP upregulation has been implicated in cancer [46] and so we use the set of cancer drugs undergoing clinical development in [184] as a reference set for defining "good quality" targets. In particular, we shall focus on ovarian cancer drugs since Fig. 1a is based on Chinese hamster ovary cell. The set of known drug targets is chosen based on the effect of these ovarian cancer drugs (Table 5).

The reference drug targets are curated from [184] by searching for relevant key words (e.g., ovarian cancer), filtering the results for relevant studies involving drugs, identifying unique drugs from the filtered studies and then performing a literature survey to identify targets of these drugs. For instance, a search using "ovarian cancer" as key word yielded 1417 studies. However, only 845 studies involve drugs specific for the purpose of ovarian cancer study while the rest involve questionnaires, radiation treatment, polycystic ovary syndrome, cytomegalovirus infection for cancer (including ovarian cancer) patients undergoing transplant or general terms such as chemotherapy. The same drug can be used in multiple studies. Hence, duplicated drugs are removed from the 845 studies, resulting in a total of 342 unique drugs. Amongst these 342 drugs, some of the drugs target other networks. For instance, cisplatin targets the DNA synthesis network by crosslinking to DNA to trigger apoptosis [55]. The targets of the 342 drugs were identified using literature survey (Appendix A) and only those that are relevant to the MAPK-PI3K network are considered as reference drug targets (Table 5).

The *MinNode* are 16, 36 and 36 for PANI, MPSA, and SOBOL, respectively (Table 5). In order to examine the enrichment of known drug targets in the top ranking nodes (top-k), we vary k in the range $[0 - |V_H|]$. The normalized Receiver Operating Characteristic (ROC) curves in Fig. 3 plots the true positive rates (TPR) against the false positive rates (FPR) for the different methods. Since the range of ranks for the methods may be different, we normalize the ranks to the range $[0 - 1]$ before tabulating TPR and FPR. The area under the ROC curves (AUC) (Fig. 3a) are 0.853, 0.246 and 0.246 for PANI, MPSA and SOBOL, respectively. Paired t-test analysis on the ranks of known drug targets shows that PANI ranks drug targets higher than MPSA and SOBOL ($P<0.01$). We also compare PANI to random node prioritization. The set of 8 known drug targets are randomly prioritized 100 times. *MinNode* varies in the range $[21 - 36]$ while p-value for the paired t-test varies in the range $[0.0002 - 0.38]$. In 68 out of 100 random prioritization trials, PANI ranks drug targets higher based on paired t-test statistics ($P<0.05$). Hence, PANI *is able to identify known ovarian cancer drug targets using much fewer top scoring nodes and tends to prioritize known drug targets better than* MPSA, SOBOL *and random prioritization.*

We note that lowering ERK signaling is not the primary goal of some of these drugs and ERK regulation may happen in parallel with another "primary" effect due to interconnections in the signaling network. For example, lapatinib which inhibits ErbB4 receptors causes the down regulation of ERK activation [298]. Hence, we examine the relevance of ERK activation in the therapeutic effect of the drug. Lapatinib was found to be resistant in SKBR3 cells expressing H-ras mutant or overexpressing H-ras. In these cell lines, phosphorylation levels of ERK remains high. Ras-mediated lapatinib resistance can be overcome with the MEK inhibitor U0126 which results in down regulation of phosphorylated ERK [298], implying that the apoptotic effect of lapatinib requires the regulation of ERK via its inhibition of ERK's upstream regulator. Similarly, sorafenib-mediated growth inhibition was found to be dependent on ERK phosphorylation level. Cells expressing low basal phosphorylated ERK expression are less sensitive to sorafenib [293]. Similar phenomenon was also reported for ISIS 5132. A study involving over 100 different tumor cell lines found that cell lines such as OVCAR3 and SKOV-3 which exhibit high constitutive ERK activation are more sensitive to ISIS 5132 while OVCAR5 which shows minimal constitutive ERK activation fails to inhibit cell growth with ISIS 5132 [170]. ECO-4601 has a similar drug effect as ISIS 5132. Hence, its efficacy is likely to be dependent on ERK phosphorylation level. AZD6244 targets MEK1/2 kinases which have unique specificity to ERK1/2 and phosphorylate the tyrosine and threonine residues on ERK, activating it [63]. *Hence, regulation of the level of phosphorylated* ERK *is found to be critical to the therapeutic effect of these drugs.* In the case of XL147, it inhibits the activity of PI3K [230] and mediates apoptosis through Akt. Based on Fig. 1a, we would expect XL147 to upregulate phosphorylated ERK which would reduce its apoptotic effect. However, XL147 exhibits an inhibitory effect on ERK activity [230] and this is likely to happen through a pathway different from the one in Fig. 1a. In contrast, LY294002, another PI3K inhibitor, inhibits PI3K activation and induces ERK activation as predicted from Fig. 1a. It was found that U0126 (MEK inhibitor) when combined with LY294002 led to synergistic effect [266] and this was likely due to U0126 downregulating the level of phosphorylated ERK to further enhance the apoptotic effect of LY294002. We could not find record of combination studies of XL147 with U0126. However, it would not be surprising to find this combination having synergistic effect. Similarly, the PI3K inhibitors, PKI-587, PKI-179 and BKM120 are likely to combine synergistically with U0126. Perifosine, which targets Akt, behaves in a similar fashion as LY294002 and combining it with U0126 led to significant synergistic activity [100]. *Although regulation of the level of phosphorylated* ERK *may be a secondary effect of these drugs, the therapeutic effect of the drugs is closely related to the level of phosphorylated* ERK.

From Table 2, we note that PANI's top-3 drug target classes are phospholipids, kinases and GTPases with average putative score of 5, 13.6 and 23, respectively. For MPSA, the top-3 drug target classes are adaptor molecule, others (ligands and receptors) and phosphatase with average putative score of 9.75, 10 and 11, respectively. Similarly, SOBOL's top-3 drug target classes are phosphatases, adaptor molecules, and others with average putative score of 7.5, 9.75 and 12.5, respectively. Protein kinase is the second largest group of drug targets and has been targeted for many years, yielding drugs ranging from fasudil hydrochloride to Gleevec [58]. Although phospholipids, phosphatases and GTPases are generally not considered good drug targets, they have been seriously considered recently [95, 169, 156]. PANI *identifies classes with relevance as drug targets but which are distinct from* MPSA *and* SOBOL.

Finally, we examine the biological relevance of nodes having significantly different ranks (rank difference of $\frac{|T|}{2}$ or more) in the different approaches. First, we look at the set

Atrial Fibrillation Drugs in [184]	Mechanism of Action	Drug Effect	Rank		
			PANI	MPSA	SOBOL
Amiodarone (Phase IV)[187]	Bind to Ca^{2+}-calmodulin complex to prevent binding of enzyme substrate.	↓MLCK.Ca^{2+}.CaM	44	105	15
		↓MLCK.2Ca^{2+}.CaM	54	80	87
		↓MLCK.3Ca^{2+}.CaM	18	79	86
		↓MLCK.4Ca^{2+}.CaM	20	78	85
Dabigatran (Phase III)[241]	Bind to thrombin and block interaction with substrate	↓thrombinR active	30	95	103
Simvastatin (Phase IV) [76, 202]	Inhibit rate of thrombin generation by directly interfering with tissue factor (TF).	↓thrombin	93	30	23
	Inhibit Rho geranylgeranylation (Rho-kinase activation).	↓Rho.GTP.Rho-kinase	3	15	12
Celivarone (Phase II) [83]	Multi-channel blocker. Blocks Na^+ inward current and l-type Ca^{2+} current.	↓intracellular Ca^{2+}	45	23	35
AZD1305 (Phase II) [44]	A combined ion channel blocker. AZD1305 predominantly blocked the human ether-a-go-go related gene (hERG), the L-type calcium and the human voltage-gated Na^+ channel (hNav1.5) channels in a concentration-dependent manner.	↓intracellular Ca^{2+}	45	23	35
Ximelagatran (Phase II) [168]	Inhibits fluid-phase and clot-bound thrombin with similar high potency. Binding to the active site of thrombin is direct and competitive and does not require the presence of co-factors.	↓thrombin	93	30	23
Edoxaban (Phase II) [273]	Reversibly blocks the active site of thrombin.	↓thrombin	93	30	23
Apixaban (Phase II)[273]	Reversibly blocks the active site of thrombin.	↓thrombin	93	30	23
Verapamil (Phase III) [146]	Competes with external Ca^{2+} for binding on Ca^{2+} channel.	↓intracellular Ca^{2+}	45	23	35
Spironolactone (Phase II) [173]	Interacts at a binding site of the calcium entry blocker receptor complex in vascular membranes and allosterically modulates the binding of calcium entry blockers to this complex.	↓intracellular Ca^{2+}	45	23	35
Magnesium sulphate (Phase III) [73]	Competes with calcium for binding sites, in this case for voltage-operated calcium channels (VOCC). Decreased calcium channel activity lowers intracellular calcium, causing relaxation and vasodilation.	↓intracellular Ca^{2+}	45	23	35
K201 (Phase II) [117]	Non-specific blocker of sodium (I_{Na}), potassium (I_{Kl}) and calcium (I_{Ca}) channels, inhibiting sodium influx, K^+ efflux and Ca^{2+} influx.	↓intracellular Ca^{2+}	45	23	35
Diltiazem (Phase III) [146]	Competes with external Ca^{2+} for binding on Ca^{2+} channel.	↓intracellular Ca^{2+}	45	23	35
Calcium antagonist (Phase IV) [77]	Blocks entry of Ca^{2+} into cells.	↓intracellular Ca^{2+}	45	23	35
AZD0837 (Phase II) [241]	An anticoagulant that binds selectively to thrombin and blocks its interaction with its substrates. AZD0837 is the prodrug of ARH06737, a potent, competitive, reversible inhibitor of free and fibrin-bound thrombin.	↓thrombinR active	30	95	103
ATI-2042 (Phase II) [225] [187]	An oral, rapidly metabolized chemical analogue of amiodarone with a half-life of 7h, which is expected to have a similar efficacy profile to amiodarone but without the side effects attributable to long-term dosing and tissue accumulation. Amiodarone binds to Ca^{2+}-calmodulin complex to prevent binding of enzyme substrate.	↓MLCK.Ca^{2+}.CaM	44	105	15
		↓MLCK.2Ca^{2+}.CaM	54	80	87
		↓MLCK.3Ca^{2+}.CaM	18	79	86
		↓MLCK.4Ca^{2+}.CaM	20	78	85
% **of known drug targets in top-47 rank**			75%	37.5%	50%

Table 6: Atrial fibrillation drugs found in [184] and ranks of corresponding target based on different approaches.

of nodes ranked high in PANI, but low in MPSA or SOBOL, denoted as V_A = {ERKP, ERKPP, RHRG2, PIP3, RP†, AktPIP†, AktPIP3†, AktPIPP†, PI3K*†, MEKPP†}. We shall not elaborate further on nodes marked with †which are known ovarian cancer drug targets. ERKP and ERKPP are obvious targets for regulating ERKPP. The other potential targets are RHRG2 and PIP3. RHRG2 is the dimerized ligand-bound ErbB4 receptor which results in receptor autophosphorylation and activation of the signaling cascade in Fig. 1a. Besides ErbB4-ErbB4 homodimers, ErbB4-Her2 heterodimers can also result in receptor autophosphorylation. Pertuzumab, a drug that prevents Her2 dimerization, is currently in phase II trial for advanced, refractory ovarian cancer [84]. PIP3 is the main substrate of phosphatase PTEN [65] and PTEN mutation is found to occur at high frequency in endometrioid ovarian tumors [98]. Hence, targeting PIP3 via PTEN may be beneficial for some form of ovarian cancer. Therefore, *V_A contains nodes with high biological relevance as potential ovarian cancer drug targets, of which, a majority are known drug targets.* Next, we look at the set of nodes ranked high in MPSA or SOBOL, but low in PANI, denoted as V_B = {E,R,PP2A,Shc,GS,ShP,HRG,internalization}. We will not discuss E which is an unidentified enzyme, but will instead focus on R (ErbB4), PP2A, Shc, GS, ShP, HRG and internalization. ErbB4 receptors are found to be overexpressed in several cancers including ovarian cancer [158]. Regulating the level of ErbB4 receptors using methods such as receptor internalization can help to attenuate receptor signaling by regulating the amount of RP [3]. PP2A is a phosphatase found to inhibit ERK signaling in ovarian cells expressing ErbB4 receptors [290]. However, the inhibition effect is dependent on the expression level of ErbB4 [290], thus making PP2A a difficult target to control. Shc, GS and ShP are adaptor proteins implicated in ovarian cancer as they play a role in recruiting secondary messenger proteins in the signaling cascade [290]. Targeting these proteins may interfere and attenuate the signaling. Heregulin (HRG) is the ligand for the ErbB4 receptor which leads to its activation upon receptor binding. A ligand sequestering approach similar to that of Bevacizumab [269] may be used to regulate ErbB4 receptor signaling. However, the efficacy may be dependent on the expression level of HER2 since heregulin has been found to inhibit growth of breast and ovarian cancer cells overexpressing HER2 [143]. Hence, *V_B contains nodes with high biological relevance as potential ovarian cancer drug targets. However, the efficacy of hitting some of these targets may be dependent on the expression level of other proteins.*

Node	PANI	MPSA	SOBOL
ATP-dependent motor protein			
ppMLC	1	100	21
MLC	5	1	3
pMLC	2	32	14
G protein related			
$G_q\alpha$:GTP	10	90	98
$G\beta\gamma1$	76	64	71
$G\beta\gamma2$	81	63	70
$G_{12}\alpha\beta\gamma$	67	103	22
$G_{12}\alpha$:GDP	39	60	67
$G_{12}\alpha$:GTP	21	59	66
$G_q\alpha$:GDP	40	58	65
$G_q\alpha\beta\gamma$	66	20	20
RGS	35	31	32
$G_q\alpha$:RGS	27	91	99
Nucleotide			
GTP	91	25	30
GDP	-1	29	97
Phospholipase			
PLCβ	53	18	29
Phospholipid			
PIP2	90	22	24
PC	-1	86	93
Ion related			
Ca^{2+}†	45	23	35
Ca^{2+} trunsp	74	21	27
$2Ca^{2+}$:Ca^{2+} trunsp	64	55	62
Ca^{2+} ext leak	92	8	11
Ca ext	89	10	8
Ca^{2+} int leak	92	19	39
IP3R	69	14	28
Ca^{2+} pump	87	13	10
Ca^{2+} pump:Ca^{2+}	83	54	61
Ca^{2+} store	80	16	19
Ca^{2+}:CaM	65	102	25
$2Ca^{2+}$:CaM	77	83	90
$3Ca^{2+}$:CaM	79	82	89
$4Ca^{2+}$:CaM	85	81	88
CaM	82	98	13
Inositol related			
Inositol	-1	94	102
IP3	8	28	34
3IP3:IP3R	52	89	96

Node	PANI	MPSA	SOBOL
GTPase related			
Rho:RhoGEF	33	85	92
Rho:GTP	6	104	17
Rho:GDP	16	7	6
RhoGAP	42	6	7
p115RhoGEF	9	9	9
RhoGEF active	-1	84	91
p115RhoGEF:GTPα	13	61	68
Rho.RhoGAP	28	87	94
Kinase			
Rho-kinase	37	5	4
MLCK	11	2	2
PKC	58	17	31
PKC active 1	25	24	38
PKC active 2	48	12	26
PKC active 3	23	76	83
Phosphatase related			
MYPT1_PPase	14	3	1
pMYPT1_PPase	17	4	5
CPI-17	70	27	16
pCPI-17	7	65	72
pCPI-17:MYPT1_PPase	88	69	76
CPI-17:MYPT1_PPase	86	68	75
Glyceride			
DAG	12	88	95
Protease			
thrombin†	93	30	23
thrombin_ligand	-1	96	104
Kinase:ATP-dependent motor protein complex			
Rho-kinase:MLC	51	67	74
Rho-kinase:pMLC	43	66	73
MLCK:pMLC	55	46	53
MLCK:MLC	46	45	52
Kinase:ion:ion-binding protein complex			
MLCK:Ca^{2+}:CaM†	44	105	15
MLCK:$2Ca^{2+}$:CaM†	54	80	87
MLCK:$3Ca^{2+}$:CaM†	18	79	86
MLCK:$4Ca^{2+}$:CaM†	20	78	85
Kinase:phosphatase inhibitor complex			
PKC active 1:CPI	63	72	79
PKC active 2:CPI	75	71	78
PKC active 3:CPI	32	70	77

Node	PANI	MPSA	SOBOL
Phosphatase:ATP-dependent motor protein complex			
pMYPT1:ppMLC	19	50	57
MYPT1:ppMLC	26	49	56
pMYPT1:pMLC	38	48	55
MYPT1:pMLC	57	47	54
Kinase:ion:ion-binding protein:ATP-dependent motor protein complex			
MLCK:$4Ca^{2+}$:CaM:pMLC	34	43	50
MLCK:$3Ca^{2+}$:CaM:pMLC	29	42	49
MLCK:$4Ca^{2+}$:CaM:MLC	59	41	48
MLCK:$3Ca^{2+}$:CaM:MLC	68	40	47
MLCK:$2Ca^{2+}$:CaM:pMLC	78	39	46
MLCK:$2Ca^{2+}$:CaM:MLC	84	38	45
MLCK:Ca^{2+}:CaM:pMLC	73	37	44
MLCK:Ca^{2+}:CaM:MLC	72	36	43
Protease:G protein-coupled receptor complex			
thrombin_R	71	97	105
pro_thrombinR	94	101	18
thrombinR active†	30	95	103
thrombinR	-1	92	100
G protein:protease:G protein-coupled receptor complex			
$G_{12}\alpha\beta\gamma$:thrombinR active	62	62	69
$G_q\alpha\beta\gamma$:thrombinR active	56	57	64
Other complexes			
Rho:GTP:Rho-kinase†	3	15	12
Rho:GTP:Rho-kinase:pMLC	22	53	60
Rho:GTP:Rho-kinase:MLC	49	52	59
PKC:DAG	47	77	84
PKC:Ca^{2+}	60	99	36
PKC:Ca^{2+}:DAG	61	34	41
MYPT1:Rho:GTP:Rho-kinase	41	44	51
MYPT1:Rho-kinase	50	51	58
PLCβ:$G_q\alpha$:GTP	36	56	63
PLCβ:$G_q\alpha$:GTP:Ca^{2+}	4	35	42
PLCβ:G_q:GTP:Ca:PIP2	15	33	40
PLCβ:Ca^{2+}	24	26	33
PLCβ:Ca:PIP2	31	11	37
Others			
sa40_degraded	-1	93	101
csa39_degraded	-1	75	82
csa36_degraded	-1	74	81
csa35_degraded	-1	73	80

Table 7: Node ranking result with ppMLC as output node. Nodes marked with †are known drug targets for atrial fibrillation (Table 6). Rank of -1 indicates that the protein is not considered a relevant target based on the reachability rule.

MLC phosphorylation network. For the MLC phosphorylation network [160], the Spearman's ranked coefficients for the pairs of methods (MPSA, PANI), (MPSA, SOBOL) and (PANI, SOBOL) are -0.1264, 0.6722, and -0.2194, respectively. This implies that rankings obtained by PANI are significantly different from GSA-based ranking.

The MLC phosphorylation network [160] is implicated in the control of transient MLC phosphorylation by Ca^{2+}/calmodulin-dependent MLC kinase (MLCK) and Rho-kinase. Transient MLC phosphorylation results in transient cell contraction and changes in MLC expression has been observed in animal models of atrial fibrillation (a condition of sustained disorder in the cardiac rhythm) [43]. Hence, we will choose phosphorylated MLC (ppMLC) as the output node and use atrial fibrillation drugs in [184] as benchmark (Table 6). Analysis was done using BIOMD0000000088 obtained from Biomodels.net [144]. Except for the initial concentration of thrombin which was modified from 0μM to 0.01μM to initiate the phosphorylation signaling cascade, the rest of the kinetic constants and initial concentrations follow those specified in BIOMD0000000088. The concentration-time profiles of the nodes are obtained using *Copasi* with the following parameters: $\{duration = 3600seconds, intervals = 12seconds\}$. From the pruning phase in PANI, we obtain 95 relevant target nodes ($|T| = 95$). The reference drug targets are curated from [184] by searching for "atrial fibrillation drug" and filtering for unique drugs relevant for atrial fibrillation that are targeting the MLC phosphorylation pathway. The uncurated result consists of 375 studies, of which 219 studies involve drugs relevant for atrial fibrillation. The rest of the studies involve ablation studies, catheter procedures and more general conditions such as cardiovascular disease. Appendix B contains the 99 unique drugs from the 219 studies. The drug targets are identified using literature survey. Only drug targets that are relevant for the MLC phosphorylation network are considered as reference drug targets for subsequent analysis.

The *MinNode* are 93, 105 and 103 for PANI, MPSA, and SOBOL, respectively (Table 6). In terms of normalized ROC curves' AUC, they are 0.705, 0.458, 0.533, respectively (Fig. 3b). Paired t-test analysis on the ranks of known drug targets shows that PANI ranks drug targets higher than MPSA (t=-

1.492, P=0.09) and SOBOL (t=-0.949, P=0.19). For random prioritization (100 trials), *MinNode* varies in the range [53 – 105] while paired t-test p-value varies in the range [0.005 – 0.97]. Of these trials, 35% had *MinNode*<93 and 74% had p-value<=0.3. Hence, *compared to* MPSA, SOBOL *and random prioritization,* PANI *is able to prioritize a majority of known atrial fibrillation drug targets.* We next examine the biological relevance of the putative target nodes.

Similarly, we examine the relevance of MLC phosphorylation in the therapeutic effect of the drug. Simvastatin targets the RhoA/Rho kinase (ROCK) signaling pathway which regulates the vascular tone via inhibition of MLC phosphatase [137]. Dysregulation of vascular tone is an effect of atrial fibrillation [185]. Ca^{2+}-calmodulin complex can activate MLCK which induces phosphorylation of MLC, resulting in modulation of vascular tone [149]. Amiodarone [187] and ATI-2042 [225, 187] antagonize calmodulin, thus hindering activation of MLCK and the phosphorylation of MLC. Similarly, calivarone [83], AZD1305 [44], spironolactone [173], verapamil [146], magnesium sulphate [73], K201 [117], diltiazem [146] and calcium antagonist [77] which reduce intracellular Ca^{2+} level cause inhibition of MLCK and hence, inhibit the phosphorylation of MLC. Thrombin stimulation inhibits MLC phosphatase via the RhoA/ROCK pathway [12]. Hence, simvastatin [76], ximelagatran [168], edoxaban [273] and apixaban [273] which block the active site of thrombin reduce the level of thrombin activity, thereby allowing MLC phosphatase to dephosphorylate ppMLC. Similarly, AZD0837 and dabigatran which disrupt the binding of thrombin to its substrate [241] result in increased level of MLC phosphatase dephosphorylating ppMLC. Hence, *pp*MLC *is likely to be an important mediator in the regulation of vascular tone by these drugs.*

From Table 7, we see that PANI's top-3 drug target classes are ATP-dependent motor protein, glyceride and GTPase with average putative target score of 2.67, 12 and 30.25, respectively; MPSA's are phospholipase, kinase and nucleotide with average putative target score of 18, 22.67 and 27, respectively; SOBOL's are ATP-dependent motor protein, phospholipase and kinase with average putative target score of 12.67, 29 and 30.67, respectively. Apart from kinases which has long been regarded as good drug targets [58], ATP-dependent motor protein, glyceride, GTPase and phospholipase are also being explored as potential drug targets. Several synthetic, small molecule human kinesin (ATP-dependent motor protein) inhibitors [47], and phospholipase inhibitors such as darapladib [245] are currently in clinical trials. There are also drugs such as Fasudil [81] which target the Rho GTPase pathway to prevent atrial electrical remodeling in atrial fibrillation. Glyceride such as diacylglycerol (DAG) has been suggested as a novel therapeutic target for atrial fibrillation [103]. Hence, PANI *identifies classes with relevance as drug targets which tend to be different from* MPSA *and* SOBOL.

Finally, we examine the set of nodes ranked high in PANI, but low in MPSA or SOBOL, denoted as V_A = {thrombinR active†, $G_q\alpha$.RGS, $G_q\alpha$.GTP, MLCK.3Ca^{2+}.CaM†, Rho.RhoGAP, MLCK.4Ca^{2+}.CaM†, RhoGEF, p115RhoGEF.GTPα, pCPI-17, PKC active, DAG}. Nodes marked with †are known atrial fibrillation drug targets. $G_q\alpha$.RGS and $G_q\alpha$.GTP represent $G_q\alpha$ bound to regulator of G-protein signaling protein (RGS) and GTP, respectively. $G_q\alpha$ has recently been implicated in atrial fibrillation in mouse model [258] and specific G-protein inhibition using cell-penetrating C-terminal peptides [6] could be beneficial for atrial fibrillation treatment. RGS controls the activity of active $G_q\alpha$ ($G_q\alpha$.GTP). In mouse model, knockout of RGS4, a GTPase-activating protein for $G_q\alpha$ [99], showed increased susceptibility to atrial fibrillation [56]. Hence, regulation of different RGS may be useful in treatment of atrial fibrillation. p115RhoGEF is the $G_{13}\alpha$-specific RGS [274] and activated $G_{13}\alpha$ is involved in phosphorylation of MLC_{20} [177]. Hence, $G_{13}\alpha$-specific cell-penetrating peptides similar to that used in [6] may be a potential atrial fibrillation treatment via regulation of MLC phosphorylation. Diacylglycerol kinase ζ was found to inhibit $G_q\alpha$-induced atrial remodeling in mouse model by degenerating diacylglycerol (DAG) and suggested as a novel therapeutic target for atrial fibrillation [103]. In mouse models, cardiac-specific overexpression of RhoA results in sinus and atrioventricular nodal dysfunction and contractile failure [222]. Hence, RhoGEF and Rho.RhoGAP, which regulate the activity of RhoA, can be targeted to control RhoA activity, which in turn provide better regulation of cardiac cell contraction. PKC activation was found to be critical for activation of the cardiac delayed rectifier K^+ current channel and regulation of this channel has direct implications on heart rhythm regulation [166]. CPI-17 is a phosphatase-inhibitory protein whose inhibitory potency increases with phosphorylation of Thr38 [192] and phosphorylated CPI-17 (pCPI-17) inhibits MLC phosphatase activity [127]. Hence, regulation of pCPI-17 is another means of regulating MLC phosphorylation. Thus, V_A contains nodes with high relevance as drug tar-

NCT ID (Phase)	Drugs	Conditions
00257556 (4)	follitrophin α, menotrophin	infertility
00417144 (4)	arvekap, ganirelix	polycystic ovary syndrome, hyperstimulation syndrome
00441324 (4)	recombinant human LH (Luveris)	infertility
00505752 (2)	AS900672, follitrophin α	infertility
00571870 (-)	cetrorelix acetate	infertility
00575302 (4)	follitrophin α	infertility
00696800 (3)	corifollitrophin α, follitrophin β	in vitro fertilization
00696878 (3)	corifollitrophin α	in vitro fertilization
00702845 (3)	corifollitrophin α, follitrophin β	infertility
00802360 (4)	menopur, endometrin, follistim pen, progesterone	infertility
00805935 (4)	menopur, endometrin, follistim pen, progesterone	polycystic ovarian syndrome, infertility
00866008 (4)	GnRH agonist	in vitro fertilization
00884221 (3)	menotrophin, follitrophin β	infertility
00954265 (3)	urinary human chorionic gonadotrophin (hCG), recombinant hCG	embryonic development, pregnancy
01035099 (-)	letrozole	breast cancer, infertility
01043120 (2)	barusiban	infertility
01058252 (-)	letrozole, follitrophin β	infertility
01112111 (-)	gonadotropin	polycystic ovarian syndrome
01115725 (4)	follitrophin α	infertility
01121991 (3)	Luveris	infertility, ovulation reduction
01144416 (3)	corifollitrophin α, follitrophin β	infertility
01202643 (1)	G-CSF, saline	infertility, female endometrium
01202656 (1)	G-CSF, saline	infertility, female endometrium
01225835 (4)	menotrophin, follitrophin α	infertility

Table 8: Drugs-related trials from [184] using "embryonic development" for keyword search.

Transcription Factor

Node	PANI	Node	PANI
Protein E Bra	4	Protein M UbiqSoxB1	27
Protein M cB	5	Protein P UbiqEts1	28
Protein E cB	6	Protein M Gcm	29
Protein P cB	7	Protein P UbiqHesC	30
Protein P UbiqHnf6	8	mRNA E SoxB1	31
Protein P Snail	9	mRNA M SoxB1	31
Protein E Gcm	10	Protein P Erg	33
Protein M SoxB1	11	mRNA M Otx	34
Protein E SoxB1	12	mRNA E Otx	35
Protein M Otx	13	Protein P Dri	36
Protein E Otx	14	mRNA P Otx	37
Protein P Hex	15	Protein M Bra	38
Protein P Otx	16	Protein P Hnf6	40
Protein E Hox	17	Protein P Pmar1	41
Protein P Ets1	18	Protein P GataE	44
Protein P Hox	19	Protein E GataE	46
Protein M Pmar1	20	mRNA P GataE	47
Protein E Pmar1	21	Protein M GataE	51
Protein M Hox	22	Protein P UbiqSoxC	52
mRNA P Ets1	23	Protein P UbiqTel	52
Protein P Bra	24	Protein P Pmar1	55
Protein P Tgif	26	Protein M Pmar1	56
Protein E UbiqSoxB1	27		

Glycoprotein

Node	PANI	Node	PANI
Protein E Wnt8	1	mRNA M Wnt8	42
Protein M Wnt8	2	mRNA E Wnt8	43
Protein P Wnt8	3	mRNA P Wnt8	45

Ligand

Node	PANI	Node	PANI
Protein M Delta	39	mRNA M Delta	50
Protein P Delta	48		

Others

Node	PANI	Node	PANI
mRNA E Gcad	25	Protein M Notch	49
mRNA M Gcad	25	Protein P VEGFSignal	53
mRNA P Gcad	25	Protein P Sm30	54
mRNA P VEGFR	32		

Table 9: Top-61 ranked nodes of endomesoderm network with Protein E Endo16 as the output node.

gets for atrial fibrillation. Next, we look at the set of nodes ranked high in MPSA and SOBOL, but low in PANI, denoted as V_B = {thrombin†, GTP, PIP2, Ca^{2+} store, Ca^{2+} trunsp, Ca^{2+} pump,Ca^{2+} ext leak, Ca^{2+} ext, Ca^{2+} int leak}. Similarly, we will not elaborate further on thrombin which is a known drug target. GTP is a energy storage molecule that is used ubiquitously in the cell to perform many different and important biological functions. Hence, GTP may not be a suitable target. In contrast to the effect of PKC, PIP2 depletion was found to be critical for inhibition of the cardiac delayed rectifier K^+ current channel and regulation of this channel has direct implications on heart rhythm regulation [166]. The rest of the nodes in V_B regulates the intracellular concentration of Ca^{2+}. Altered Ca^{2+} signaling has been observed in atrial fibrillation and methods such as targeting of $I_{Ca,L}$ and normalization of RYR2 dysfunction have been suggested as potential treatments [67]. Note that besides identifying highly relevant potential target nodes, MPSA and SOBOL also identify node such as GTP whose extensive involvement in different biological functions makes it a difficult target.

Endomesoderm network. For the sea urchin endomesoderm gene regulatory network [138], we could not perform Spearman's ranked coefficient analysis since MPSA and SOBOL fail to analyze this network due to memory error.

The endomesoderm network which is used for studying embryonic development (BIOMD0000000235) is obtained from Biomodels.net [144] and the concentration-time profiles of the nodes are obtained using *Copasi* with the following parameters: $\{duration = 70hours, intervals = 0.1hours\}$. The network in [138] describes the gastrulation phase involving the formation of the endoderm and the mesoderm. Endo16 (Protein E Endo16) is found to be essential for gastrulation [213], a phase early in embryonic development, and will be selected as the output node. A search in [184] using "embryonic development" did not yield any drugs that were targeted at the endomesoderm network. Of the 82 trials in the search result, 25 trials involved drugs (Table 8) and of these 25 trials, only trial NCT00954265 is associated to embryonic development. However, the drug (recombinant human chorionic gonadotrophin) involved is a promoter of corpus luteal progesterone production. This drug targets the LH/hCG receptors on the spiral arteries [59] which is not part of the endomesoderm gene regulatory network in [138]. With no relevant drug targets in [184], we are unable to evaluate the results in the same way we have done for the above two networks. Instead, we will assess a small subset of the top ranked nodes (Table 9) in terms of their relevance in the regulation of endo16 using literature survey. The size of the candidate node set is 610 after the pruning process. For a more manageable assessment of the top ranked nodes, we fix the size of the small subset as 61 (top-10%).

cB is a transcription factor of *cis*-regulatory Module B of endo16 [288]. Otx was found to be necessary for the initial activation of endo16 in the endomesoderm [286] and the β1/2 transcription unit of this gene interacts with both Krox and GataE to form a positive feedback loop [287]. Brachyury (Bra), a target gene of Otx, also activates Otx to form a positive feedback loop and the expression of Bra is inhibited by presence of hox11/13b [199]. Wnt8 is activated by Krox which positively autoregulates and together they form a positive feedback loop [62] leading to the activation of endo16. SoxB1 inhibits the transcriptional activation of $\beta-$catenin [10] which activates Wnt8 [275]. Delta is the ligand for the notch receptor whose activation is required for the expression of GataE [102]. Micromere ablation prevents normal gastrulation and normal expression of endo16 [206]. Pmar1 expression induces endo16 and rescues cadherin-inhibited specification of micromeres [189] by inhibiting HesC which in turns inhibits delta [41]. In [219], ERK inhibition was found to significantly reduce delta expression via Ets1 mediation. *Hence, of the 61 putative nodes, 44 (72.13%) are implicated in the regulation of endo16.*

From Table 9, we see that PANI's top-61 ranked nodes consist of a mix of various classes of drug targets and the top-3 classes of target are transcription factors, glycoproteins and ligands accounting for 73.8%, 9.8% and 4.9% of drug targets, respectively. Traditionally, transcription factors are not considered good targets. However, with increasing knowledge and technological advances, they have recently been seriously considered as drug targets [207]. Compounds, such as 3-deazaneplanocin A (DZNep), an S-adenosylhomocysteine hydrolase inhibitor which depletes EZH2 in breast cancer cells, are currently investigated as potential cancer treatment [250]. Several proteins in the glycoprotein family have been targeted by drugs. For instance, tariquidar is a potent and specific non-competitive inhibitor of P-glycoprotein [78] while BMS-378806 can bind to gp120 to hinder

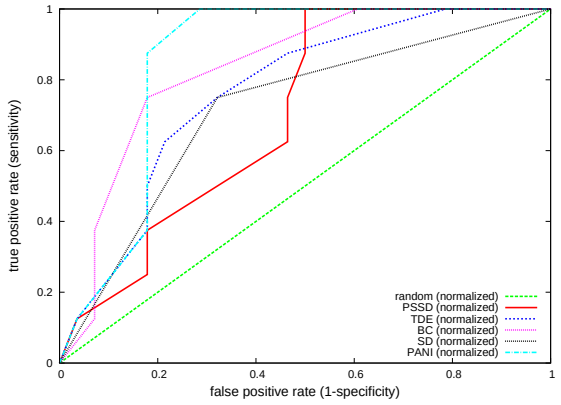

(a)

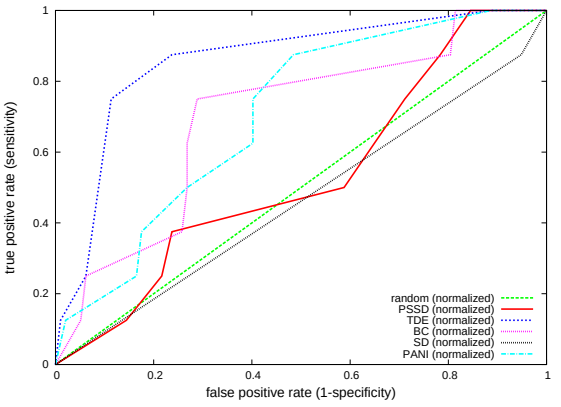

(b)

Figure 4: Effect of PSSD, TDE, BC and SD on (a) MAPK-PI3K and (b) MLC phosphorylation network prioritization results.

the interaction between the HIV-1 envelope and cellular CD4 receptors [151]. When the entire endomesoderm network is considered, PANI's top-3 classes of target for the endomesoderm network are adaptor protein-transcription factor complexes, actin binding proteins and cytoskeletal-associated proteins with average putative target score of 90, 202.67 and 203.89, respectively. These drug classes too, are promising drug targets. For instance, drugs targeting interaction of adaptor proteins and other proteins have been developed. An example is **difopein** which inhibits the interaction of 14-3-3 and Raf [268]; INS115644, a **latrunculin B** compound which behaves like a **gelsolin** mimetic (actin binding proteins) is in clinical trials for glaucoma [184]. It may look surprising that the top-3 classes of the top-61 ranked nodes differ from that of the entire network. On closer examination, we find that this difference is most likely due to the size of these target classes in the endomesoderm network. Transcription factors, glycoproteins and ligands account for 53.2%, 5.9% and 4% of drug targets in this 622-node network, respectively while adaptor protein-transcription factor complexes, actin binding proteins and cytoskeletal-associated proteins account for 0.5%, 1.4% and 1.4%, respectively. Hence, even though adaptor protein-transcription factor complexes, actin binding proteins and cytoskeletal-associated proteins have lower putative target score, it is still highly probably that transcription factors,

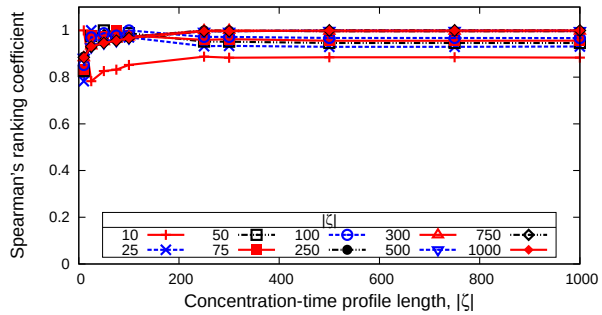

(a)

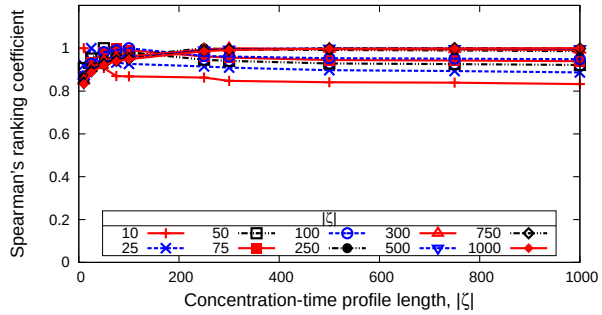

(b)

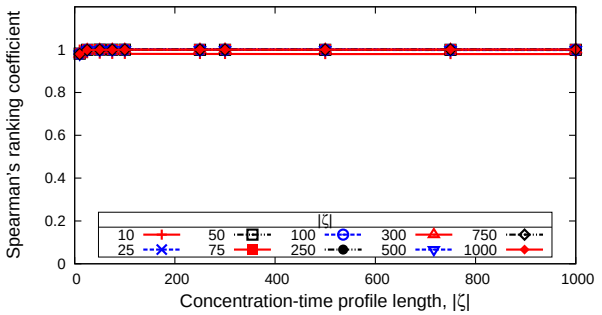

(c)

Figure 5: Effect of $|\zeta|$ on ranking result of (a) MAPK-PI3K, (b) MLC phosphorylation and (c) endomesoderm network using PANI.

glycoproteins and ligands appear in the top-61 ranked nodes since they are much more abundant by comparison.

5.4 Effects of Multiple Properties on Prioritization Result.

In this set of experiments, we investigate the effects of aggregate ranking on the prediction quality by comparing ranking results based on PANI with results based solely on PSSD, TDE, BC or signaling distance to output node (SD). We perform ROC analysis on the MAPK-PI3K and MLC phosphorylation network. From the ROC analysis, we find that aggregating the ranking can help to moderate the rank of the putative target nodes and even improve the prioritization result. Although SD can also prioritize many known drug targets, its low granularity (assigning multiple nodes to the same rank) limits its usage in networks with large SCC. In the case of the endomesoderm network, the ROC analysis could not be carried out as there is no relevant drug in [184].

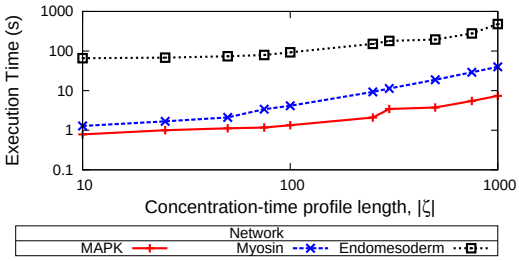

Figure 6: Effect of $|\zeta|$ on execution time.

MAPK-PI3K network. The Spearman's ranked coefficients for the pairs of properties $(\frac{1}{\text{PSSD}}, \frac{1}{\text{TDE}})$, $(\frac{1}{\text{PSSD}}, \text{BC})$, $(\text{BC}, \frac{1}{\text{TDE}})$, $(\frac{1}{\text{PSSD}}, \frac{1}{\text{SD}})$, $(\frac{1}{\text{TDE}}, \frac{1}{\text{SD}})$ and $(\text{BC}, \frac{1}{\text{SD}})$ are 0.3997, 0.2513, 0.1992, 0.3006, 0.9368 and 0.0758, respectively. Apart from TDE and SD, the coefficients of the rest of the pairs of properties are at most 0.3997. Statistically, the variables are not perfectly correlated and evaluating the putative target score based on all the properties can improve prioritization results [88]. The normalized ROC curves of SD and TDE are similar (Fig. 4a), although TDE performs slightly better than SD. The ROC analysis (Fig. 4a) shows that for FPR greater than 0.2, the aggregate ranking performed better than individual ranking. This is likely due to different properties complementing each other to improve the prioritization results. For instance, ranking based on only TDE misses PI3K* (a well-known ovarian cancer drug target) as a putative target node. Incorporating additional properties improved the ranking of PI3K* and result in its prioritization as a putative target node. The AUC of the ROC is 0.701, 0.763, 0.833 and 0.714 for PSSD, TDE, BC and SD, respectively. This suggests that nodes having smaller PSSD, smaller TDE, larger BC and smaller SD values may be potential drug targets in the case of MAPK-PI3K network in the context of ovarian cancer.

MLC phosphorylation network. The Spearman's ranked coefficients for the pairs of properties $(\frac{1}{\text{PSSD}}, \frac{1}{\text{TDE}})$, $(\frac{1}{\text{PSSD}}, \text{BC})$, $(\text{BC}, \frac{1}{\text{TDE}})$, $(\frac{1}{\text{PSSD}}, \frac{1}{\text{SD}})$, $(\frac{1}{\text{TDE}}, \frac{1}{\text{SD}})$ and $(\text{BC}, \frac{1}{\text{SD}})$ are 0.4529, 0.4998, 0.63, -0.2426, -0.2103 and -0.2664, respectively. In this network, TDE performed better than PANI and other individual ranking. This is likely due to the tendency of TDE assigning multiple nodes to the same rank. For instance, 42 nodes are assigned the same rank (rank=14). The lack of granularity provides poor distinction between nodes. Hence, even though TDE can rank nodes much better than other individual properties for this network, additional properties are needed to improve granularity of the ranking. The AUC of the ROC is 0.531, 0.859, 0.699 and 0.463 for PSSD, TDE, BC and SD, respectively. In this network, we note that SD did not perform as well as the other properties. This is probably due to SD assigning a large number of nodes to the same rank, especially for networks with large SCC resulting in both high TPR and high FPR. Hence, it has a smaller AUC as compared to other properties. In summary, nodes having smaller TDE and larger BC values may be potential drug targets in the case of MLC phosphorylation network in the context of atrial fibrillation.

5.5 Effects of Profile Length ($|\zeta|$).

In this experiment, we examine the effect of varying the number of time points in the concentration-time profile ζ ($|\zeta|$) on the ranking. The profiles are obtained using *Copasi*

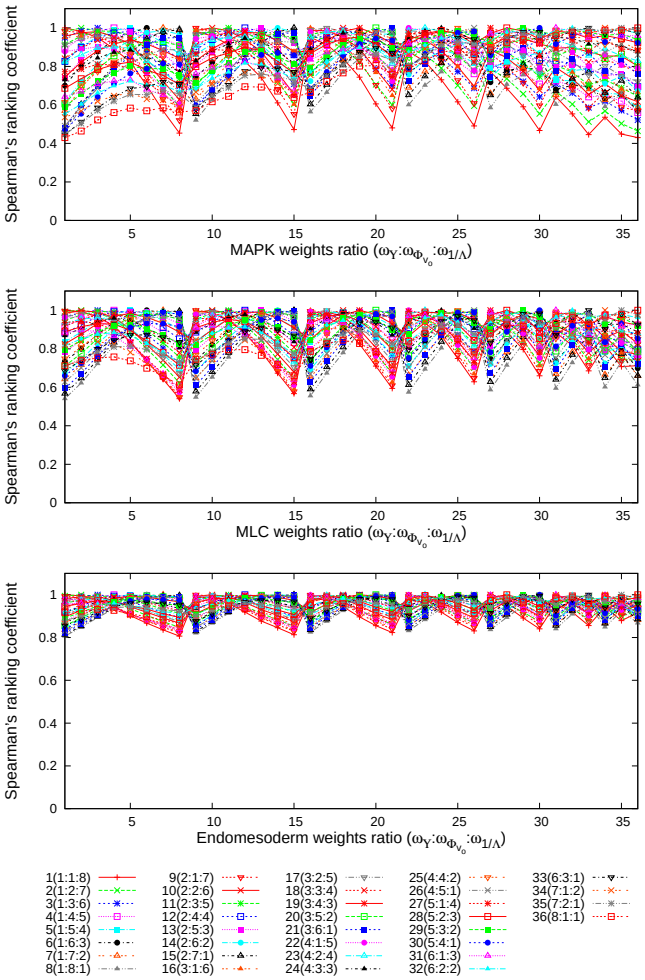

Figure 7: Effect of property-weights on relative ranking result of nodes.

where $|\zeta|$ varies in the range of $\{10, 25, 50, 75, 100, 250, 300, 500, 750, 1000\}$. For MPSA and SOBOL, the SBML-SAT tool [297] used for performing the sensitivity analysis does not permit editing of $|\zeta|$.

MAPK-PI3K network. We observe that $|\zeta| = 10$ has a much lower coefficient with respect to the rankings obtained for other values of $|\zeta|$ (Fig. 5a), probably due to insufficient time points to capture profile changes. At $|\zeta| > 100$, the correlation coefficient approaches a constant value of $\sim 100\%$ when compared with other values of $|\zeta|$ greater than 100. In this paper, we set $|\zeta|$ as 300 for this network. Lastly, as reported in Fig. 6, execution times of PANI increase with increasing value of $|\zeta|$ while that of MPSA and SOBOL remains constant at about 16 minutes and 3 hours, respectively since $|\zeta|$ is not a modifiable parameter for SBML-SAT sensitivity analysis.

MLC phosphorylation network. Similar to the MAPK-PI3K network, we observe that $|\zeta| = 10$ has a much lower coefficient with respect to the rankings obtained for other values of $|\zeta|$ (Fig. 5b). At $|\zeta| > 100$, the correlation coefficient approaches a constant value of $\sim 95\%$ when compared with other values of $|\zeta|$ greater than 100. In this paper, we set $|\zeta|$ as 300 for this network. Lastly, as reported in Fig. 6, execution times of PANI increase with increasing value of $|\zeta|$

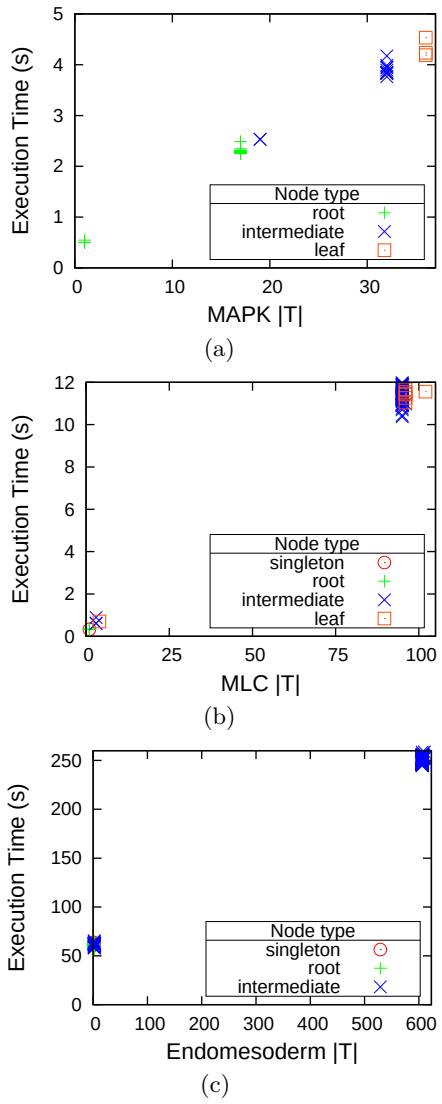

Figure 8: Relationship of execution time (s) and $|T|$ for (a)MAPK-PI3K, (b)MLC phosphorylation and (c)endomesoderm network. Singletons are nodes with no in-coming or out-going edges.

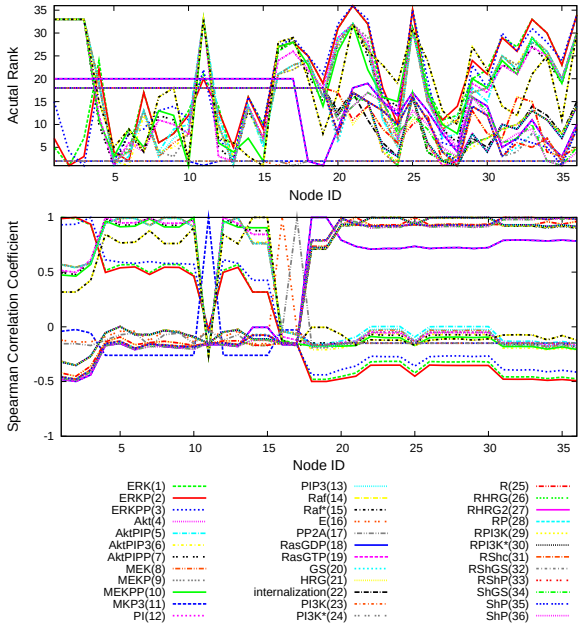

Figure 9: Effect of varying output node on MAPK-PI3K ranking result using PANI.

while that of MPSA and SOBOL remains constant at about 2 and 21 hours, respectively.

Endomesoderm network. Similar to the two previous networks, we observe that $|\zeta| = 10$ has a lower coefficient with respect to the rankings obtained for other values of $|\zeta|$ (Fig. 5c). In addition, we note that in this network, even for $|\zeta| = 10$, the coefficients with respect to the rankings of other $|\zeta|$ values are consistently above 98%. At $|\zeta| > 25$, the correlation coefficient approaches a constant value of $\sim 100\%$ when compared with other values of $|\zeta|$ greater than 25. In this paper, we set $|\zeta|$ as 700 for this network. Lastly, as reported in Fig. 6, execution times of PANI increase with increasing value of $|\zeta|$. Both MPSA and SOBOL analysis failed for the endomesoderm network due to memory error.

5.6 Effects of Weights ($\omega_{\Phi_{v_o}}$, ω_{Υ} and $\omega_{\frac{1}{\Lambda}}$).

In this set of experiments, we investigate the effects of different scalar weight factors on the ranking result by examining how the percentage of common putative target nodes and known drug targets vary as the weights are modified. We vary each weight in the range of $\{0.1, 0.2, 0.3, 0.4, 0.5, 0.6, 0.7, 0.8, 0.9\}$ while ensuring that $\omega_{\Phi_{v_o}} + \omega_{\Upsilon} + \omega_{\frac{1}{\Lambda}} = 1$. This produces 36 different weight-ratios. For each weight-ratio, the putative target score of each node is calculated. Then, the Spearman's correlation coefficient of the rankings of each pair of weight-ratio is evaluated. We find that many of the weight-ratios contain common putative target nodes and can identify a majority of known drug targets. This implies that although the rankings of the targets vary, most of the targets are still ranked high enough to be considered as a putative target node in most weight-ratios. Interestingly, we note that as the size of the network increases, the impact of the weight ratios on the ranking result seems to reduce. For instance, the coefficient ranges between ~ 0.45 to 1 for the MAPK-PI3K network which contains 36 nodes while it ranges between ~ 0.8 to 1 for the endomesoderm network which contains 622 nodes. This implies that for larger networks, the choice of weight ratios may not be as important in influencing the ranking result. As knowledge of signaling networks and drug targets grow, there will be more well-established networks with associated well-known drug targets, which would facilitate training of these weights to provide improved node ranking and prioritization.

MAPK-PI3K network. The coefficient ranges between ~ 0.45 to 1 (Fig. 7), implying that using different weight-ratio affects the rankings quite significantly. Since putative target prioritization is dependent on the node rankings, we check how this affects the prioritization. Across the entire range of weights we tested, the minimum number of top ranking targets (*MinNode*) required to identify at least 75% of the relevant known drug targets is 19 for this 36-node network. In addition, 66.7% of the top-50% putative target nodes in 88.9% of the ratios are common.

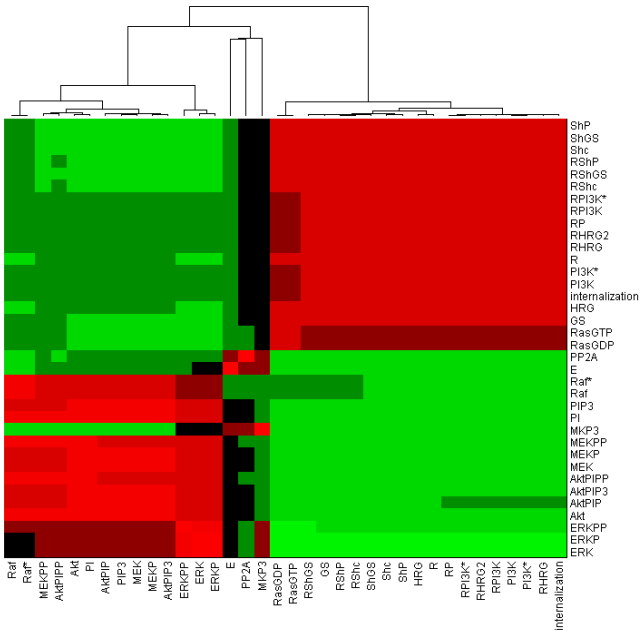

Figure 10: Clustergram analysis of Spearman's correlation coefficient of MAPK-PI3K ranking result when output node is varied.

MLC phosphorylation network. The coefficient ranges between ~ 0.6 to 1 (Fig. 7). The *MinNode* required to identify at least 75% of known drug targets for this 105-node network is 72. Besides that, 60% of the top-50% putative target nodes in all the ratios are common.

Endomesoderm network. The coefficient ranges between ~ 0.8 to 1 (Fig. 7) and 76.9% of the top-50% putative target nodes in all the ratios are common.

5.7 Effects of Selecting Different Output Node.

In this experiment, we examine the effect of selecting different output node on the execution time and the prioritization results. As reported in Fig. 8, the number of pruned targets $|T|$ depends on the network structure and location of v_o where leaf nodes (nodes with no out-going edges) resulted in larger $|T|$. The execution time varies linearly with $|T|$ for PANI and remains constant for MPSA and SOBOL, as these approaches are oblivious to pruning. When we vary the output node, the prioritization results changes. We perform Spearman's rank correlation coefficient and clustergram analysis to investigate the effect of selecting different output node on the prioritization results. For the purpose of computing the Spearman's ranked correlation coefficient, candidate nodes that are pruned ($V_H \backslash T$) are assigned the lowest rank value to reflect their low relevance as putative target node. We find that some output nodes share more similar rank correlation coefficient then others. Particularly, selecting for output nodes in the same SCC produces closer rank correlation coefficient and hence more similar prioritization results. The choice of output nodes affect the ranking in two ways, namely, the decision of whether a candidate is pruned and the candidate node's PSSD value. Hence, output nodes in the same SCC have similar reachability property and are likely to share similar PSSD. In gene regulatory network, profiles of genes in the same module are highly correlated [254]. This

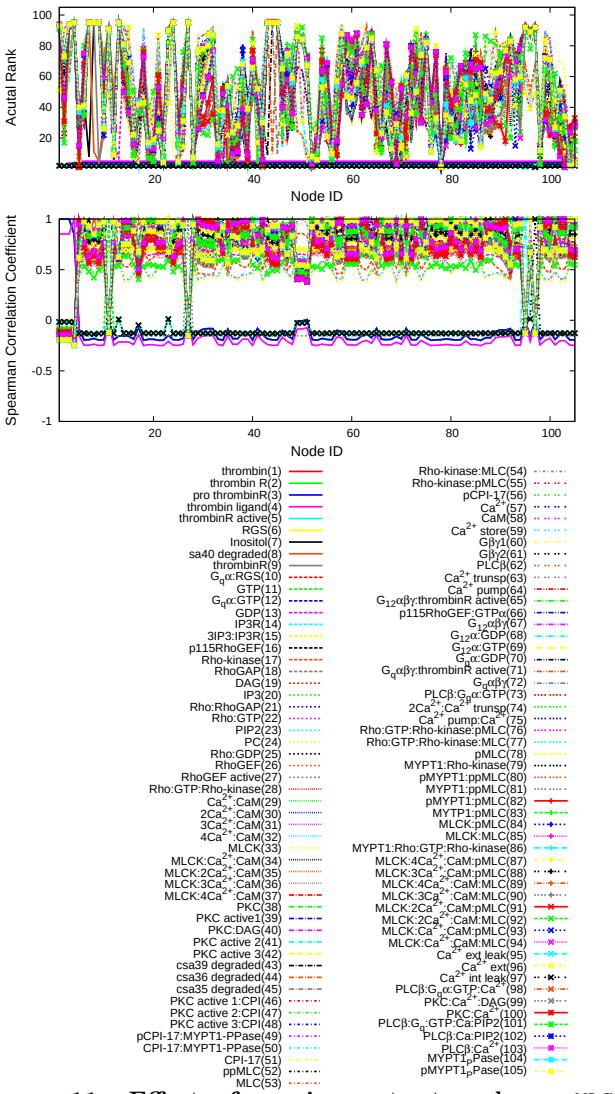

Figure 11: Effect of varying output node on MLC ranking result using PANI.

observation may also hold true for signaling network where protein post-translational profiles in the same SCC are highly correlated

MAPK-PI3K network. Selecting different output node results in changes in the ranking. From the Spearman's correlation coefficient analysis (Fig. 9), we observe that some nodes share more similar rank correlation coefficient than others. We further perform a clustergram analysis (Fig. 10) and find that selecting for output nodes in the same SCC leads to closer rank correlation coefficient and hence more similar ranking results. In the MAPK-PI3K network, we make several observations. First, nodes in the same SCC have closer rank correlation coefficient. Second, sub-clusters exist within SCC. For instance, {RP, RPI3K*, RHRG2, RPI3K, PI3K, PI3K*, RHRG, internalization} form a sub-cluster within the SCC represented by meta node $v_{meta:1}$. Third, SCCs that are separated by a shorter node distance in the hypergraph tend to be nearer in terms of clustering distance. Lastly, root nodes (nodes with no in-coming edges) tend to be clustered together since the pruning process would result in $|T| = 1$

in most instances. Consequently, the nodes that are pruned ($V_H \backslash T$) would be allocated a rank of 2, resulting in highly correlated ranking results when the root nodes are selected as the output node. Hence, nodes that are closer within the hypergraph tend to have more similar ranking result.

MLC phosphorylation network. The MLC phosphorylation network (Fig. 11) appears to have a much closer Spearman's correlation coefficient across the entire range of output node as compared to the MAPK-PI3K network (Fig. 9). The MLC phosphorylation network's correlation coefficient seems to fall into two different clusters. When we performed the clustergram analysis (Fig. 12a), we find similar observations seen in the MAPK-PI3K network. There are two main clusters. The first main cluster (blue box in Fig. 12b) contains the set of root nodes {GTP, RhoGEF active, Ca^{2+} ext leak, Ca^{2+} int leak} and thrombin, thrombin R, pro thrombin R and thrombin ligand. Amongst these nodes, thrombin, thrombin R and pro thrombin R are in the same SCC. The second main cluster contains the rest of the nodes which all fall into one large clusters. Within the second main cluster, there are smaller sub-clusters containing nodes involved in the same reactions. For instance, in the sub-cluster containing {PKC:Ca^{2+}, Ca^{2+}:CaM, CaM, Ca^{2+}} (magenta box in Fig. 12a), CaM combines with Ca^{2+} to form Ca^{2+}:CaM while PKC combines with Ca^{2+} to produce PKC:Ca^{2+}.

Endomesoderm network. Similarly, the endomesoderm network (Fig. 13) appears to have a much closer Spearman's correlation coefficient across the entire range of output node as compared to the MAPK-PI3K network (Fig. 9). The endomesoderm network's correlation coefficient seems to fall into two different clusters. This network contains 217 root, 4 singleton and 401 intermediate nodes. Amongst the intermediate nodes, 25 are not in any SCCs. In total, there are 8 SCCs containing 2 nodes and one SCC containing 360 nodes. When we perform the clustergram analysis (Fig. 14a), we find similar observations seen in the two previous networks. There are two main clusters. The first main cluster (magenta box in Fig. 14a) contains the set of root nodes, singleton nodes and intermediate nodes which are not in any SCC; the second main cluster contains nodes in the 8 two-node SCCs and the 360-node SCC. For the two-node SCCs, nodes in the same SCC were clustered together. For the larger-sized SCC, nodes of the same types tend to form sub-clusters. For instance, nodes associated to Blimp1 and FoxA cluster together to form a sub-cluster {mRNA E Blimp1, mRNA E FoxA, mRNA M Blimp1, mRNA M FoxA, mRNA P Blimp1, mRNA P FoxA, mRNA P GataC} (blue box in Fig. 14b).

6. CONCLUSION AND FUTURE WORK

In this paper, we propose PANI, a novel algorithm for the problem of selecting a set of putative target nodes from a given signaling network. It exploits network structural properties associated with off-target effects to filter out targets with higher probability of side effects, and a dynamic network property associated with efficacy to select for targets with strong influence on the output. Testing PANI on several networks reveals it to be faster and more effective in prioritizing known drug targets. Poor GSA performance may be because the sensitivity criterion seeks high-magnitude correlations, while PANI seeks robust correlations with few off-target effects. Great caution should be exercised when utilizing GSA for a physiological context beyond its original model. Last but not least, PANI is orders of magnitude faster than GSA-based methods.

A key future direction of this research is to continue producing curated datasets showing the known targets of drugs against additional diseases, so that target prioritization methods can be evaluated across a statistical number of problems, and so the computational community will have convenient access to test sets for predicting actual clinical targets. Meanwhile, given that manifestations of a disease may result from dysfunctions in various points instead of a single point of the networks, we will extend PANI to handle multiple output nodes. Our approach requires a boolean-type trigger event, or a pre-specified dosing of the input stimuli, at time zero in the signaling network models and cannot handle models built around a variable dose input (e.g., bistable models). The dimensionality of the trigger, the concentration-time profiles and the shape similarity distance measure of PANI could naturally be extended to make our approach useful for these models. A potentially useful application of our approach is in analyzing incomplete signaling networks with missing rate constants which cannot be analyzed by GSA-based methods. PANI performs analysis based on network topology, and concentration-time profile data such as experimental time-series measurements of protein abundance. Proteomic methods such as SILAC are now providing an explosive increase in available data for this purpose, but in the event that no rate parameters and incomplete concentrations are available, PANI can perform a partial analysis with concentration-time profiles of a partial set of nodes, and identify putative target nodes from within this partial set.

The current study maintains clarity of comparison by contrasting pure GSA-based approaches with pure heuristic or empirical method, but future work for target prioritization may choose to design versions of GSA-based approaches that use heuristics from PANI. Possible integration of methods might occur by filtering out molecules that are very poor by off-target criteria, prior to GSA-based computation, which would also improve speed rather than adding additional burdens to GSA-based approaches. Lastly, we note the unexpected trend of PANI predicting actual clinical targets at a higher rate than mathematically rigorous GSA-based approaches. Hence, this work constitutes anecdotal evidence that heuristic common sense is still needed and useful for bridging the gap between the analysis of quantitative models, and the medical reasons why we build these models.

7. ACKNOWLEDGMENTS

The authors are supported by grant from the Singapore-MIT Alliance Programme in Computational and Systems Biology.

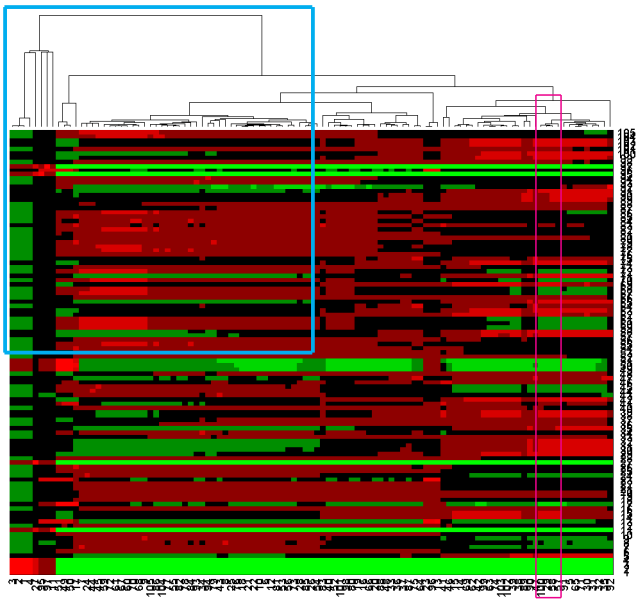

(a)

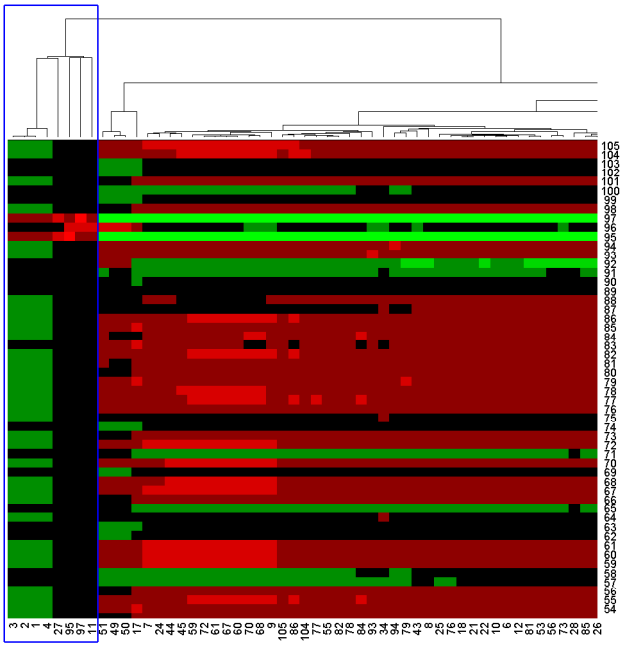

(b)

Figure 12: (a)Clustergram analysis of Spearman's correlation coefficient of `MLC` ranking result when output node is varied and (b)zoom-in view of area enclosed by cyan box in (a). Numbering on axes correspond to Node ID in Fig. 11.

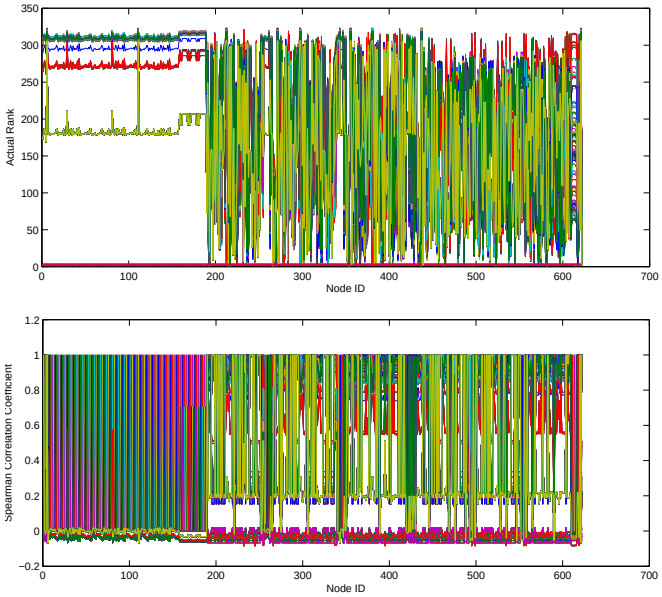

Figure 13: Effect of varying output node on endomesoderm ranking result using PANI. Node names of the corresponding node ID can be found in Table 10.

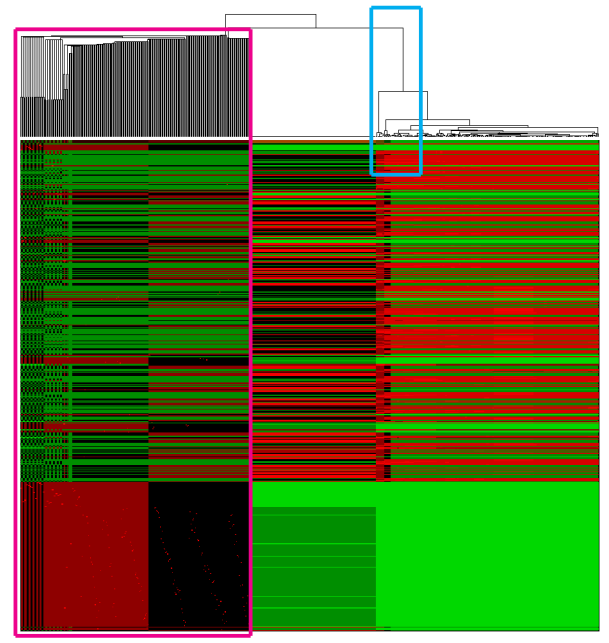

(a)

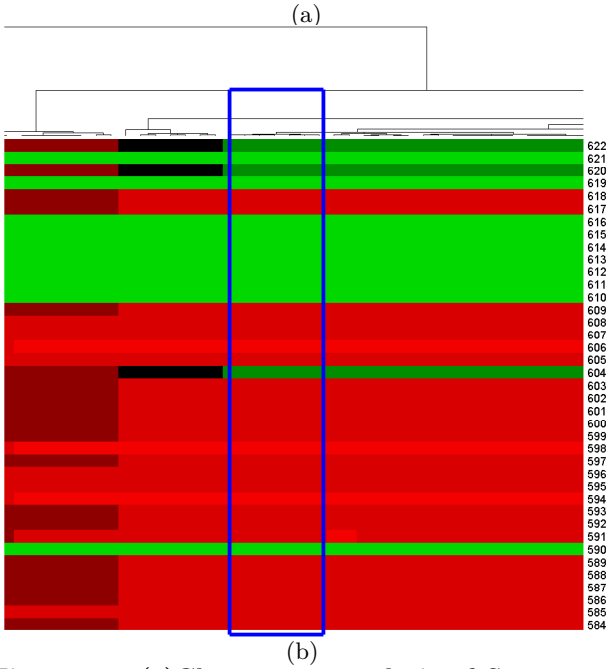

(b)

Figure 14: (a)Clustergram analysis of Spearman's correlation coefficient of endomesoderm ranking result when output node is varied and (b)zoom-in view of area enclosed by cyan box in (a). Numbering on axes correspond to Node ID in Table 10.

ID	Node Name	ID	Node Name	ID	Node Name	ID	Node Name	ID	Node Name	ID	Node Name	ID	Node Name
1	GENE E Alx1	90	GENE M Otx	179	PRE P Gcad	268	PROTEIN E VEGFSignal	357	PROTEIN M nBTCF	446	mRNA E CAPK	535	mRNA M Notch
2	GENE E Apobec	91	GENE M Pks	180	PRE P L1	269	PROTEIN E Wnt8	358	PROTEIN M z13	447	mRNA E CyP	536	mRNA M Nrl
3	GENE E Blimp1	92	GENE M Pmar1	181	PRE P Otx	270	PROTEIN E cB	359	PROTEIN P Alx1	448	mRNA E Delta	537	mRNA M OrCt
4	GENE E Bra	93	GENE M Sm27	182	PRE P UbiqAlx1	271	PROTEIN E frizzled a	360	PROTEIN P Apobec	449	mRNA E Dpt	538	mRNA M Otx
5	GENE E Brn	94	GENE M Sm30	183	PRE P UbiqES	272	PROTEIN E frizzled i	361	PROTEIN P Blimp1	450	mRNA E Dri	539	mRNA M Pks
6	GENE E CAPK	95	GENE M Sm50	184	PRE P UbiqEts1	273	PROTEIN E nBTCF	362	PROTEIN P Bra	451	mRNA E ES	540	mRNA M Pmar1
7	GENE E CyP	96	GENE M Snail	185	PRE P UbiqHesC	274	PROTEIN E z13	363	PROTEIN P Brn	452	mRNA E Endo16	541	mRNA M Sm27
8	GENE E Delta	97	GENE M SoxB1	186	PRE P UbiqHnf6	275	PROTEIN GCM	364	PROTEIN P CAPK	453	mRNA E Erg	542	mRNA M Sm30
9	GENE E Dpt	98	GENE M SoxC	187	PRE P UbiqSoxC	276	PROTEIN M Alx1	365	PROTEIN P CyP	454	mRNA E Ets1	543	mRNA M Sm50
10	GENE E Dri	99	GENE M SuTx	188	PRE P UbiqTel	277	PROTEIN M Apobec	366	PROTEIN P Delta	455	mRNA E Eve	544	mRNA M Snail
11	GENE E ES	100	GENE M TBr	189	PRE P cB	278	PROTEIN M Blimp1	367	PROTEIN P Delta2	456	mRNA E Ficolin	545	mRNA M SoxB1
12	GENE E Endo16	101	GENE M Tel	190	PROTEIN E Alx1	279	PROTEIN M Bra	368	PROTEIN P Dpt	457	mRNA E FoxA	546	mRNA M SoxC
13	GENE E Erg	102	GENE M Tgif	191	PROTEIN E Apobec	280	PROTEIN M Brn	369	PROTEIN P Dri	458	mRNA E FoxB	547	mRNA M SuH
14	GENE E Ets1	103	GENE M VEGFR	192	PROTEIN E Blimp1	281	PROTEIN M CAPK	370	PROTEIN P Endo16	459	mRNA E FoxN23	548	mRNA M SuTx
15	GENE E Eve	104	GENE M Wnt8	193	PROTEIN E Bra	282	PROTEIN M CyP	371	PROTEIN P Erg	460	mRNA E FoxO	549	mRNA M TBr
16	GENE E Ficolin	105	GENE M z13	194	PROTEIN E Brn	283	PROTEIN M Delta	372	PROTEIN P Ets1	461	mRNA E FvMo	550	mRNA M Tel
17	GENE E FoxA	106	GENE P Alx1	195	PROTEIN E CAPK	284	PROTEIN M Delta2	373	PROTEIN P Eve	462	mRNA E GataC	551	mRNA M Tgif
18	GENE E FoxB	107	GENE P Apobec	196	PROTEIN E CyP	285	PROTEIN M Dpt	374	PROTEIN P Ficolin	463	mRNA E GataE	552	mRNA M UMADelta
19	GENE E FoxN23	108	GENE P Blimp1	197	PROTEIN E Delta	286	PROTEIN M Dri	375	PROTEIN P FoxA	464	mRNA E Gcad	553	mRNA M UMANrl
20	GENE E FoxO	109	GENE P Bra	198	PROTEIN E Delta2	287	PROTEIN M Endo16	376	PROTEIN P FoxB	465	mRNA E Gcm	554	mRNA M UMR
21	GENE E FvMo	110	GENE P Brn	199	PROTEIN E Dpt	288	PROTEIN M Erg	377	PROTEIN P FoxN23	466	mRNA E Gelsolin	555	mRNA M UbiqSoxB1
22	GENE E GataC	111	GENE P CAPK	200	PROTEIN E Dri	289	PROTEIN M Ets1	378	PROTEIN P FoxO	467	mRNA E HesC	556	mRNA M VEGFR
23	GENE E GataE	112	GENE P CyP	201	PROTEIN E ES	290	PROTEIN M Eve	379	PROTEIN P FvMo	468	mRNA E Hex	557	mRNA M Wnt8
24	GENE E Gcad	113	GENE P Delta	202	PROTEIN E Endo16	291	PROTEIN M Ficolin	380	PROTEIN P GSK3 a	469	mRNA E Hnf6	558	mRNA M cB
25	GENE E Gcm	114	GENE P Dpt	203	PROTEIN E Erg	292	PROTEIN M FoxA	381	PROTEIN P GSK3 i	470	mRNA E Hox	559	mRNA M z13
26	GENE E Gelsolin	115	GENE P Dri	204	PROTEIN E Ets1	293	PROTEIN M FoxB	382	PROTEIN P GataC	471	mRNA E Kakapo	560	mRNA P Alx1
27	GENE E HesC	116	GENE P Endo16	205	PROTEIN E Eve	294	PROTEIN M FoxN23	383	PROTEIN P GataE	472	mRNA E Lim	561	mRNA P Apobec
28	GENE E Hex	117	GENE P Erg	206	PROTEIN E Ficolin	295	PROTEIN M FoxO	384	PROTEIN P Gcad	473	mRNA E Msp130	562	mRNA P Blimp1
29	GENE E Hnf6	118	GENE P Ets1	207	PROTEIN E FoxA	296	PROTEIN M FvMo	385	PROTEIN P Gcm	474	mRNA E MspL	563	mRNA P Bra
30	GENE E Hox	119	GENE P Eve	208	PROTEIN E FoxB	297	PROTEIN M GSK3 a	386	PROTEIN P Gelsolin	475	mRNA E Not	564	mRNA P Brn
31	GENE E Kakapo	120	GENE P Ficolin	209	PROTEIN E FoxN23	298	PROTEIN M GSK3 i	387	PROTEIN P Gro	476	mRNA E Notch	565	mRNA P CAPK
32	GENE E Lim	121	GENE P FoxA	210	PROTEIN E FoxO	299	PROTEIN M GataC	388	PROTEIN P GroTCF	477	mRNA E Nrl	566	mRNA P CyP
33	GENE E Msp130	122	GENE P FoxB	211	PROTEIN E FvMo	300	PROTEIN M GataE	389	PROTEIN P GroTFC	478	mRNA E OrCt	567	mRNA P Delta
34	GENE E MspL	123	GENE P FoxN23	212	PROTEIN E GSK3 a	301	PROTEIN M Gcad	390	PROTEIN P HesC	479	mRNA E Otx	568	mRNA P Dpt
35	GENE E Not	124	GENE P FoxO	213	PROTEIN E GSK3 i	302	PROTEIN M Gcm	391	PROTEIN P Hex	480	mRNA E Pks	569	mRNA P Dri
36	GENE E Nrl	125	GENE P FvMo	214	PROTEIN E GataC	303	PROTEIN M Gelsolin	392	PROTEIN P Hnf6	481	mRNA E Pmar1	570	mRNA P Endo16
37	GENE E OrCt	126	GENE P GataC	215	PROTEIN E GataE	304	PROTEIN M Gro	393	PROTEIN P Hox	482	mRNA E Sm27	571	mRNA P Erg
38	GENE E Otx	127	GENE P GataE	216	PROTEIN E Gcad	305	PROTEIN M GroTCF	394	PROTEIN P Kakapo	483	mRNA E Sm30	572	mRNA P Ets1
39	GENE E Pks	128	GENE P Gcad	217	PROTEIN E Gcm	306	PROTEIN M GroTFC	395	PROTEIN P L1	484	mRNA E Sm50	573	mRNA P Eve
40	GENE E Pmar1	129	GENE P Gcm	218	PROTEIN E Gelsolin	307	PROTEIN M HesC	396	PROTEIN P Lim	485	mRNA E Snail	574	mRNA P Ficolin
41	GENE E Sm27	130	GENE P Gelsolin	219	PROTEIN E Gro	308	PROTEIN M Hex	397	PROTEIN P Msp130	486	mRNA E SoxB1	575	mRNA P FoxA
42	GENE E Sm30	131	GENE P HesC	220	PROTEIN E GroTCF	309	PROTEIN M Hnf6	398	PROTEIN P MspL	487	mRNA E SoxC	576	mRNA P FoxB
43	GENE E Sm50	132	GENE P Hex	221	PROTEIN E GroTFC	310	PROTEIN M Hox	399	PROTEIN P Not	488	mRNA E SuH	577	mRNA P FoxN23
44	GENE E Snail	133	GENE P Hnf6	222	PROTEIN E HesC	311	PROTEIN M Kakapo	400	PROTEIN P Notch	489	mRNA E SuTx	578	mRNA P FoxO
45	GENE E SoxB1	134	GENE P Hox	223	PROTEIN E Hex	312	PROTEIN M L1	401	PROTEIN P Notch2	490	mRNA E TBr	579	mRNA P FvMo
46	GENE E SoxC	135	GENE P Kakapo	224	PROTEIN E Hnf6	313	PROTEIN M Lim	402	PROTEIN P Nrl	491	mRNA E Tel	580	mRNA P GataC
47	GENE E SuTx	136	GENE P Lim	225	PROTEIN E Hox	314	PROTEIN M Msp130	403	PROTEIN P OrCt	492	mRNA E Tgif	581	mRNA P GataE
48	GENE E TBr	137	GENE P Msp130	226	PROTEIN E Kakapo	315	PROTEIN M MspL	404	PROTEIN P Otx	493	mRNA E UMR	582	mRNA P Gcad
49	GENE E Tel	138	GENE P MspL	227	PROTEIN E L1	316	PROTEIN M Not	405	PROTEIN P Pks	494	mRNA E UVAOtx	583	mRNA P Gcm
50	GENE E Tgif	139	GENE P Not	228	PROTEIN E Lim	317	PROTEIN M Notch	406	PROTEIN P Pmar1	495	mRNA E UbiqSoxB1	584	mRNA P Gelsolin
51	GENE E VEGFR	140	GENE P Nrl	229	PROTEIN E Msp130	318	PROTEIN M Notch2	407	PROTEIN P Sm27	496	mRNA E VEGF	585	mRNA P HesC
52	GENE E Wnt8	141	GENE P OrCt	230	PROTEIN E MspL	319	PROTEIN M Nrl	408	PROTEIN P Sm30	497	mRNA E VEGFR	586	mRNA P Hex
53	GENE E z13	142	GENE P Otx	231	PROTEIN E Not	320	PROTEIN M OrCt	409	PROTEIN P Sm50	498	mRNA E Wnt8	587	mRNA P Hnf6
54	GENE M Alx1	143	GENE P Pks	232	PROTEIN E Notch	321	PROTEIN M Otx	410	PROTEIN P Snail	499	mRNA E cB	588	mRNA P Hox
55	GENE M Apobec	144	GENE P Pmar1	233	PROTEIN E Notch2	322	PROTEIN M Pks	411	PROTEIN P SoxB1	500	mRNA E z13	589	mRNA P Kakapo
56	GENE M Blimp1	145	GENE P Sm27	234	PROTEIN E Nrl	323	PROTEIN M Pmar1	412	PROTEIN P SoxC	501	mRNA M Alx1	590	mRNA P L1
57	GENE M Bra	146	GENE P Sm30	235	PROTEIN E OrCt	324	PROTEIN M Sm27	413	PROTEIN P SuH	502	mRNA M Apobec	591	mRNA P Lim
58	GENE M Brn	147	GENE P Sm50	236	PROTEIN E Otx	325	PROTEIN M Sm30	414	PROTEIN P SuHN	503	mRNA M Blimp1	592	mRNA P Msp130
59	GENE M CAPK	148	GENE P Snail	237	PROTEIN E Pks	326	PROTEIN M Sm50	415	PROTEIN P SuTx	504	mRNA M Bra	593	mRNA P MspL
60	GENE M CyP	149	GENE P SoxB1	238	PROTEIN E Pmar1	327	PROTEIN M Snail	416	PROTEIN P TBr	505	mRNA M Brn	594	mRNA P Not
61	GENE M Delta	150	GENE P SoxC	239	PROTEIN E Sm27	328	PROTEIN M SoxB1	417	PROTEIN P TCF	506	mRNA M CAPK	595	mRNA P Nrl
62	GENE M Dpt	151	GENE P SuTx	240	PROTEIN E Sm30	329	PROTEIN M SoxC	418	PROTEIN P Tel	507	mRNA M CyP	596	mRNA P OrCt
63	GENE M Dri	152	GENE P TBr	241	PROTEIN E Sm50	330	PROTEIN M SuH	419	PROTEIN P Tgif	508	mRNA M Delta	597	mRNA P Otx
64	GENE M Endo16	153	GENE P Tel	242	PROTEIN E Snail	331	PROTEIN M SuHN	420	PROTEIN P UMADelta	509	mRNA M Dpt	598	mRNA P Pks
65	GENE M Erg	154	GENE P Tgif	243	PROTEIN E SoxB1	332	PROTEIN M SuTx	421	PROTEIN P UMANrl	510	mRNA M Dri	599	mRNA P Pmar1
66	GENE M Ets1	155	GENE P VEGFR	244	PROTEIN E SoxC	333	PROTEIN M TBr	422	PROTEIN P UVAOtx	511	mRNA M Endo16	600	mRNA P Sm27
67	GENE M Eve	156	GENE P Wnt8	245	PROTEIN E SuH	334	PROTEIN M TCF	423	PROTEIN P UbiqAlx1	512	mRNA M Erg	601	mRNA P Sm30
68	GENE M Ficolin	157	GENE P z13	246	PROTEIN E SuHN	335	PROTEIN M Tel	424	PROTEIN P UbiqDelta	513	mRNA M Ets1	602	mRNA P Sm50
69	GENE M FoxA	158	PRE E Gcad	247	PROTEIN E SuTx	336	PROTEIN M Tgif	425	PROTEIN P UbiqES	514	mRNA M Eve	603	mRNA P Snail
70	GENE M FoxB	159	PRE E Notch	248	PROTEIN E TBr	337	PROTEIN M UMADelta	426	PROTEIN P UbiqEts1	515	mRNA M Ficolin	604	mRNA P SoxB1
71	GENE M FoxN23	160	PRE E Otx	249	PROTEIN E TCF	338	PROTEIN M UMANrl	427	PROTEIN P UbiqGcad	516	mRNA M FoxA	605	mRNA P SoxC
72	GENE M FoxO	161	PRE E SoxB1	250	PROTEIN E Tel	339	PROTEIN M UMR	428	PROTEIN P UbiqHesC	517	mRNA M FoxB	606	mRNA P SuTx
73	GENE M FvMo	162	PRE E SuH	251	PROTEIN E Tgif	340	PROTEIN M UVAOtx	429	PROTEIN P UbiqHnf6	518	mRNA M FoxN23	607	mRNA P TBr
74	GENE M GataC	163	PRE E UMR	252	PROTEIN E UMADelta	341	PROTEIN M UbiqAlx1	430	PROTEIN P UbiqSoxB1	519	mRNA M FoxO	608	mRNA P Tel
75	GENE M GataE	164	PRE E UVAOtx	253	PROTEIN E UMANrl	342	PROTEIN M UbiqDelta	431	PROTEIN P UbiqSoxC	520	mRNA M FvMo	609	mRNA P Tgif
76	GENE M Gcad	165	PRE E UbiqSoxB1	254	PROTEIN E UMR	343	PROTEIN M UbiqES	432	PROTEIN P UbiqTel	521	mRNA M GataC	610	mRNA P UbiqAlx1
77	GENE M Gcm	166	PRE E VEGF	255	PROTEIN E UVAOtx	344	PROTEIN M UbiqEts1	433	PROTEIN P VEGFR	522	mRNA M GataE	611	mRNA P UbiqES
78	GENE M Gelsolin	167	PRE E cB	256	PROTEIN E UbiqAlx1	345	PROTEIN M UbiqGcad	434	PROTEIN P VEGFSignal	523	mRNA M Gcad	612	mRNA P UbiqEts1
79	GENE M HesC	168	PRE M Gcad	257	PROTEIN E UbiqDelta	346	PROTEIN M UbiqHesC	435	PROTEIN P Wnt8	524	mRNA M Gcm	613	mRNA P UbiqHesC
80	GENE M Hex	169	PRE M Notch	258	PROTEIN E UbiqES	347	PROTEIN M UbiqHnf6	436	PROTEIN P cB	525	mRNA M Gelsolin	614	mRNA P UbiqHnf6
81	GENE M Hnf6	170	PRE M Otx	259	PROTEIN E UbiqEts1	348	PROTEIN M UbiqSoxB1	437	PROTEIN P frizzled a	526	mRNA M HesC	615	mRNA P UbiqSoxC
82	GENE M Hox	171	PRE M SoxB1	260	PROTEIN E UbiqGcad	349	PROTEIN M UbiqSoxC	438	PROTEIN P frizzled i	527	mRNA M Hex	616	mRNA P UbiqTel
83	GENE M Kakapo	172	PRE M SuH	261	PROTEIN E UbiqHesC	350	PROTEIN M UbiqTel	439	PROTEIN P nBTCF	528	mRNA M Hnf6	617	mRNA P VEGFR
84	GENE M Lim	173	PRE M UMADelta	262	PROTEIN E UbiqHnf6	351	PROTEIN M VEGFR	440	PROTEIN P z13	529	mRNA M Hox	618	mRNA P Wnt8
85	GENE M Msp130	174	PRE M UMANrl	263	PROTEIN E UbiqSoxB1	352	PROTEIN M VEGFSignal	441	mRNA E Alx1	530	mRNA M Kakapo	619	mRNA P cB
86	GENE M MspL	175	PRE M UMR	264	PROTEIN E UbiqSoxC	353	PROTEIN M Wnt8	442	mRNA E Apobec	531	mRNA M Lim	620	mRNA P z13
87	GENE M Not	176	PRE M UbiqSoxB1	265	PROTEIN E UbiqTel	354	PROTEIN M cB	443	mRNA E Blimp1	532	mRNA M Msp130	621	ribosome
88	GENE M Nrl	177	PRE M cB	266	PROTEIN E VEGF	355	PROTEIN M frizzled a	444	mRNA E Bra	533	mRNA M MspL	622	none
89	GENE M OrCt	178	PRE P Ets1	267	PROTEIN E VEGFR	356	PROTEIN M frizzled i	445	mRNA E Brn	534	mRNA M Not		

Table 10: Node names and associated IDs for the endomesoderm network. Table is read from top to bottom and from left to right.

8. REFERENCES

[1] J. Aach et al. Aligning gene expression time series with time warping algorithms. *Bioinformatics*, 17(6):495–508, Jun 2001.

[2] Y. Abdulsattar et al. Rivaroxaban (xarelto) for the prevention of thromboembolic disease: An inside look at the oral direct factor xa inhibitor. *P T*, 34(5):238–244, May 2009.

[3] J. Abella et al. Breakdown of endocytosis in the oncogenic activation of receptor tyrosine kinases. *Am J Physiol Endocrinol Metab*, 296(5):E973–984, 2009.

[4] S. Adams et al. PT-100, a Small Molecule Dipeptidyl Peptidase Inhibitor, Has Potent Antitumor Effects and Augments Antibody-Mediated Cytotoxicity via a Novel Immune Mechanism. *Cancer Research*, 64(15):5471–5480, 2004.

[5] G. Ahmmed et al. Analysis of moricizine block of sodium current in isolated guinea-pig atrial myocytes: Atrioventricular difference of moricizine block. *Vascular Pharmacology*, 38(3):131 – 141, 2002.

[6] G. Aistrup et al. Targeted G-protein inhibition as a novel approach to decrease vagal atrial fibrillation by selective parasympathetic attenuation. *Cardiovascular Research*, 83(3):481–492, 2009.

[7] A. Almotrefi et al. Class i antiarrhythmic drug effects on ouabain binding to guinea pig cardiac na+-k+ atpase. *Canadian Journal of Physiology and Pharmacology*, 77(11):866–870, 1999.

[8] D. Altomare et al. Akt and mtor phosphorylation is frequently detected in ovarian cancer and can be targeted to disrupt ovarian tumor cell growth. *Oncogene*, 23(34):5853–5857, Jul 2004.

[9] W. Ammons et al. A novel alkylating agent, glufosfamide, enhances the activity of gemcitabine in vitro and in vivo. *Neoplasia*, 9(8):625–633, Aug 2007.

[10] L. Angerer et al. Mutual antagonism of soxb1 and canonical wnt signaling in sea urchin embryos. *Signal Transduction*, 7:174–180, 2007.

[11] J. Ansell et al. Pharmacology and Management of the Vitamin K Antagonists*. *Chest*, 133(6 suppl):160S–198S, 2008.

[12] M. Aslam et al. cAMP/PKA antagonizes thrombin-induced inactivation of endothelial myosin light chain phosphatase: role of CPI-17. *Cardiovascular Research*, 87(2):375–384, 2010.

[13] A. Asthagiri et al. A computational study of feedback effects on signal dynamics in a mitogen-activated protein kinase (MAPK) pathway model. *Biotechnol Prog*, 17(2):227–239, 2001.

[14] D. Atlas et al. Stereospecific binding of propranolol and catecholamines to the beta-adrenergic receptor. *Proc Natl Acad Sci U S A*, 71(10):4246–4248, Oct 1974.

[15] J. Avruch et al. Ras activation of the Raf kinase: Tyrosine kinase recruitment of the MAP kinase cascade. *Recent Prog Horm Res*, 56(1):127–156, 2001.

[16] J. Azuma et al. Mechanism of direct cardiostimulating actions of hydralazine. *Eur J Pharmacol*, 135(2):137–144, Mar 1987.

[17] C. Bailly et al. Altered Cleavage of DNA Sequences by Bleomycin and Its Deglycosylated Derivative in the Presence of Actinomycin. *Nucleic Acids Research*, 25(8):1516–1522, 1997.

[18] J. Baker et al. Agonist Actions of "β-Blockers" Provide Evidence for Two Agonist Activation Sites or Conformations of the Human β1-Adrenoceptor. *Molecular Pharmacology*, 63(6):1312–1321, 2003.

[19] M. Bali et al. Defining the Propofol Binding Site Location on the GABAA Receptor. *Molecular Pharmacology*, 65(1):68–76, 2004.

[20] N. Bander et al. Phase I Trial of 177Lutetium-Labeled J591, a Monoclonal Antibody to Prostate-Specific Membrane Antigen, in Patients With Androgen-Independent Prostate Cancer. *Journal of Clinical Oncology*, 23(21):4591–4601, 2005.

[21] J. Bangham. Therapeutics: Cetuximab constricts conformational contortionist. *Nature Reviews Cancer*, 5:421, June 2005.

[22] N. Banner et al. Clinical immunosuppression using the calcineurin-inhibitors ciclosporin and tacrolimus. In L. A. Pinna and P. T. Cohen, editors, *Inhibitors of Protein Kinases and Protein Phosphates*, volume 167 of *Handbook of Experimental Pharmacology*, pages 321–359. Springer Berlin Heidelberg, 2005.

[23] A. Barreras et al. Angiotensin ii receptor blockers. *BUMC Proceedings*, 16:123–126, 2003.

[24] A. Basu et al. Identification of a novel bcl-xl phosphorylation site regulating the sensitivity of taxol- or 2-methoxyestradiol-induced apoptosis. *FEBS Letters*, 538(1-3):41 – 47, 2003.

[25] J. Beebe and Others. Pharmacological Characterization of CP-547,632, a Novel Vascular Endothelial Growth Factor Receptor-2 Tyrosine Kinase Inhibitor for Cancer Therapy. *Cancer Research*, 63(21):7301–7309, 2003.

[26] A. Bender et al. Chemogenomic data analysis: prediction of small-molecule targets and the advent of biological fingerprint. *Comb Chem High Throughput Screen*, 10(8):719–731, Sep 2007.

[27] M. Benekli et al. Muromonab-cd3 (orthoclone okt3), methylprednisolone and cyclosporine for acute graft-versus-host disease prophylaxis in allogeneic bone marrow transplantation. *Bone Marrow Transplantation*, 38:365–370, 2006.

[28] P. Bennett et al. On the molecular nature of the lidocaine receptor of cardiac na+ channels : Modification of block by alterations in the alpha-subunit iii-iv interdomain. *Circ Res*, 77(3):584–592, 1995.

[29] N. Bhana et al. Indobufen: an updated review of its use in the management of atherothrombosis. *Drugs Aging*, 18(5):369–388, 2001.

[30] A. Bharucha et al. Effects of a serotonin 5-HT4 receptor antagonist SB-207266 on gastrointestinal motor and sensory function in humans. *Gut*, 47(5):667–674, 2000.

[31] A. Billiau et al. Modes of action of Freund's adjuvants in experimental models of autoimmune diseases. *Journal of Leukocyte Biology*, 70(6):849–860, 2001.

[32] N. Blijlevens et al. Palifermin (recombinant keratinocyte growth factor-1): a pleiotropic growth factor with multiple biological activities in preventing chemotherapy- and radiotherapy-induced mucositis. *Annals of Oncology*, 18(5):817–826, 2007.

[33] P. Bongioanni et al. T-cell interferon gamma receptor binding in interferon beta-1b-treated patients with multiple sclerosis. *Arch Neurol*, 56(2):217–222, 1999.

[34] J.-P. Bossavy et al. Antithrombotic efficacy of the vitamin k antagonist fluindione in a human ex vivo model of arterial thrombosis : Effect of anticoagulation level and combination therapy with aspirin. *Arterioscler Thromb Vasc Biol*, 19(9):2269–2275, 1999.

[35] F. Boudinot et al. Receptor-mediated pharmacodynamics of prednisolone in the rat. *J Pharmacokinet Biopharm*, 14(5):469–493, Oct 1986.

[36] P. Brady et al. Operative conditionŰdependent response of cardiac atp-sensitive k+ channels toward sulfonylureas. *Circ Res*, 82(2):272–278, 1998.

[37] U. Brandes. A faster algorithm for betweenness centrality. *Journal of Mathematical Sociology*, 25:163–177, 2001.

[38] J. Bridgeman et al. The Optimal Antigen Response of Chimeric Antigen Receptors Harboring the CD3-zeta Transmembrane Domain Is Dependent upon Incorporation of the Receptor into the Endogenous TCR/CD3 Complex. *The Journal of Immunology*, 2010.

[39] D. Brown. Unfinished business: target-based drug discovery. *Drug Discovery Today*, 12(23-24):1007 – 1012, 2007.

[40] A. Bullen. Microscopic imaging techniques for drug discovery. *Nat Rev Drug Discov*, 7(1):54–67, Jan 2008.

[41] C. Byrum et al. Blocking dishevelled signaling in the noncanonical wnt pathway in sea urchins disrupts endoderm formation and spiculogenesis, but not secondary mesoderm formation. *Developmental Dynamics*, 238(7):1649–1665, 2009.

[42] P. Campbell et al. Tln-4601 suppresses growth and induces apoptosis of pancreatic carcinoma cells through inhibition of ras-erk mapk signaling. *Journal of Molecular Signaling*, 5(1):18, 2010.

[43] S. Cardin et al. Contrasting Gene Expression Profiles in Two Canine Models of Atrial Fibrillation. *Circ Res*, 100(3):425–433, 2007.

[44] L. Carlsson et al. Assessment of the ion channel-blocking profile of the novel combined ion channel blocker azd1305 and its proarrhythmic potential versus dofetilide in the methoxamine-sensitized rabbit in vivo. *J Cardiovasc Pharmacol*, 54(1):82–89, Jul 2009.

[45] M. Chabert et al. Microfluidic high-throughput encapsulation and hydrodynamic self-sorting of single cells. *Proceedings of the National Academy of Sciences*, 105(9):3191–3196, 2008.

[46] D. Chan et al. Loss of mkp3 mediated by oxidative stress enhances tumorigenicity and chemoresistance of ovarian

cancer cells. *Carcinogenesis*, 29(9):1742–1750, Sep 2008.

[47] K. Y. Chan et al. Functional characterisation and drug target validation of a mitotic kinesin-13 in <italic>trypanosoma brucei</italic>. *PLoS Pathog*, 6(8):e1001050, 08 2010.

[48] N. Chandrasekharan et al. COX-3, a cyclooxygenase-1 variant inhibited by acetaminophen and other analgesic/antipyretic drugs: Cloning, structure, and expression. *Proceedings of the National Academy of Sciences of the United States of America*, 99(21):13926–13931, 2002.

[49] L. Chen et al. Stack-based algorithms for pattern matching on DAGs. In *VLDB '05: Proceedings of the 31st international conference on Very large data bases*, pages 493–504. VLDB Endowment, 2005.

[50] D. Cheng et al. Bacillus calmette-guérin interacts with the carboxyl-terminal heparin binding domain of fibronectin: implications for bcg-mediated antitumor activity. *J Urol*, 152(4):1275–1280, Oct 1994.

[51] K. Chi et al. Custirsen (ogx-011): a second-generation antisense inhibitor of clusterin for the treatment of cancer. *Expert Opinion on Investigational Drugs*, 17(12):1955–1962, 2008.

[52] K. Chianese-Bullock et al. MAGE-A1-, MAGE-A10-, and gp100-Derived Peptides Are Immunogenic When Combined with Granulocyte-Macrophage Colony-Stimulating Factor and Montanide ISA-51 Adjuvant and Administered as Part of a Multipeptide Vaccine for Melanoma. *The Journal of Immunology*, 174(5):3080–3086, 2005.

[53] Y.-W. Chin et al. Structural characterization, biological effects, and synthetic studies on xanthones from mangosteen (garcinia mangostana), a popular botanical dietary supplement. *Mini-Reviews in Organic Chemistry*, 5:355–364(10), November 2008.

[54] A. Choppin et al. Effect of tecarfarin, a novel vitamin k epoxide reductase inhibitor, on coagulation in beagle dogs. *Br J Pharmacol*, 158(6):1536–1547, Nov 2009.

[55] G. Chu. Cellular responses to cisplatin. The roles of DNA-binding proteins and DNA repair. *Journal of Biological Chemistry*, 269(2):787–790, 1994.

[56] C. Cifelli et al. Regulator of G-protein signalling 4 (RGS4) KO mice show increased susceptibility to atrial fibrillation. *FASEB J.*, 24(1 MeetingAbstracts):855.1–, 2010.

[57] F. Ciruela et al. Adenosine deaminase affects ligand-induced signalling by interacting with cell surface adenosine receptors. *FEBS Letters*, 380(3):219 – 223, 1996.

[58] P. Cohen. Protein kinases–the major drug targets of the twenty-first century? *Nat Rev Drug Discov*, 1(4):309–315, Apr 2002.

[59] L. Cole. New discoveries on the biology and detection of human chorionic gonadotropin. *Reprod Biol Endocrinol*, 7:8, 2009.

[60] J. Cooper et al. A phase i study examining weekly dosing and pharmacokinetics (pk) of a novel spectrum selective kinase inhibitor, xl999, in patients (pts) with advanced solid malignancies (asm). *Journal of Clinical Oncology*, 24(18S), 2006.

[61] C. Cunningham et al. A phase i trial of c-raf kinase antisense oligonucleotide isis 5132 administered as a continuous intravenous infusion in patients with advanced cancer. *Clin Cancer Res*, 6(5):1626–1631, May 2000.

[62] E. Davidson et al. A Genomic Regulatory Network for Development. *Science*, 295(5560):1669–1678, 2002.

[63] B. Davies et al. AZD6244 (ARRY-142886), a potent inhibitor of mitogen-activated protein kinase/extracellular signal-regulated kinase kinase 1/2 kinases: mechanism of action in vivo, pharmacokinetic/pharmacodynamic relationship, and potential for combination in preclinical models. *Molecular Cancer Therapeutics*, 6(8):2209–2219, 2007.

[64] C. de Kogel et al. Imatinib. *Oncologist*, 12(12):1390–1394, 2007.

[65] A. Di Cristofano et al. The multiple roles of pten in tumor suppression. *Cell*, 100(4):387 – 390, 2000.

[66] I. Diaz-Padilla et al. Cyclin-dependent kinase inhibitors as potential targeted anticancer agents. *Investigational New Drugs*, 27:586–594, 2009.

[67] D. Dobrev. Atrial ca2+ signaling in atrial fibrillation as an antiarrhythmic drug target. *Naunyn-Schmiedeberg's Archives of Pharmacology*, 381:195–206, 2010. 10.1007/s00210-009-0457-1.

[68] M. Drake et al. Bisphosphonates: Mechanism of Action and Role in Clinical Practice. *Mayo Clinic Proceedings*, 83(9):1032–1045, 2008.

[69] K. Duggan et al. Renoprotective differences between perindopril and enalapril in the diabetic hypertensive rat do not reflect glomerular angiotensin-converting enzyme activity. *Clinical Science*, 94:511–516, 1998.

[70] I. Dukes et al. Tedisamil inactivates transient outward K+ current in rat ventricular myocytes. *American Journal of Physiology - Heart and Circulatory Physiology*, 257(5):H1746–H1749, 1989.

[71] W. Dun et al. Diverse phenotypes of outward currents in cells that have survived in the 5-day-infarcted heart. *American Journal of Physiology - Heart and Circulatory Physiology*, 289(2):H667–H673, 2005.

[72] J. Engelfiet et al. A comparison of boundary graph grammars and context-free hypergraph grammars. *Information and Computation*, 84(2):163 – 206, 1990.

[73] A. Euser et al. Magnesium sulfate for the treatment of eclampsia: A brief review. *Stroke*, 40(4):1169–1175, 2009.

[74] M. Fabiani et al. Comparative in vivo effects of irbesartan and losartan on angiotensin ii receptor binding in the rat kidney following oral administration. *Clin. Sci.*, 99(4):331–341, 2000.

[75] D. Fedida et al. The mechanism of atrial antiarrhythmic action of rsd1235. *J Cardiovasc Electrophysiol*, 16(11):1227–1238, Nov 2005.

[76] D. Ferro et al. Inhibition of tissue-factor-mediated thrombin generation by simvastatin. *Atherosclerosis*, 149(1):111–116, Mar 2000.

[77] A. Fleckenstein et al. Mechanism of action of calcium antagonists in heart and vascular smooth muscle. *European Heart Journal*, 9(suppl H):95–99, 1988.

[78] E. Fox et al. Tariquidar (xr9576): a p-glycoprotein drug efflux pump inhibitor. *Expert Review of Anticancer Therapy*, 7(4):447–459, 2007.

[79] B. Freestone et al. The renin-angiotensin-aldosterone system in atrial fibrillation: a new therapeutic target? *J Hum Hypertens*, 18(7):461–465, Jul 2004.

[80] W. Frishman. Beta-adrenergic blockers. *Circulation*, 107(18):e117–119, 2003.

[81] H. Furusho et al. Rho-kinase inhibitor fasudil prevents atrial electrical remodeling in atrial fibrillation. *Circ J*, 68:362, 2004.

[82] M. Garcia-Calvo et al. The target of ezetimibe is niemann-pick c1-like 1 (npc1l1). *Proc Natl Acad Sci U S A*, 102(23):8132–8137, Jun 2005.

[83] P. Gautier et al. In vivo and in vitro characterization of the novel antiarrhythmic agent ssr149744c: electrophysiological, anti-adrenergic, and anti-angiotensin ii effects. *J Cardiovasc Pharmacol*, 44(2):244–257, Aug 2004.

[84] M. S. Gordon et al. Clinical Activity of Pertuzumab (rhuMAb 2C4), a HER Dimerization Inhibitor, in Advanced Ovarian Cancer: Potential Predictive Relationship With Tumor HER2 Activation Status. *J Clin Oncol*, 24(26):4324–4332, 2006.

[85] M. Goren et al. Reduction of Dimesna to Mesna by the Isolated Perfused Rat Liver. *Cancer Research*, 58(19):4358–4362, 1998.

[86] C. Goulding et al. Sdz psc 833 the drug resistance modulator activates cellular ceramide formation by a pathway independent of p-glycoprotein. *Cancer Lett*, 149(1-2):143–151, Feb 2000.

[87] S. Gunn et al. In vitro modeling of the clinical interactions between octreotide and 111in-pentetreotide: Is there evidence of somatostatin receptor downregulation? *J Nucl Med*, 47(2):354–359, 2006.

[88] I. Guyon et al. An introduction to variable and feature selection. *J. Mach. Learn. Res.*, 3:1157–1182, 2003.

[89] P. Hanley et al. Halothane, isoflurane and sevoflurane inhibit NADH: ubiquinone oxidoreductase (complex I) of cardiac mitochondria. *The Journal of Physiology*, 544(3):687–693, 2002.

[90] R. Hannon et al. Effects of the src kinase inhibitor saracatinib (azd0530) on bone turnover in healthy men: a randomized, double-blind, placebo-controlled, multiple-ascending-dose phase i trial. *J Bone Miner Res*, 25(3):463–471, Mar 2010.

[91] D. Hao et al. A Phase I and Pharmacokinetic Study of Squalamine, an Aminosterol Angiogenesis Inhibitor. *Clinical Cancer Research*, 9(7):2465–2471, 2003.

[92] S. Hashemy et al. Motexafin gadolinium, a tumor-selective drug targeting thioredoxin reductase and ribonucleotide reductase. *J Biol Chem*, 281(16):10691–10697, Apr 2006.

[93] M. Hatakeyama et al. A computational model on the modulation of mitogen-activated protein kinase (MAPK) and Akt pathways in heregulin-induced ErbB signalling. *Biochem J*, 373(Pt 2):451–463, Jul 2003.

[94] R. Hawtin et al. Voreloxin is an anticancer quinolone derivative that intercalates dna and poisons topoisomerase ii. *PLoS ONE*, 5(4):e10186, 04 2010.

[95] J. He et al. Antiphosphatidylserine antibody combined with irradiation damages tumor blood vessels and induces tumor immunity in a rat model of glioblastoma. *Clin Cancer Res*, 15(22):6871–6880, Nov 2009.

[96] X. He et al. Why do hubs tend to be essential in protein networks? *PLoS Genetics*, 2(6):e88, 06 2006.

[97] M. Hellerstein. A critique of the molecular target-based drug discovery paradigm based on principles of metabolic control: Advantages of pathway-based discovery. *Metabolic Engineering*, 10(1):1 – 9, 2008.

[98] B. Hennessy et al. Ovarian cancer: homeobox genes, autocrine/paracrine growth, and kinase signaling. *Int J Biochem Cell Biol*, 38(9):1450–1456, 2006.

[99] J. Hepler et al. RGS4 and GAIP are GTPase-activating proteins for GqÎś and block activation of phospholipase CÎš byâĂLÎş-thio-GTP-GqÎś. *Proceedings of the National Academy of Sciences of the United States of America*, 94(2):428–432, 1997.

[100] T. Hideshima et al. Perifosine, an oral bioactive novel alkylphospholipid, inhibits akt and induces in vitro and in vivo cytotoxicity in human multiple myeloma cells. *Blood*, 107(10):4053–4062, May 2006.

[101] F. Hilberg et al. BIBF 1120: Triple Angiokinase Inhibitor with Sustained Receptor Blockade and Good Antitumor Efficacy. *Cancer Research*, 68(12):4774–4782, 2008.

[102] V. Hinman et al. Evolutionary plasticity of developmental gene regulatory network architecture. *Proceedings of the National Academy of Sciences*, 104(49):19404–19409, 2007.

[103] M. Hirose et al. Diacylglycerol kinase ζ inhibits $g\alpha q$-induced atrial remodeling in transgenic mice. *Heart Rhythm*, 6(1):78 – 84, 2009.

[104] J. Hirsh et al. Heparin: Mechanism of Action, Pharmacokinetics, Dosing Considerations, Monitoring, Efficacy, and Safety. *Chest*, 108(4 Supplement):258S–275S, 1995.

[105] J. Hirsh et al. Oral Anticoagulants: Mechanism of Action, Clinical Effectiveness, and Optimal Therapeutic Range. *Chest*, 119(1 suppl):8S–21S, 2001.

[106] L. Hood et al. Systems biology and new technologies enable predictive and preventative medicine. *Science*, 306(5696):640–643, Oct 2004.

[107] A. Hopkins. Network pharmacology: the next paradigm in drug discovery. *Nat Chem Biol*, 4(11):682–690, Nov 2008.

[108] D. Hu et al. Time-dependent sensitivity analysis of biological networks: Coupled MAPK and PI3K signal transduction pathways. *The Journal of Physical Chemistry A*, 110(16):5361–5370, 2006.

[109] X. Hu et al. Molecular mechanisms of mineralocorticoid receptor antagonism by eplerenone. *Mini Rev Med Chem*, 5(8):709–718, Aug 2005.

[110] J. Hurst, N. Prinz, M. Lorenz, S. Bauer, J. Chapman, K. J. Lackner, and P. von Landenberg. Tlr7 and tlr8 ligands and antiphospholipid antibodies show synergistic effects on the induction of il-1[beta] and caspase-1 in monocytes and dendritic cells. *Immunobiology*, 214(8):683 – 691, 2009.

[111] W.-C. Hwang et al. Identification of information flow-modulating drug targets: a novel bridging paradigm for drug discovery. *Clin Pharmacol Ther*, 84(5):563–572, Nov 2008.

[112] Y. Ishikawa et al. Cardiac Myosin Light Chain Kinase: A New Player in the Regulation of Myosin Light Chain in the Heart. *Circ Res*, 102(5):516–518, 2008.

[113] Z. Israili. Clinical pharmacokinetics of angiotensin ii (at1) receptor blockers in hypertension. *J Hum Hypertens*, 14 Suppl 1:S73–S86, Apr 2000.

[114] P. Jahn et al. Beta 1-adrenoceptor subtype selective antagonism of esmolol and its major metabolite in vitro and in man. investigations using tricresylphosphate as red blood cell carboxylesterase inhibitor. *Arzneimittelforschung*, 45(5):536–541, May 1995.

[115] S. Kageyama et al. Humoral immune responses in patients vaccinated with 1-146 her2 protein complexed with cholesteryl pullulan nanogel. *Cancer Sci*, 99(3):601–607, Mar 2008.

[116] C. Kahn et al. Unraveling the mechanism of action of thiazolidinediones. *The Journal of Clinical Investigation*, 106(11):1305–1307, 12 2000.

[117] N. Kaneko et al. Pharmacological characteristics and clinical applications of k201. *Current Clinical Pharmacology*, 4:126–131(6), May 2009.

[118] T. Karlberg et al. Crystal structure of the catalytic domain of human parp2 in complex with parp inhibitor abt-888. *Biochemistry*, 49(6):1056–1058, 2010.

[119] A. Katz et al. Selectivity of Digitalis Glycosides for Isoforms of Human Na,K-ATPase. *Journal of Biological Chemistry*, 285(25):19582–19592, 2010.

[120] T. Kažić et al. [potassium channels and the development of new drugs]. *Med Pregl*, 51(11-12):481–488, 1998.

[121] E. Keogh et al. Derivative dynamic time warping. In *In First SIAM International Conference on Data Mining (SDMŠ2001*, 2001.

[122] M. Kiaei et al. Thalidomide and lenalidomide extend survival in a transgenic mouse model of amyotrophic lateral sclerosis. *J. Neurosci.*, 26(9):2467–2473, 2006.

[123] C. Kiesecker et al. Class ia anti-arrhythmic drug ajmaline blocks herg potassium channels: mode of action. *Naunyn-Schmiedeberg's Archives of Pharmacology*, 370:423–435, 2004.

[124] W. Kiesman et al. A1 adenosine receptor antagonists, agonists, and allosteric enhancers. In C. N. Wilson and S. J. Mustafa, editors, *Adenosine Receptors in Health and Disease*, volume 193 of *Handbook of Experimental Pharmacology*, pages 25–58. Springer Berlin Heidelberg, 2009.

[125] Y. Kim et al. Substrate-dependent control of mapk phosphorylation in vivo. *Mol Syst Biol*, 7:467, Feb 2011.

[126] M. Kindermann et al. Carvedilol but not metoprolol reduces beta-adrenergic responsiveness after complete elimination from plasma in vivo. *Circulation*, 109(25):3182–3190, 2004.

[127] T. Kitazawa et al. Reconstitution of protein kinase C-induced contractile Ca2+ sensitization in Triton X-100-demembranated rabbit arterial smooth muscle. *The Journal of Physiology*, 520(1):139–152, 1999.

[128] S. Klamt et al. Hypergraphs and cellular networks. *PLoS Comput Biol*, 5(5):e1000385, May 2009.

[129] T. Knudsen et al. Effects of (r)-deoxycoformycin (pentostatin) on intrauterine nucleoside catabolism and embryo viability in the pregnant mouse. *Teratology*, 45(1):91–103, Jan 1992.

[130] H. Koch et al. Evidence for the intercalation of thalidomide into dna: clue to the molecular mechanism of thalidomide teratogenicity? *Z Naturforsch C*, 41(11-12):1057–1061, 1986.

[131] R. Kohli et al. Efficacy of once daily bisoprolol in stable angina pectoris: an objective comparison with atenolol and long term follow-up. *European Heart Journal*, 6(10):845–850, 1985.

[132] M. Köller et al. Influence of low molecular weight heparin (certoparin) and unfractionated heparin on the release of cytokines from human leukocytes. *Inflammation*, 25:331–337, 2001.

[133] S. Kondapaka et al. Perifosine, a novel alkylphospholipid, inhibits protein kinase b activation. *Mol Cancer Ther*, 2(11):1093–1103, Nov 2003.

[134] J. Kortmansky et al. Bryostatin-1: a novel pkc inhibitor in clinical development. *Cancer Invest*, 21(6):924–936, 2003.

[135] S. Koumi et al. Disopyramide block of cardiac sodium current after removal of the fast inactivation process in guinea pig ventricular myocytes. *Journal of Pharmacology and Experimental Therapeutics*, 261(3):1167–1174, 1992.

[136] C. Kreutz et al. An error model for protein quantification. *Bioinformatics*, 23(20):2747–2753, Oct 2007.

[137] T. Kuang et al. Combination of sildenafil and simvastatin ameliorates monocrotaline-induced pulmonary hypertension in rats. *Pulmonary Pharmacology & Therapeutics*, 23(5):456 – 464, 2010.

[138] C. Kuhn et al. Monte carlo analysis of an ode model of the sea urchin endomesoderm network. *BMC Systems Biology*, 3(1):83, 2009.

[139] R. Kumar et al. Pharmacokinetic-pharmacodynamic correlation from mouse to human with pazopanib, a multikinase angiogenesis inhibitor with potent antitumor and antiangiogenic activity. *Molecular Cancer Therapeutics*, 6(7):2012–2021, 2007.

[140] Y.-K. Kwon et al. Coherent coupling of feedback loops: a design principle of cell signaling networks. *Bioinformatics*, 24(17):1926–1932, Sep 2008.

[141] L. Lad et al. Mechanism of inhibition of human ksp by ispinesib. *Biochemistry*, 47(11):3576–3585, 2008.

[142] S. Lapenna et al. Cell cycle kinases as therapeutic targets for cancer. *Nature Reviews Drug Discovery*, 8:547–566, July 2009.

[143] X.-F. Le et al. Anti-HER2 Antibody and Heregulin Suppress Growth of HER2-Overexpressing Human Breast Cancer Cells through Different Mechanisms. *Clinical Cancer Research*, 6(1):260–270, 2000.

[144] N. Le Novère et al. Biomodels database: a free, centralized database of curated, published, quantitative kinetic models of biochemical and cellular systems. *Nucleic Acids Res*, 34(Database issue):D689–D691, Jan 2006.

[145] B. Lee et al. Procainamide Is a Specific Inhibitor of DNA Methyltransferase 1. *Journal of Biological Chemistry*, 280(49):40749–40756, 2005.

[146] K. Lee et al. Mechanism of calcium channel blockade by verapamil, d600, diltiazem and nitrendipine in single dialysed heart cells. *Nature*, 302(5911):790–794, Apr 1983.

[147] J. Lees-Miller et al. Molecular Determinant of High-Affinity Dofetilide Binding toHERG1 Expressed in Xenopus Oocytes: Involvement of S6 Sites. *Molecular Pharmacology*, 57(2):367–374, 2000.

[148] L. Leoni et al. Bendamustine (Treanda) Displays a Distinct Pattern of Cytotoxicity and Unique Mechanistic Features Compared with Other Alkylating Agents. *Clinical Cancer Research*, 14(1):309–317, 2008.

[149] J. Levy et al. *Cardiac surgical pharmacology*. New York: McGraw-Hill, 2008.

[150] D. Liebler et al. Elucidating mechanisms of drug-induced toxicity. *Nat Rev Drug Discov*, 4(5):410–420, May 2005.

[151] P.-F. Lin et al. A small molecule HIV-1 inhibitor that targets the HIV-1 envelope and inhibits CD4 receptor binding. *Proceedings of the National Academy of Sciences of the United States of America*, 100(19):11013–11018, 2003.

[152] P.-H. Lin et al. Antithrombin binding of low molecular weight heparins and inhibition of factor xa. *Biochimica et Biophysica Acta (BBA) - General Subjects*, 1526(1):105 – 113, 2001.

[153] J. Liu et al. Calcineurin is a common target of cyclophilin-cyclosporin a and fkbp-fk506 complexes. *Cell*, 66(4):807–815, Aug 1991.

[154] M. Los et al. *Apoptotic pathways as targets for novel therapies in cancer and other diseases*. Springer, 2005.

[155] J. Low et al. Phenotypic fingerprinting of small molecule cell cycle kinase inhibitors for drug discovery. *Curr Chem Genomics*, 3:13–21, 2009.

[156] Q. Lu et al. Signaling through rho gtpase pathway as viable drug target. *Current Medicinal Chemistry*, 16:1355–1365(11), April 2009.

[157] J. Luo et al. Targeting the PI3K-Akt pathway in human cancer: Rationale and promise. *Cancer Cell*, 4(4):257 – 262, 2003.

[158] J. Maatta et al. Proteolytic Cleavage and Phosphorylation of a Tumor-associated ErbB4 Isoform Promote Ligand-independent Survival and Cancer Cell Growth. *Mol. Biol. Cell*, 17(1):67–79, 2006.

[159] H. Mackay et al. Targeting the protein kinase c family: are we there yet? *Nat Rev Cancer*, 7(7):554–562, Jul 2007.

[160] A. Maeda et al. Ca2+-independent phospholipase a2-dependent sustained rho-kinase activation exhibits all-or-none response. *Genes to Cells*, 11:1071–1083, 2006.

[161] N. Mamoulis et al. Efficient top-k aggregation of ranked inputs. *ACM Trans. Database Syst.*, 32(3):19, 2007.

[162] M. Manoach et al. Sotalol: the mechanism of its antiarrhythmic-defibrillating effect. *Cardiovasc Drug Rev*, 19(2):172–182, 2001.

[163] E. Mantzourani et al. Peptides as therapeutic agents or drug leads for autoimmune, hormone dependent and cardiovascular diseases. *Anti-Inflammatory & Anti-Allergy Agents in Medicinal Chemistry (Formerly Cu rrent Medicinal Chemistry - Anti-Inflammatory and Anti-Allergy Agents)*, 7:294–306(13), December 2008.

[164] A. Markham et al. Valsartan. a review of its pharmacology and therapeutic use in essential hypertension. *Drugs*, 54(2):299–311, Aug 1997.

[165] S. Marusic et al. Therapeutic efficacy of acenocoumarol in a warfarin-resistant patient with deep venous thrombosis: a case report. *European Journal of Clinical Pharmacology*, 65:1265–1266, 2009.

[166] A. Matavel et al. Pkc activation and pip2 depletion underlie biphasic regulation of iks by gq-coupled receptors. *Journal of Molecular and Cellular Cardiology*, 46(5):704 – 712, 2009.

[167] C. Mathias et al. Indium-111-dtpa-folate as a potential folate receptor-targeted radiopharmaceutical. *J Nucl Med*, 39(9):1579–1585, 1998.

[168] C. Mattsson et al. Mechanism of action of the oral direct thrombin inhibitor ximelagatran. *Seminars in Vascular Medicine*, 5(3):235–244, 2005.

[169] J. McConnell et al. Targeting protein serine/threonine phosphatases for drug development. *Molecular Pharmacology*, 75(6):1249–1261, 2009.

[170] F. McPhillips et al. Association of c-raf expression with survival and its targeting with antisense oligonucleotides in ovarian cancer. *Br J Cancer*, 85(11):1753–1758, Nov 2001.

[171] R. Mehvar et al. Stereospecific pharmacokinetics and pharmacodynamics of beta-adrenergic blockers in humans. *J Pharm Pharmaceut Sci*, 4(2):185–200, 2001.

[172] S. Meisel et al. Clinical pharmacokinetics of ramipril. *Clin Pharmacokinet*, 26(1):7–15, Jan 1994.

[173] J. Mironneau et al. Interactions of spironolactone with (+)-[3h]-isradipine and (-)-[3h]-desmethoxyverapamil binding sites in vascular smooth muscle. *Br J Pharmacol*, 101(1):6–7, Sep 1990.

[174] E. Mohler et al. *Advanced therapy in hypertension and vascular disease*. PMPH Inc., April 2006.

[175] D. Morré et al. Ecto-nox target for the anticancer isoflavene phenoxodiol. *Oncol Res*, 16(7):299–312, 2007.

[176] D. Morrone et al. Role of raas inhibition in preventing left ventricular remodeling in patients post myocardial infarction. *Heart and Metabolism*, (47):9–13, 2010.

[177] K. Murthy et al. Differential signalling by muscarinic receptors in smooth muscle: m2-mediated inactivation of myosin light chain kinase via gi3, cdc42/rac1 and p21-activated kinase 1 pathway, and m3-mediated mlc20 (20 kda regulatory light chain of myosin ii) phosphorylation via rho-associated kinase/myosin phosphatase targeting subunit 1 and protein kinase c/cpi-17 pathway. *Biochem. J.*, 374(1):145–155, 2003.

[178] S. Mustafa et al. Adenosine receptors and the heart: Role in regulation of coronary blood flow and cardiac electrophysiology. In C. N. Wilson and S. J. Mustafa, editors, *Adenosine Receptors in Health and Disease*, volume 193 of *Handbook of Experimental Pharmacology*, pages 161–188. Springer Berlin Heidelberg, 2009.

[179] J. Nagasawa et al. Novel her2 selective tyrosine kinase inhibitor, tak-165, inhibits bladder, kidney and androgen-independent prostate cancer in vitro and in vivo. *International Journal of Urology*, 13(5):587 – 592, 2006.

[180] NCI. Nci drug dictionary. http://www.cancer.gov/drugdictionary/, August 2010.

[181] NCI. Nci thesaurus. http://ncit.nci.nih.gov/, 2011.

[182] P. Nell et al. 4 the adenosine a1 receptor and its ligands. volume 47 of *Progress in Medicinal Chemistry*, pages 163 – 201. Elsevier, 2009.

[183] S. Neschen et al. n-3 Fatty Acids Preserve Insulin Sensitivity In Vivo in a Peroxisome ProliferatorŮActivated Receptor-aŮDependent Manner. *Diabetes*, 56(4):1034–1041, April 2007.

[184] NIH. Clinicaltrials.gov, 2009. Accessed 2 Feb 2010.

[185] D. Nikitovic et al. Plasma levels of nitrites/nitrates in patients with chronic atrial fibrillation are increased after electrical restoration of sinus rhythm. *Journal of Interventional Cardiac Electrophysiology*, 7:171–176, 2002. 10.1023/A:1020841906241.

[186] L. Niu et al. High-affinity binding to the gm-csf receptor requires intact n-glycosylation sites in the extracellular domain of the beta subunit. *Blood*, 95(11):3357–3362, 2000.

[187] P. Nokin et al. Amiodarone is a potent calmodulin antagonist. *Naunyn-Schmiedeberg's Archives of Pharmacology*, 339:367–373, 1989. 10.1007/BF00736049.

[188] D. Norwood et al. Olmesartan medoxomil for hypertension: A clinical review. *Drug Forecast*, 27(12):611–618, December 2002.

[189] P. Oliveri et al. Activation of pmar1 controls specification of micromeres in the sea urchin embryo. *Developmental Biology*, 258(1):32 – 43, 2003.

[190] K. Olkkola et al. Midazolam and other benzodiazepines. In J. Schüttler and H. Schwilden, editors, *Modern Anesthetics*, volume 182 of *Handbook of Experimental Pharmacology*,

pages 335–360. Springer Berlin Heidelberg, 2008.

[191] S. Orosz et al. Pharmacokinetics of amoxicillin plus clavulanic acid in blue-fronted amazon parrots (amazona aestiva aestiva). *Journal of Avian Medicine and Surgery*, 14(2):107–112, June 2000.

[192] H. Pang et al. RhoA-Rho kinase pathway mediates thrombin- and U-46619-induced phosphorylation of a myosin phosphatase inhibitor, CPI-17, in vascular smooth muscle cells. *Am J Physiol Cell Physiol*, 289(2):C352–360, 2005.

[193] D. Pant et al. Automated oncogene detection in complex protein networks with applications to the mapk signal transduction pathway. *Biophysical Chemistry*, 113(3):275 – 288, 2005.

[194] M. Pásek et al. Quantitative modelling of interaction of propafenone with sodium channels in cardiac cells. *Medical and Biological Engineering and Computing*, 42:151–157, 2004.

[195] P. Pauwels et al. The receptor binding profile of the new antihypertensive agent nebivolol and its stereoisomers compared with various beta-adrenergic blockers. *Molecular Pharmacology*, 34(6):843–851, 1988.

[196] A. Pecora et al. Phase i clinical experience with intravenous administration of pv701, an oncolytic virus. In K. K. Hunt, S. A. Vorburger, and S. G. Swisher, editors, *Gene Therapy for Cancer*, Cancer Drug Discovery and Development, pages 399–411. Humana Press, 2007.

[197] M. Perry et al. Structural Determinants of HERG Channel Block by Clofilium and Ibutilide. *Molecular Pharmacology*, 66(2):240–249, 2004.

[198] F. Persson et al. Blocking characteristics of herg, hnav1.5, and hkvlqt1/hmink after administration of the novel anti-arrhythmic compound azd7009. *J Cardiovasc Electrophysiol*, 16(3):329–341, Mar 2005.

[199] I. Peter et al. The endoderm gene regulatory network in sea urchin embryos up to mid-blastula stage. *Developmental Biology*, 340(2):188 – 199, 2010. Special Section: Gene Regulatory Networks for Development.

[200] G. Piatigorskaia et al. [dna interaction with the antitumor agent thiophosphamide]. *Mol Biol (Mosk)*, 20(2):423–429, 1986.

[201] B. Pitt et al. Aldosterone receptor antagonists for heart failure: current status, future indications. *Cleveland Clinic Journal of Medicine*, 73(3):257–260, 2006.

[202] K. Porter et al. Simvastatin reduces human atrial myofibroblast proliferation independently of cholesterol lowering via inhibition of RhoA. *Cardiovascular Research*, 61(4):745–755, 2004.

[203] C. Qiu et al. Mechanism of activation and inhibition of the her4/erbb4 kinase. *Structure*, 16(3):460–467, Mar 2008.

[204] R. Ramakrishnan et al. Pharmacodynamics and Pharmacogenomics of Methylprednisolone during 7-Day Infusions in Rats. *Journal of Pharmacology and Experimental Therapeutics*, 300(1):245–256, 2002.

[205] E. Ramos et al. State-dependent trapping of flecainide in the cardiac sodium channel. *The Journal of Physiology*, 560(1):37–49, 2004.

[206] A. Ransick et al. Micromeres are required for normal vegetal plate specification in sea urchin embryos. *Development*, 121(10):3215–3222, 1995.

[207] A. Redmond et al. Defining and targeting transcription factors in cancer. *Genome Biology*, 10(7):311, 2009.

[208] M. Remko. Molecular structure, lipophilicity, solubility, absorption, and polar surface area of novel anticoagulant agents. *Journal of Molecular Structure: THEOCHEM*, 916(1-3):76 – 85, 2009.

[209] B. Rini. Temsirolimus, an Inhibitor of Mammalian Target of Rapamycin. *Clinical Cancer Research*, 14(5):1286–1290, 2008.

[210] M. Robertson et al. Clinical and Biological Effects of Recombinant Human Interleukin-18 Administered by Intravenous Infusion to Patients with Advanced Cancer. *Clinical Cancer Research*, 12(14):4265–4273, 2006.

[211] S. Robinette et al. Cluster analysis statistical spectroscopy using nuclear magnetic resonance generated metabolic data sets from perturbed biological systems. *Analytical Chemistry*, 81(16):6581–6589, 2009. PMID: 19624161.

[212] D. Roden. Antiarrhythmic drugs: from mechanisms to clinical practice. *Heart*, 84(3):339–346, 2000.

[213] L. Romano et al. Endo16 is required for gastrulation in the sea urchin lytechinus variegatus. *Dev Growth Differ*, 48(8):487–497, Oct 2006.

[214] C. Rommel et al. Differentiation stage-specific inhibition of the raf-mek-erk pathway by akt. *Science*, 286(5445):1738–1741, Nov 1999.

[215] J. Rosen et al. The search for safer glucocorticoid receptor ligands. *Endocr Rev*, 26(3):452–464, 2005.

[216] P. Rosen et al. Amg 102, an hgf/sf antagonist, in combination with anti-angiogenesis targeted therapies in adult patients with advanced solid tumors. *Journal of Clinical Oncology*, 26(15S):3570, May 2008.

[217] R. Roskoski Jr. Sunitinib: A vegf and pdgf receptor protein kinase and angiogenesis inhibitor. *Biochemical and Biophysical Research Communications*, 356(2):323 – 328, 2007.

[218] S. Rost et al. Site-directed mutagenesis of vkorc1, the target protein of coumarin-type anticoagulants. pages 242–244. Springer Berlin Heidelberg, 2006.

[219] E. Röttinger et al. A Raf/MEK/ERK signaling pathway is required for development of the sea urchin embryo micromere lineage through phosphorylation of the transcription factor Ets. *Development*, 131(5):1075–1087, 2004.

[220] V. Roukos, T. Misteli, and C. K. Schmidt. Descriptive no more: the dawn of high-throughput microscopy. *Trends in Cell Biology*, 20(9):503 – 506, 2010.

[221] H. Ruan et al. Ing-1(hemab), a monoclonal antibody to epithelial cell adhesion molecule, inhibits tumor metastases in a murine cancer model. *Neoplasia*, 5(6):489–494, 2003.

[222] V. Sah et al. Cardiac-specific overexpression of rhoa results in sinus and atrioventricular nodal dysfunction and contractile failure. *The Journal of Clinical Investigation*, 103(12):1627–1634, 6 1999.

[223] S. Salvadore et al. Fastdtw: Toward accurate dynamic time warping in linear time and space. In *3rd Workshop on Mining Temporal and Sequential Data*, 2004.

[224] R. Santos et al. Angiotensin-(1Ű7) is an endogenous ligand for the G protein-coupled receptor Mas. *Proceedings of the National Academy of Sciences of the United States of America*, 100(14):8258–8263, 2003.

[225] I. Savelieva et al. Anti-arrhythmic drug therapy for atrial fibrillation: current anti-arrhythmic drugs, investigational agents, and innovative approaches. *Europace*, 10(6):647–665, 2008.

[226] E. Schadt et al. A network view of disease and compound screening. *Nat Rev Drug Discov*, 8(4):286–295, Apr 2009.

[227] M. a. Schittenhelm. Dasatinib (BMS-354825), a Dual SRC/ABL Kinase Inhibitor, Inhibits the Kinase Activity of Wild-Type, Juxtamembrane, and Activation Loop Mutant KIT Isoforms Associated with Human Malignancies. *Cancer Research*, 66(1):473–481, 2006.

[228] H. Schlebusch et al. A monoclonal antiidiotypic antibody aca 125 mimicking the tumor-associated antigen ca 125 for immunotherapy of ovarian cancer. *Hybridoma*, 14(2):167–174, Apr 1995.

[229] J. Shao et al. Characterization of the interacting mechanisms between triapine (3-aminopyridine-2-carboxaldehyde thiosemicarbazone) and the small subunits of human ribonucleotide reductase. *AACR Meeting Abstracts*, 46(1):969–a, 2005.

[230] G. Shapiro et al. Phase I dose-escalation study of XL147, a PI3K inhibitor administered orally to patients with solid tumors. *J Clin Oncol (Meeting Abstracts)*, 27(15S):3500–, 2009.

[231] Y. Shi et al. Induction of grp78 by valproic acid is dependent upon histone deacetylase inhibition. *Bioorganic & Medicinal Chemistry Letters*, 17(16):4491 – 4494, 2007.

[232] H. Shionoiri et al. [angiotensin-converting enzyme inhibitors: recent therapeutic aspect]. *Nippon Rinsho*, 55(8):2067–2074, Aug 1997.

[233] A. Shiroshita-Takeshita et al. Effect of simvastatin and antioxidant vitamins on atrial fibrillation promotion by atrial-tachycardia remodeling in dogs. *Circulation*, 110(16):2313–2319, 2004.

[234] S. Simons et al. Dexamethasone 21-mesylate: an affinity label of glucocorticoid receptors from rat hepatoma tissue culture cells. *Proc Natl Acad Sci U S A*, 78(6):3541–3545, Jun 1981.

[235] N. Singh et al. Molecular modeling and molecular dynamics studies of hydralazine with human dna methyltransferase 1. *ChemMedChem*, 4(5):792–799, May 2009.

[236] E. Slater et al. Glucocorticoid receptor binding and activation of a heterologous promoter by dexamethasone by the first intron of the human growth hormone gene. *Mol. Cell. Biol.*,

5(11):2984–2992, 1985.

[237] C. Smith et al. Beta-blocker selectivity at cloned human beta1- and beta2-adrenergic receptors. *Cardiovascular Drugs and Therapy*, 13:123–126, 1999.

[238] I. Sobolá. Global sensitivity indices for nonlinear mathematical models and their Monte Carlo estimates. *Math. Comput. Simul.*, 55(1-3):271–280, 2001.

[239] H. Sondermann et al. Structural analysis of autoinhibition in the Ras activator Son of sevenless. *Cell*, 119(3):393–405, Oct 2004.

[240] J. Spratlin et al. Clinical Applications of Metabolomics in Oncology: A Review. *Clinical Cancer Research*, 15(2):431–440, 2009.

[241] A. Squizzato et al. New direct thrombin inhibitors. *Internal and Emergency Medicine*, 4:479–484, 2009. 10.1007/s11739-009-0314-8.

[242] C. Stancu et al. Statins: mechanism of action and effects. *Journal of Cellular and Molecular Medicine*, 5(4):378–387, 2001.

[243] R. Steinman et al. Activation of Stat3 by cell confluence reveals negative regulation of Stat3 by cdk2. *Oncogene*, 22(23):3608–3615, Jun 2003.

[244] R. Steinmetz et al. Mechanisms Regulating the Constitutive Activation of the Extracellular Signal-Regulated Kinase (ERK) Signaling Pathway in Ovarian Cancer and the Effect of Ribonucleic Acid Interference for ERK1/2 on Cancer Cell Proliferation. *Mol Endocrinol*, 18(10):2570–2582, 2004.

[245] K. Suckling. Phospholipase a2s: Developing drug targets for atherosclerosis. *Atherosclerosis*, 212:357–366, 2010.

[246] N. Suh et al. Arzoxifene, a New Selective Estrogen Receptor Modulator for Chemoprevention of Experimental Breast Cancer. *Cancer Research*, 61(23):8412–8415, 2001.

[247] D. Szklarczyk et al. The string database in 2011: functional interaction networks of proteins, globally integrated and scored. *Nucleic Acids Research*, 39(suppl 1):D561–D568, 2011.

[248] L. Tabernero et al. Crystal Structure of a Statin Bound to a Class II Hydroxymethylglutaryl-CoA Reductase. *Journal of Biological Chemistry*, 278(22):19933–19938, 2003.

[249] G. Taglialatela et al. Acetyl-l-carnitine enhances the response of pc12 cells to nerve growth factor. *Developmental Brain Research*, 59(2):221 – 230, 1991.

[250] J. Tan et al. Pharmacologic disruption of Polycomb-repressive complex 2-mediated gene repression selectively induces apoptosis in cancer cells. *Genes & Development*, 21(9):1050–1063, 2007.

[251] R. Tarjan. Depth-first search and linear graph algorithms. *SIAM Journal on Computing*, 1(2):146–160, 1972.

[252] I. Telik. Telcyta. http://www.telik.com/pipe_telcyta.html, 2010.

[253] A. Terando et al. Vaccine therapy for melanoma: Current status and future directions. *Vaccine*, 25(Supplement 2):B4 – B16, 2007.

[254] S. Tornow et al. Functional modules by relating protein interaction networks and gene expression. *Nucleic Acids Res*, 31(21):6283–6289, Nov 2003.

[255] D. M. Townsend and K. D. Tew. Pharmacology of a mimetic of glutathione disulfide, nov-002. *Biomedicine & Pharmacotherapy*, 63(2):75 – 78, 2009.

[256] S. Trißl et al. Fast and practical indexing and querying of very large graphs. In *SIGMOD '07: Proceedings of the 2007 ACM SIGMOD international conference on Management of data*, pages 845–856, New York, NY, USA, 2007. ACM.

[257] C. Tse et al. ABT-263: A Potent and Orally Bioavailable Bcl-2 Family Inhibitor. *Cancer Research*, 68(9):3421–3428, 2008.

[258] J. Tuomi et al. Evidence for enhanced M3 muscarinic receptor function and sensitivity to atrial arrhythmia in the RGS2-deficient mouse. *Am J Physiol Heart Circ Physiol*, 298(2):H554–561, 2010.

[259] H. van Beeren et al. Dronerarone acts as a selective inhibitor of 3,5,3'-triiodothyronine binding to thyroid hormone receptor-alpha1: In vitro and in vivo evidence. *Endocrinology*, 144(2):552–558, 2003.

[260] J. Vane et al. The mechanism of action of aspirin. *Thrombosis Research*, 110(5-6):255 – 258, 2003.

[261] A. Venkatesan et al. Bis(morpholino-1,3,5-triazine) derivatives: Potent adenosine 5'-triphosphate competitive phosphatidylinositol-3-kinase/mammalian target of rapamycin inhibitors: Discovery of compound 26 (pki-587), a highly efficacious dual inhibitor. *Journal of Medicinal Chemistry*, 53(6):2636–2645, 2010.

[262] P. Verhamme et al. A new era for oral anticoagulation. *Belgian Journal of Hematology*, 1(1):6–13, September 2010.

[263] D. Villaret et al. A multicenter phase ii study of tgdcc-e1a for the intratumoral treatment of patients with recurrent head and neck squamous cell carcinoma. *Head Neck*, 24(7):661–669, Jul 2002.

[264] F. Vincenti et al. Interleukin-2-receptor blockade with daclizumab to prevent acute rejection in renal transplantation. daclizumab triple therapy study group. *N Engl J Med*, 338(3):161–165, Jan 1998.

[265] D. Vitagliano et al. The tyrosine kinase inhibitor zd6474 blocks proliferation of ret mutant medullary thyroid carcinoma cells. *Endocr Relat Cancer*, 18(1):1–11, 2011.

[266] A. von Gise et al. Apoptosis suppression by raf-1 and mek1 requires mek- and phosphatidylinositol 3-kinase-dependent signals. *Mol Cell Biol*, 21(7):2324–2336, Apr 2001.

[267] B. Walker et al. Comparative effects of azimilide and ambasilide on the human ether-a-go-go-related gene (HERG) potassium channel. *Cardiovascular Research*, 48(1):44–58, 2000.

[268] B. Wang et al. Isolation of high-affinity peptide antagonists of 14-3-3 proteins by phage display. *Biochemistry*, 38(38):12499–12504, 1999.

[269] Y. Wang et al. Biological activity of bevacizumab, a humanized anti-vegf antibody *in vitro*. *Angiogenesis*, 7:335–345, 2004. 10.1007/s10456-004-8272-2.

[270] Y. Wang et al. The toll-like receptor 7 (tlr7) agonist, imiquimod, and the tlr9 agonist, cpg odn, induce antiviral cytokines and chemokines but do not prevent vaginal transmission of simian immunodeficiency virus when applied intravaginally to rhesus macaques. *J. Virol.*, 79(22):14355–14370, 2005.

[271] Y. Wang et al. Reconstruct gene regulatory network using slice pattern model. *BMC Genomics*, 10(Suppl 1):S2, 2009.

[272] J. Weber. Overcoming immunologic tolerance to melanoma: Targeting ctla-4 with ipilimumab (mdx-010). *Oncologist*, 13(suppl_4):16–25, 2008.

[273] J. Weitz et al. New Antithrombotic Drugs*. *Chest*, 133(6 suppl):234S–256S, 2008.

[274] N. Wettschureck et al. Mammalian G Proteins and Their Cell Type Specific Functions. *Physiol. Rev.*, 85(4):1159–1204, 2005.

[275] A. Wikramanayake et al. Nuclear beta-catenin-dependent wnt8 signaling in vegetal cells of the early sea urchin embryo regulates gastrulation and differentiation of endoderm and mesodermal cell lineages. *Genesis*, 39(3):194–205, 2004.

[276] S. Wilhelm et al. Discovery and development of sorafenib: a multikinase inhibitor for treating cancer. *Nat Rev Drug Discov*, 5(10):835–844, Oct 2006.

[277] S. Willatts et al. Effect of the antiendotoxic agent, taurolidine, in the treatment of sepsis syndrome: A placebo-controlled, double-blind trial. *Critical Care Medicine*, 23(6):1033–1039, 1995.

[278] L. Wilson et al. Characterization of acetyl-3h-labeled vinblastine binding to vinblastine-tubulin crystals. *Journal of Molecular Biology*, 121(2):255 – 268, 1978.

[279] D. Wishart et al. Drugbank: a knowledgebase for drugs, drug actions and drug targets. *Nucleic Acids Res*, 36(Database issue):D901–D906, Jan 2008.

[280] J. Wu. Mycophenolate mofetil: Molecular mechanisms of action. *Perspectives in Drug Discovery and Design*, 2:185–204, 1994.

[281] L. Wu, L. Zhou, D. Q. Liu, F. G. Vogt, and A. S. Kord. Lc-ms/ms and density functional theory study of copper(ii) and nickel(ii) chelating complexes of elesclomol (a novel anticancer agent). *Journal of Pharmaceutical and Biomedical Analysis*, 54(2):331 – 336, 2011.

[282] G. Würthwein et al. Activation of beclomethasone dipropionate by hydrolysis to beclomethasone-17-monopropionate. *Biopharm Drug Dispos*, 11(5):381–394, Jul 1990.

[283] H. Yan et al. Molecular characterization of an alpha interferon receptor 1 subunit (ifnar1) domain required for tyk2 binding and signal transduction. *Mol. Cell. Biol.*, 16(5):2074–2082, 1996.

[284] X. Yang et al. From xenomouseő technology to panitumumab (abx-egf). In W. J. LaRochelle and R. A. Shimkets, editors, *The Oncogenomics Handbook*, Cancer Drug Discovery and Development, pages 647–657. Humana Press, 2005.

[285] T. Yeh et al. Biological characterization of arry-142886

(azd6244), a potent, highly selective mitogen-activated protein kinase kinase 1/2 inhibitor. *Clin Cancer Res*, 13(5):1576–1583, Mar 2007.

[286] C.-H. Yuh et al. Correct expression of spec2a in the sea urchin embryo requires both otx and other cis-regulatory elements. *Developmental Biology*, 232(2):424 – 438, 2001.

[287] C.-H. Yuh et al. An otx cis-regulatory module: a key node in the sea urchin endomesoderm gene regulatory network. *Developmental Biology*, 269(2):536 – 551, 2004.

[288] C.-H. Yuh et al. Brn1/2/4, the predicted midgut regulator of the endo16 gene of the sea urchin embryo. *Developmental Biology*, 281(2):286 – 298, 2005.

[289] K. Yuki et al. Sevoflurane binds and allosterically blocks integrin lymphocyte function-associated antigen-1. *Anesthesiology*, 113(3):600–609, Sep 2010.

[290] N. Yumoto et al. Expression of the erbb4 receptor causes reversal regulation of pp2a in the shc signal transduction pathway in human cancer cells. *Mol Cell Biochem*, 285(1-2):165–171, Apr 2006.

[291] M. Zaki et al. Cnto 328, a monoclonal antibody to il-6, inhibits human tumor-induced cachexia in nude mice. *Int J Cancer*, 111(4):592–595, Sep 2004.

[292] X.-W. Zhang et al. Arsenic Trioxide Controls the Fate of the PML-RARa Oncoprotein by Directly Binding PML. *Science*, 328(5975):240–243, 2010.

[293] Z. Zhang et al. Phosphorylated erk is a potential predictor of sensitivity to sorafenib when treating hepatocellular carcinoma: evidence from an in vitro study. *BMC Med*, 7:41, 2009.

[294] Y. Zheng et al. Comparative study of parameter sensitivity analyses of the TCR-activated Erk-MAPK signalling pathway. *IEE Proceedings - Systems Biology*, 153(4):201–211, 2006.

[295] X. Zhu et al. Toll like receptor-3 ligand poly-iclc promotes the efficacy of peripheral vaccinations with tumor antigen-derived peptide epitopes in murine cns tumor models. *J Transl Med*, 5:10, 2007.

[296] Z. Zi et al. In silico identification of the key components and steps in IFN-gamma induced JAK-STAT signaling pathway. *FEBS Lett*, 579(5):1101–1108, Feb 2005.

[297] Z. Zi et al. SBML-SAT: a systems biology markup language (SBML) based sensitivity analysis tool. *BMC Bioinformatics*, 9:342, 2008.

[298] G. Zoppoli et al. Ras-induced resistance to lapatinib is overcome by mek inhibition. *Curr Cancer Drug Targets*, 10(2):168–175, Mar 2010.

APPENDIX

A. OVARIAN CANCER DRUGS

Ovarian Cancer Drugs	NCT ID	Drug Effect	Mechanism of Action
DNA/RNA			
5-fluorouracil [180]	00004206, 00664911, 00003135, 00433407, 00957905, 00983541, 00178802, 00413322, 00959647	↓RNA	In vivo, fluoruracil is converted to the active metabolite 5-fluoroxyuridine monophosphate (F-UMP); replacing uracil, F-UMP incorporates into RNA and inhibits RNA processing, thereby inhibiting cell growth. Another active metabolite, 5-5-fluoro-2'-deoxyuridine-5'-O-monophosphate (F-dUMP), inhibits thymidylate synthase, resulting in the depletion of thymidine triphosphate (TTP), one of the four nucleotide triphosphates used in the in vivo synthesis of DNA.
antineoplaston A10 [180]	00003532	↓DNA	Intercalates into DNA, resulting in cell cycle arrest in G1 phase, reduction of mitosis, and decreased protein synthesis.
aroplatin [180] [Liposomal NDDP, L-NDDP]	00057395	↓DNA	Third-generation platinum complex analogue of cisplatin. liposomal NDDP alkylate DNA, forming both inter- and intra-strand DNA crosslinks and inhibiting DNA synthesis.
camptothecin [180] [CT-2106, 9-aminocamptothecin]	00001427, 00002671, 00003523, 00003548, 00333502, 00291837	↓active topoisomerase I	Binds to the nuclear enzyme, thereby inhibiting topoisomerase I repair of single-strand DNA breakages.
becatecarin [180]	00006262	↓DNA	Intercalates into DNA and stabilizes the DNA-topoisomerase I complex, thereby interfering with the topoisomerase I-catalyzed DNA breakage-reunion reaction and initiating DNA cleavage and apoptosis.
bendamustine hydrochloride [148]	00867503, 01110135	↓DNA	DNA cross-linking agent that causes DNA breaks.
bleomycin sulfate [17]	01042522, 00053352, 00276718, 00274950, 00003811	↓DNA, ↓RNA	Very potent cleaver of RNA as well as DNA in the presence of transition metal ions such as iron and copper.
brostallicin [180]	00410462	↓DNA	A synthetic, alpha-bromoacrylic, second-generation minor groove binder (MGB), related to distamycin A, with potential antineoplastic activity. Brostallicin binds to DNA minor groove DNA, after having formed a highly reactive glutathione (GSH)-brostallicin complex in the presence of the enzyme glutathione S-transferase (GST), which is overexpressed in cancer cells.
busulfan [180]	00003926, 00638898	↓DNA	Appears to act through the alkylation of DNA. Following systemic absorption of busulfan, carbonium ions are formed, resulting in DNA alkylation, breaks and inhibition of DNA replication and RNA transcription.
doxorubicin [180] [caelyx, adriamycin, doxil, SGN-15]	00002477, 00002489, 00002526, 00002641, 00002764, 00003135, 00003214, 00003334, 00003380, 00003385, 00003896, 00006235, 00011986, 00020514, 00025441, 00032162, 00043082, 00051584, 00057720, 00102973, 00113607, 00157560, 00170573, 00178802, 00179725, 00182767, 00183742, 00189410, 00189553, 00191607, 00216645, 00237627, 00248248, 00262990, 00312650, 00326456, 00350948, 00410462, 00484432, 00523380, 00538603, 00562185, 00575952, 00610792, 00628251, 00635193, 00653328, 00653952, 00657878, 00659178, 00662233, 00664911, 00698451, 00720096, 00722592, 00727961, 00743431, 00758732, 00770536, 00780039, 00815945, 00846612, 00861120, 00862355, 00862836, 00887796, 00903630, 00913835, 00945139, 00976911, 01004380, 01016054, 01035658, 01100372, 01113957, 01121406, 01145430, 01170650, 01202890, 01214668, 01227941	↓DNA, ↓active topoisomerase II	Intercalates between base pairs in the DNA helix, thereby preventing DNA replication and ultimately inhibiting protein synthesis. Additionally, doxorubicin inhibits topoisomerase II which results in an increased and stabilized cleavable enzyme-DNA linked complex during DNA replication and subsequently prevents the ligation of the nucleotide strand after double-strand breakage.
canfosfamide hydrochloride [252] [TLK286, Telcyta]	00022347, 00051948, 00052065, 00038428, 00102973, 00350948, 00057720	↓DNA, ↓active GST P1-1	Activation occurs when GST P1-1 splits Telcyta into two active fragments: a glutathione analog fragment and an active cytotoxic fragment. The cytotoxic fragment reacts with important cell components, including RNA, DNA and proteins, leading to cell death. The glutathione analog fragment of Telcyta may remain bound to GST P1-1, which may limit the ability of GST P1-1 to inactivate other cancer drugs.
capecitabine [180]	01081262, 00403429, 00664911, 00006812, 00004012, 00354601, 00118300, 01233505	↓DNA, ↓RNA	As a prodrug, capecitabine is selectively activated by tumor cells, producing two active metabolites, 5-fluoro-2-deoxyuridine monophosphate (FdUMP) and 5-fluorouridine triphosphate (FUTP). FdUMP inhibits DNA synthesis and cell division by reducing normal thymidine production, while FUTP inhibits RNA and protein synthesis by competing with uridine triphosphate for incorporation into the RNA strand.

Continued on next page

Table A.1 – continued from previous page

Ovarian Cancer Drugs	NCT ID	Drug Effect	Mechanism of Action
carboplatin [180] [Paraplatin]	00002477, 00002489, 00002508, 00002515, 00002558, 00002600, 00002819, 00002854, 00002894, 00002931, 00002943, 00003064, 00003072, 00003136, 00003214, 00003378, 00003385, 00003386, 00003560, 00003597, 00003636, 00003644, 00003657, 00003732, 00003733, 00003852, 00003880, 00003944, 00003998, 00004082, 00004221, 00004876, 00004921, 00004934, 00005026, 00005049, 00005051, 00005612, 00006155, 00006235, 00006356, 00006453, 00006454, 00007813, 00008138, 00011986, 00017303, 00021385, 00025441, 00028743, 00028912, 00030446, 00031954, 00032162, 00043082, 00045461, 00052468, 00059618, 00059787, 00060359, 00063401, 00069901, 00075712, 00079430, 00085358, 00086892, 00090610, 00096200, 00098878, 00102973, 00112086, 00117442, 00129727, 00138242, 00157560, 00170664, 00181701, 00189371, 00189410, 00189553, 00189566, 00191646, 00193297, 00214058, 00217529, 00217568, 00226915, 00228319, 00230542, 00231075, 00247988, 00262847, 00267696, 00274950, 00276718, 00293293, 00303940, 00316173, 00316407, 00317434, 00321633, 00322881, 00325351, 00326456, 00331422, 00352300, 00369954, 00373217, 00382811, 00390611, 00391118, 00401674, 00407407, 00408070, 00408655, 00421889, 00423852, 00432094, 00434642, 00452985, 00467051, 00473954, 00483782, 00489359, 00490711, 00501644, 00516724, 00520013, 00529022, 00535119, 00538603, 00544973, 00561795, 00562185, 00565851, 00583622, 00610714, 00647062, 00652119, 00652691, 00657878, 00660842, 00664911, 00672295, 00698451, 00737243, 00744718, 00748527, 00750386, 00756847, 00758732, 00772798, 00780039, 00788125, 00815945, 00838656, 00877253, 00886717, 00891605, 00910000, 00919984, 00929162, 00937560, 00945191, 00951496, 00954174, 00979082, 00989651, 00993616, 00993655, 01000896, 01001910, 01004380, 01016054, 01042522, 01074411, 01081262, 01081951, 01097746, 01124435, 01133756, 01144442, 01146795, 01164995, 01167712, 01188876, 01196429, 01219777, 01237067, 01239732, 01248962, 01249443, 01253681, 01256268	↓DNA	Bind to nucleophilic groups such as GC-rich sites in DNA, thereby inducing intrastrand and interstrand DNA cross-links, as well as DNA-protein cross-links.
carmustine [180]	00003413	↓DNA	Alkylates and cross-links DNA during all phases of the cell cycle.
CP-4055 [180]	00831636	↓DNA	As a prodrug, CP-4055 is converted intracellularly into cytarabine triphosphate by deoxycytidine kinase and subsequently competes with cytidine for incorporation into DNA, thereby inhibiting DNA synthesis.
cyclophosphamide [180] [cytophosphan]	00001426, 00003136, 00652691, 00003214, 00004221, 00652899, 00004921, 00002477, 01105650, 00072566, 00005612, 00002819, 00551265, 00002600, 00003386, 00381173, 00228358, 00562640, 00550784, 00003944, 01212887, 00003425, 00003269, 00002489, 00002943, 00007813, 00293384, 00553683, 00025441, 00003852, 00662233, 00856180, 00538031, 00002854, 00499733, 00844506, 01238770, 01175772	↓DNA	In the liver, cyclophosphamide is converted to the active metabolites aldophosphamide and phosphoramide mustard, which bind to DNA, thereby inhibiting DNA replication and initiating cell death.
epirubicin	00004934, 00025441, 00003852	↓DNA	Intercalates into DNA and interacts with topoisomerase II, thereby

Continued on next page

Table A.1 – continued from previous page

Ovarian Cancer Drugs	NCT ID	Drug Effect	Mechanism of Action
hydrochloride [180]		↓RNA	inhibiting DNA replication and repair and RNA and protein synthesis.
cisplatin [180]	00436657, 01138137, 01083537, 00942838, 00006356, 00003322, 00003896, 00002717, 00003214, 00002894, 00993655, 00772863, 00002913, 00314678, 00003636, 00006028, 00003345, 00006942, 00702299, 00028743, 00002477, 00003413, 00964626, 00005051, 00091377, 00003358, 00003386, 01042522, 00002568, 01104259, 00951496, 00814086, 00550784, 00083122, 00005049, 00081276, 00020696, 00588237, 00003624, 00002559, 00470366, 00003269, 00006036, 00335998, 00003569, 00551122, 00575952, 00053352, 00274950, 00003811, 00002854, 00582205, 00004083, 00001426, 00889733	↓DNA	Bind to nucleophilic groups such as GC-rich sites in DNA, inducing intrastrand and interstrand DNA cross-links, as well as DNA-protein cross-links.
trabectedin [180] [ET-743]	00113607, 00569673, 00437047, 00003939, 00786838, 00050414	↓DNA	Binding to the minor groove of DNA, trabectedin interferes with the transcription-coupled nucleotide excision repair machinery to induce lethal DNA strand breaks and blocks the cell cycle in the G2 phase.
etoposide phosphate [180] [VP16]	00312988, 00005612, 00003967, 00003380, 00002478, 00002931, 00003657, 00003269, 00002489, 00002943, 00007813, 00432094, 00025441, 00003852, 00053352, 00002558, 00002508, 00276718, 00274950, 00003811, 00662233, 00002854, 00003597, 00003064, 01042522, 00788125, 00250094	↓active topoisomerase II	Binds to and inhibits topoisomerase II and its function in ligating cleaved DNA molecules, resulting in the accumulation of single- or double-strand DNA breaks, the inhibition of DNA replication and transcription, and apoptotic cell death.
fludarabine phosphate [180]	01105650, 00523809, 00652899, 01212887	↓DNA	Phosphorylated intracellularly to the active triphosphate, 2-fluoro-ara-ATP. This metabolite may inhibit DNA polymerase alpha, ribonucleotide reductase and DNA primase, thereby interrupting DNA synthesis and inhibiting tumor cell growth.
ganciclovir [180] [GCV]	00005025, 00006216, 00964756	↓active viral DNA polymerase	As the active metabolite of ganciclovir, ganciclovir-5-triphosphate (ganciclovir-TP) appears to inhibit viral DNA synthesis by competitive inhibition of viral DNA polymerases and incorporation into viral DNA, resulting in eventual termination of viral DNA elongation.
gimatecan [180]	00420485	↓active topoisomerase I	Binds to and inhibits the activity of topoisomerase I, stabilizing the cleavable complex of topoisomerase I-DNA, which inhibits the religation of single-stranded DNA breaks generated by topoisomerase I.
glufosfamide [9]	00442598	↓DNA	Glucose-coupled iphosphoramide mustard with alkylating properties. Developed to avoid the need for the activation of ifosfamide by P450 in the liver, thus reducing toxicities associated with systemic exposure to multiple metabolites of ifosfamide, including acrolein. Phosphoramide mustard induces DNA interstrand and DNA-protein cross-links.
hydralazine [235] [16]	00533299	↑intracellular Ca^{2+}, ↓active DNA methyltransferase	Inhibitory activity of hydralazine toward DNMT may be rationalized at the molecular level by similar interactions within the binding pocket (e.g., by a similar pharmacophore) as established by substrate-like deoxycytidine analogues. These interactions involve a complex network of hydrogen bonds with arginine and glutamic acid residues that also play a major role in the mechanism of DNA methylation. Has direct effect on the myocardium to increase Ca^{2+} inflow. The increased Ca^{2+} influx and inward slow current is due partly to activation of beta-adrenoceptors, with resultant elevation of cyclic AMP, and partly to another mechanism.
ifosfamide [180]	00954174, 00045461, 00002559, 00470366, 00002931, 00467051, 00003657, 00423852, 00551122, 00432094, 00788125, 00025441, 00003852, 00002558, 00274950, 00002641, 00002764, 00662233, 00002526, 00002854, 00003597	↓DNA	Alkylates and forms DNA crosslinks, thereby preventing DNA strand separation and DNA replication.
irinotecan hydrochloride [180] [CPT-11,NKTR-102]	00003345, 00053833, 00031681, 00047242, 00959647, 01040312, 00806156	↓active topoisomerase I	Irinotecan, a prodrug, is converted to a biologically active metabolite 7-ethyl-10-hydroxy-camptothecin (SN-38), which inhibits topoisomerase I activity by stabilizing the cleavable complex between topoisomerase I and DNA, resulting in DNA breaks that inhibit DNA replication and trigger apoptotic cell death.
irofulven [180]	00019552, 00053365	↓DNA	Alkylates DNA and protein macromolecules, forms adducts, and arrests cells in the S-phase of the cell cycle.
IT-101 [180]	00753740	↓active topoisomerase I	Contains camptothecin-polymer, which during the S phase of the cell cycle, selectively stabilizes topoisomerase I-DNA covalent complexes, thereby inhibiting religation of topoisomerase I-mediated single-strand DNA breaks and producing potentially lethal double-strand DNA breaks when encountered by the DNA replication machinery.

Continued on next page

Table A.1 – continued from previous page

Ovarian Cancer Drugs	NCT ID	Drug Effect	Mechanism of Action
karenitecin [180]	00477282, 00054119	↓active topoisomerase I	Stabilizes the cleavable complex between topoisomerase I and DNA, resulting in DNA breaks and consequently triggering apoptosis.
levofloxacin [180]	00005590	↓active DNA gyrase	Diffuses through the bacterial cell wall and acts by inhibiting DNA gyrase (bacterial topoisomerase II), an enzyme required for DNA replication, RNA transcription, and repair of bacterial DNA.
melphalan [180]	00583622, 00003080, 00002977, 00004921, 00003413, 00523809, 00550784, 00003425, 00003926, 00002750, 00638898	↓DNA, ↓RNA	Alkylates DNA at the N7 position of guanine and induces DNA interstrand cross-linkages, resulting in the inhibition of DNA and RNA synthesis and cytotoxicity against both dividing and non-dividing tumor cells.
mitoxantrone hydrochloride [180]	00003080, 00002819, 00003297	↓DNA, ↓RNA, ↓active topoisomerase II	Intercalates into and crosslinks DNA, thereby disrupting DNA and RNA replication. This agent also binds to topoisomerase II, resulting in DNA strand breaks and inhibition of DNA repair.
moxifloxacin hydrochloride [180]	00324324	↓active DNA gyrase, ↓active topoisomerase IV	Binds to and inhibits the bacterial enzymes DNA gyrase (topoisomerase II) and topoisomerase IV, resulting in inhibition of DNA replication and repair and cell death in sensitive bacterial species.
lurtotecan [180] [OSI-211]	00046800, 00010179, 00006036	↓active topoisomerase I	A semisynthetic analogue of camptothecin, selectively stabilizes the topoisomerase I-DNA covalent complex and forms an enzyme-drug-DNA ternary complex during S phase of the cell cycle, thereby inhibiting religation of topoisomerase I-mediated single-stranded DNA breaks.
oxaliplatin [180]	00004206, 01081262, 00664911, 00296816, 00005836, 00313612, 00006391, 00075543, 00692900, 01233505, 00957905, 00091182, 00418093, 00959647	↓DNA	An organoplatinum complex. Active oxaliplatin derivatives, such as monoaquo and diaquo DACH platinum, alkylate macromolecules, forming both inter- and intra-strand platinum-DNA crosslinks, which result in inhibition of DNA replication and transcription and cell-cycle nonspecific cytotoxicity.
palifosfamide-tris [180]	01242072	↓DNA	An active metabolite of ifosfamide covalently linked to the amino acid lysine for stability, palifosfamide irreversibly alkylates and cross-links DNA through GC base pairs, resulting in irreparable 7-atom inter-strand cross-links; inhibition of DNA replication and cell death follow.
pemetrexed [180] [Alimta]	00230542, 00109096, 01001910, 00489359, 00315861, 00461786, 00868192, 00702299, 00087087, 01172028, 00055432	↓active thymidylate synthase	Binds to and inhibits the enzyme thymidylate synthase (TS) which catalyses the methylation of 2'-deoxyuridine-5'-monophosphate (dUMP) to 2'-deoxythymidine-5'-monophosphate (dTMP), an essential precursor in DNA synthesis.
picoplatin [180]	00465725, 00710697	↓DNA	Designed to overcome platinum drug resistance, picoplatin alkylates DNA, forming both inter- and intra-strand cross-linkages, resulting in inhibition of DNA replication and transcription, and the induction of apoptosis.
topotecan [180] [Hycamtin]	00253461, 00194935, 00102375, 00526799, 00770536, 00429559, 00316173, 00312988, 01177501, 00720096, 00003732, 00189566, 01121406, 00170677, 00250094, 00061308, 00314678, 00976911, 00437307, 00343044, 00179712, 00317772, 00193297, 00315861, 00157560, 00231855, 00523432, 00888810, 00046111, 00477282, 00002734, 00003733, 00003064, 00652691, 00014690, 00004221, 00057720, 00002913, 00006454, 00072267, 00313612, 00006391, 00028743, 00287859, 00003382, 00005051, 00005612, 01012817, 00005026, 00003967, 00011986, 00550784, 00003944, 00005029, 00114166, 00217555, 00436644, 00055614, 00045175, 00842452, 00002515, 00638898, 00765973, 00170625, 00484666	↓active topoisomerase I	During the S phase of the cell cycle, topotecan selectively stabilizes topoisomerase I-DNA covalent complexes, inhibiting religation of topoisomerase I-mediated single-strand DNA breaks and producing potentially lethal double-strand DNA breaks when complexes are encountered by the DNA replication machinery.
rubitecan [180]	00006230, 00006267	↓active topoisomerase I	Binds to and inhibits the enzyme topoisomerase I and induces protein-linked DNA single-strand breaks.
SJG-136 [180]	01200797, 01199796	↓DNA	Binds to the minor groove of DNA and induces interstrand cross-links between two N-2 guanine positions, thereby inhibiting DNA replication and transcription.
temozolomide [180]	01113957, 00526617, 00005952, 00006043, 00303940, 00020150, 00003718	↑methylated DNA	Converted at physiologic pH to the short-lived active compound, monomethyl triazeno imidazole carboxamide (MTIC), which causes the methylation of DNA at the O6 and N7 positions of guanine, resulting in inhibition of DNA replication.
thalidomide [130]	00016224, 00004876, 00041080, 00049296	↓DNA	Intercalates into DNA, resulting in cell cycle arrest in G1 phase, reduction of mitosis, and decreased protein synthesis.
thiotepa [200]	00003297, 00003080, 00002977, 00003064, 00003173, 00003926, 00002515, 00432094, 00003852	↓DNA	Thiotepa binding results in destabilization of the DNA secondary structure and formation of cross-links. An increased amount of bounded thiotepa results in DNA denaturation; prolonged alkylation causes breaks in the sugar-phosphate backbone.
tirapazamine [180]	00020696	↓DNA, ↓active topoisomerase II	Selectively activated by multiple reductases to form free radicals in hypoxic cells, thereby inducing single-and double-strand breaks in DNA, base damage, and cell death. This agent also sensitizes hypoxic cells to ionizing radiation and inhibits the repair of radiation-induced DNA strand breaks via inhibition of topoisomerase II.

Continued on next page

Table A.1 – continued from previous page

Ovarian Cancer Drugs	NCT ID	Drug Effect	Mechanism of Action
treosulfan [180]	00170690	↓DNA	Under physiological conditions, treosulfan converts nonenzymatically to L-diepoxybutane via a monoepoxide intermediate. The monoepoxide and L-diepoxybutane alkylate DNA at guanine residues and produce DNA intermediate interstrand crosslinks, resulting in DNA fragmentation and apoptosis.
voreloxin [94]	00408603	↓DNA, ↓active topoisomerase II	Intercalates DNA and inhibits topoisomerase II, resulting in replication-dependent, site-selective DNA damage, G2 arrest and apoptosis.
AEZS-108 [180]	00569257	↓GnRH-1R, ↓DNA	Binds to GnRH-1Rs, which may be highly expressed on endometrial and ovarian tumor cell membrane surfaces, and is internalized. Once inside the cell, the doxorubicin moiety of this agent intercalates into DNA and inhibits the topoisomerase II activity, which may result in the inhibition of tumor cell DNA replication and tumor cell proliferation.
azacitidine [180]	00842582, 00529022	↓active DNA methyltransferase	Incorporated into DNA, where it reversibly inhibits DNA methyltransferase, thereby blocking DNA methylation.
belinostat [180]	00421889, 00301756, 00993616, 00413075, 00413322	↓active HDAC	A histone deacetylase (HDAC) inhibitor. Belinostat targets HDAC enzymes, thereby inhibiting tumor cell proliferation, inducing apoptosis, promoting cellular differentiation, and inhibiting angiogenesis.
dactinomycin [180]	00002489, 00025441	↓RNA	Intercalates between adjacent guanine-cytosine base pairs, blocking the transcription of DNA by RNA polymerase.
decitabine [180]	00477386, 00748527, 00887796	↓DNA methyltransferase	Incorporates into DNA and inhibits DNA methyltransferase, resulting in hypomethylation of DNA and intra-S-phase arrest of DNA replication.
magnesium valproate [180]	00533299	↓active histone deacetylases	Dissociates in the gastrointestinal tract and is absorbed into the circulation as magnesium ions and valproic acid ions; valproic acid may inhibit histone deacetylases, inducing tumor cell differentiation, apoptosis, and growth arrest.
romidepsin [180]	00085527, 00091195	↓active histone deacetylases	After intracellular activation, romidepsin binds to and inhibits histone deacetylase (HDAC), resulting in alterations in gene expression and the induction of cell differentiation, cell cycle arrest, and apoptosis.
valproic acid [231]	00529022	↓active HDAC	Binds acetylase active site on HDAC, inhibiting it.
vorinostat [180]	00772798, 00910000, 00976183, 00132067, 01249443	↓active HDAC	Binds to the catalytic domain of the histone deacetylases (HDACs). This allows the hydroxamic moiety to chelate zinc ion located in the catalytic pockets of HDAC, thereby inhibiting deacetylation and leading to an accumulation of both hyperacetylated histones and transcription factors. Hyperacetylation of histone proteins results in the upregulation of the cyclin-dependant kinase p21, followed by G1 arrest.
lenalidomide [122] [CC-5013]	01202890, 01111903, 00903630, 00179725, 00179712	↓TNFα mRNA	Inhibits TNFα production by destabilizing its mRNA.
exatecan mesylate [180]	00004060	↓active topoisomerase I	Inhibits topoisomerase I activity by stabilizing the cleavable complex between topoisomerase I and DNA and inhibiting religation of DNA breaks, thereby inhibiting DNA replication and triggering apoptotic cell death.
gemcitabine [180] [gemzar]	00102414, 01016054, 00583622, 00312650, 00191334, 00003449, 00183794, 00096395, 00490711, 01121406, 01133756, 01196559, 00061308, 01131039, 00910000, 00390182, 00434642, 00157560, 00418093, 00191607, 00191646, 00983541, 00429559, 00312988, 00267696, 00838656, 00052468, 00031954, 00006453, 00006028, 00003382, 00003358, 00620295, 00003378, 01100372, 00011986, 00227721, 00093496, 00217555, 00369954, 00014456, 00410553, 00551122, 00003518, 00004082, 00004066, 00055432, 00051584, 00928642, 00610740	↓active ribonucleotide reductase	dFdCDP is the metabolite of gemcitabine. dFdCDP inhibits ribonucleotide reductase, thereby decreasing the deoxynucleotide pool available for DNA synthesis; dFdCDP is incorporated into DNA, resulting in DNA strand termination and apoptosis.
O6-benzylguanine [180]	00020150	↓active AGT	Binds the DNA repair enzyme O(6)-alkylguanine DNA alkyltransferase (AGT), transferring the benzyl moiety to the active-site cysteine and resulting in inhibition of AGT-mediated DNA repair.
oblimersen sodium [180]	00003103	↓bcl-2	The sodium salt of a phosphorothioate antisense oligonucleotide targeted to the initiation codon region of mRNA for the anti-apoptotic gene Bcl-2. Oblimersen inhibits Bcl-2 mRNA translation, which may result in decreased expression of the Bcl-2 protein and tumor cell apoptosis.
PF-01367338 [180]	00664781	↓active PARP1	Selectively binds to PARP1 and inhibits PARP1-mediated DNA repair, thereby enhancing the accumulation of DNA strand breaks and promoting genomic instability and apoptosis.
ABT-888 [118] [veliparib]	01113957, 00526617, 01145430, 00892736, 01012817, 00535119, 01104259, 00989651, 01233505	↓active PARPs	Inhibits PARPs by binding at the NAD+ binding site, thereby inhibiting DNA repair and potentiating the cytotoxicity of DNA-damaging agents.
iniparib [180] [BSI-201]	01033123, 01033292, 00677079	↓active PARP-1	In vivo, iniparib is converted to the active drug, which selectively binds to PARP-1 and inhibits PARP-1-mediated DNA repair.

Continued on next page

Table A.1 – continued from previous page

Ovarian Cancer Drugs	NCT ID	Drug Effect	Mechanism of Action
KU-0059436 [180] [AZD2281, olaparib]	00494442, 00516373, 00516724, 01081951, 01116648, 01115829, 01237067, 01078662, 00628251, 00679783, 00647062, 00753545	↓active PARP	Selectively binds to and inhibits PARP, inhibiting PARP-mediated repair of single strand DNA breaks.
MK4827 [180]	01227941, 00749502	↓active PARP	Inhibits PARP activity, enhancing the accumulation of DNA strand breaks and promoting genomic instability and apoptosis.
plevitrexed [180]	00014690	↓active thymidylate synthetase	Transported into the cell via the physiological reduced folate carrier (RFC) system. Intracellularly, this agent selectively binds to the folate binding site of thymidylate synthase and inhibits thymidine synthesis, which may result in DNA synthesis inhibition and apoptosis.
Diagnostic Imaging			
perflutren [180]	00626873	-	An injectable suspension of liposome-encapsuled microspheres containing the fluorocarbon gas perflutren for contrast enhancement in ultrasound procedures. Because the acoustic impedance of perflutren lipid microspheres is much lower than that of blood, impinging ultrasound waves are scattered and reflected at the microsphere-blood interface and may be visualized with ultrasound imaging.
fludeoxyglucose F 18 [180]	00253461	-	The radioactive form of glucose used in positron emission tomography (PET), a diagnostic imaging procedure.
Tc 99m sestamibi [180]	00972205	-	Sestamibi is a large synthetic molecule of the isonitrile family, which can be labeled with Tc99m. It passes through cells membranes passively, collecting in cells with large numbers of mitochondria. It is often used for imaging of the thyroid and parathyroid.
Diagnostic - Detection of Oxygen Level			
EF5 [180]	00107445, 00087191	-	Effective in accessing oxygen levels in tumor tissue through its adduct formation to intracellular macromolecules in the absence of oxygen.
Microtubule			
ABT-751 [180]	00036959	↓microtubule	Binds to the colchicine-binding site on beta-tubulin and inhibits the polymerization of microtubules, thereby preventing tumor cell replication.
docetaxel [180] [ATI-1123, Taxotere]	01041235, 00216112, 00583622, 00183794, 00484666, 00758732, 00474669, 00772863, 00452985, 00296816, 00003998, 00004037, 00138242, 00217568, 00217529, 00069160, 00003560, 00321633, 00214058, 00539669, 00565851, 00303888, 00066456, 00085358, 00227721, 00436501, 00872989, 00569673, 00075543, 00004081, 00692900, 00354601, 00504257, 00003103, 00287885, 00433407, 00014456, 01172028, 00002901, 00471432, 00004082, 00002903, 00020514, 00004066, 00268918, 00539968, 00183742, 00487786, 00049296, 00473954, 00431054, 00247988, 00231855, 00090610	↑microtubule	Binds to and stabilizes tubulin, thereby inhibiting microtubule disassembly which results in cell-cycle arrest at the G2/M phase and cell death.
dolastatin 10 [180] [24]	00003778	↓microtubule, ↑phosphorylated Bcl2, ↑phosphorylated Bcl-xL, ↑phosphorylated Mcl-1	Binding to tubulin, dolastatin 10 inhibits microtubule assembly, resulting in the formation of tubulin aggregates and inhibition of mitosis. This agent also phosphorylate Bcl2, Bcl-xL and Mcl-1.
epothilone [180] [EPO906, Patupilone, epothilone b, BMS753493, epofolate]	00546247, 00550017, 00262990, 00035100	↑microtubules	Epothilone induces microtubule polymerization and stabilizes microtubules against depolymerization conditions.
eribulin mesylate [180]	00334893, 00410553	↓microtubule	Eribulin binds to the vinca domain of tubulin and inhibits the polymerization of tubulin and the assembly of microtubules, resulting in inhibition of mitotic spindle assembly, induction of cell cycle arrest at G2/M phase, and, potentially, tumor regression.
estramustine [180]	00433407	↓microtubule	A synthetic molecule that combines estradiol and nornitrogen mustard through a carbamate link. Estramustine and its major metabolite estramustine bind to microtubule-associated proteins (MAPs) and tubulin, thereby inhibiting microtubule dynamics and leading to anaphase arrest in a dose-dependent fashion.
T900607-sodium [180]	00043446	↓microtubule	Inhibits tubulin polymerization by binding irreversibly to colchicine binding sites, resulting in cell cycle arrest and apoptosis.
ixabepilone [180] [BMS-247550]	00182767, 00030706, 00025155, 00070096, 00030108, 00005807	↑microtubule	Binds to tubulin and promotes tubulin polymerization and microtubule stabilization, thereby arresting cells in the G2-M phase of the cell cycle and inducing tumor cell apoptosis.

Continued on next page

Table A.1 – continued from previous page

Ovarian Cancer Drugs	NCT ID	Drug Effect	Mechanism of Action
vincristine sulfate [180]	00002489, 00025441, 00662233	↓microtubule	The sulfate salt of a natural alkaloid isolated from the plant Vinca rosea Linn with antimitotic and antineoplastic activities. Vincristine binds irreversibly to microtubules and spindle proteins in S phase of the cell cycle and interferes with the formation of the mitotic spindle, thereby arresting tumor cells in metaphase. This agent also depolymerizes microtubules and may also interfere with amino acid, cyclic AMP, and glutathione metabolism; calmodulin-dependent Ca^{2+}-transport ATPase activity; cellular respiration; and nucleic acid and lipid biosynthesis.
MKC-1 [180]	00607607	↓microtubule	MKC-1 and its metabolites inhibit tubulin polymerization, blocking the formation of the mitotic spindle, which may result in cell cycle arrest at the G2-M phase and apoptosis.
panzem nanocrystal colloidal dispersion [181] [NCD]	00400348	↓microtubule	Binds to tubulin and disrupts microtubule formation, thereby preventing mitosis and subsequent cellular proliferation.
sagopilone [180] [BAY86-5302, ZK219477]	00751205, 00246688, 00325351	↑microtubule	Binds to tubulin and induces microtubule polymerization while stabilizing microtubules against depolymerization, which may result in the inhibition of cell division, the induction of G2-M arrest, and apoptosis.
vinblastine sulfate [278]	00274950	↓microtubule	Disrupts microtubule formation by binding to tubulin.
paclitaxel [180] [Abraxane, ABI-007, CT-2103, Taxol, Paclical, Genexol]	00069901, 00666991, 00772798, 01138137, 00929162, 00585052, 00373217, 00102622, 01081951, 01083537, 00326456, 00390611, 00919984, 00189371, 00001426, 00421889, 00189553, 00750386, 00002928, 00003449, 00945191, 00228319, 01081262, 00002734, 00003733, 00889382, 00129727, 00003322, 00003644, 00003732, 00003896, 00490711, 00664911, 00003160, 01239732, 00657878, 00189566, 00003064, 00391118, 00002717, 01146795, 00002474, 00004221, 00415207, 00415181, 01121406, 00231075, 00170664, 00002894, 00954174, 00993655, 01144442, 01196741, 01091428, 00002913, 01196429, 00003072, 00017303, 00979082, 00838656, 00538603, 00517621, 00003120, 00314678, 00052468, 00840450, 01256268, 01000896, 01219777, 00976911, 00937560, 00031954, 01097746, 00006454, 00004921, 00005046, 00003998, 00702299, 00004934, 00028743, 00483782, 00181701, 00582205, 00756847, 00158379, 00003413, 00008138, 00964626, 00005051, 00005612, 00002819, 00091377, 00544973, 01253681, 00672295, 00408070, 00652119, 00003386, 01042522, 00002568, 00075712, 00003378, 00005026, 00193297, 00011986, 00096200, 00316407, 00535119, 00226915, 00112086, 00108745, 00262847, 00063401, 00565851, 00951496, 00079430, 00888615, 00814086, 00331422, 01167712, 00989651, 00550784, 00003385, 00352300, 00003944, 00003880, 00059787, 00085358, 00023907, 00084448, 01199263, 00006227, 00479817, 00588237, 00003624, 00322881, 00520013, 00002559, 00470366, 00433407, 00002931, 00667641, 00467051, 00408655, 00003569, 00423852, 00019019, 00551122, 00003334, 00575952, 01249443, 00432094, 00003518, 00028535, 00003852, 00002558, 00117442, 00001383, 00561795, 00516724, 01209195, 00191646, 00737243, 00891605, 00972205, 00002854, 00610714, 00401674, 01204749, 00653952, 00466960, 00499252, 00313599, 00825201, 00499291, 00060359, 00045682, 00017017, 00660842, 00886717, 00034151, 00466986, 00407563, 00407407, 00877253, 00001272, 00293293, 00157560, 00989131	↑microtubule	Binds to tubulin and inhibits the disassembly of microtubules, thereby resulting in the inhibition of cell division.

Continued on next page

Table A.1 – continued from previous page

Ovarian Cancer Drugs	NCT ID	Drug Effect	Mechanism of Action
vinorelbine ditartrate [180]	01196559, 00001944, 01104259, 00020514, 01155258	↓microtubule	Binds to tubulin and prevents formation of the mitotic spindle, resulting in the arrest of tumor cell growth in metaphase.
BB-10901 [180]	00346385	↓tumor cells expressing CD56 antigen, ↓microtubule	Consist of monoclonal antibody (huN-901) and DMI. the antibody moiety selectively attaches to CD56 antigen, a neural cell adhesion molecule (NCAM)) expressed on the surface of cells of small cell lung cancer (SCLC) and other neuroendocrine (NE) tumors. Thus, the DMI conjugate is targeted specifically to CD56-expressing tumor cells, where it inhibits tubulin polymerization and assembly, resulting in inhibition of mitosis and cell cycle arrest in the S phase.
Antibody-Targeted Vaccine/Therapy			
ACA 125 [228]	00103545	↓cancer cell expressing CA 125 antigen	A murine antiidiotypic antibody. ACA 125 functionally imitating the tumor-associated antigen CA 125.
carcinoembryonic antigen RNA-pulsed DC cancer vaccine [180]	00004604	↓tumor cells expressing CEA antigen	A vaccine comprising autologous dendritic cells pulsed with mRNA-encoded Carcinoembryonic Antigen (CEA) that targets tumor cells expressing CEA.
dendritic cells/CMV pp65 peptide mixture [180]	00027534	↓cells expressing CMV pp65	A peptide derived from cytomegalovirus (CMV) internal matrix protein pp65. CMV pp65 peptide antigen is used in recombinant vaccinia virus as an HLA-A-restricted epitope to produce vaccines and specific CD8+ and CD4+ cell responses against CMV infection, a serious complication of allogeneic bone marrow transplantation (BMT).
ALVAC(2)-NY-ESO-1 (M)/TRICOM vaccine [180]	00803569, 00112957, 00887796, 00066729, 00291473	↓cancer cell expressing NY-ESO antigen	A cancer vaccine consisting of a replication-defective recombinant canarypox virus [ALVAC(2)] encoding the cancer-testis antigen NY-ESO and the TRIad of COstimulatory Molecules (B7-1, ICAM-1 and LFA-3; also called TRICOM), with potential immunostimulatory and antineoplastic activities. Upon administration, the vaccine may stimulate the host immune system to mount a cytotoxic T lymphocyte (CTL) response against NY-ESO-expressing cancer cells, which may result in the inhibition of tumor cell proliferation. NY-ESO-1, a tumor associated antigen (TAA), is found in normal testis and on the surface of various tumor cells, including bladder, breast, hepatocellular, melanoma, and prostate tumor cells. TRICOM may enhance antigen presentation and activate cytotoxic T-cells. In addition, ALVAC(2) encodes the vaccinia virus (VV) E3L and K3L genes, which may potentiate the translation of the NY-ESO and TRICOM genes.
catumaxomab [180] [Removab, anti-EpCAM x anti-CD3]	00377429, 00326885, 00836654, 00563836, 01246440, 00189345	↓tumor cells expressing EpCAM	Catumaxomab brings T cells, EpCAM-expressing epithelial tumor cells and APCs together into tricellular complexes, which may result in a potent cytotoxic T-lymphocyte (CTL) response against EpCAM-expressing epithelial tumor cells.
CDX1307 [180]	00709462, 00648102	↓tumor cells expressing hCG beta antigen	A human monoclonal antibody (B11) directed against the mannose receptor and linked to the beta-subunit of human chorionic gonadotropin (hCG beta) with potential immunostimulating and antineoplastic activities. The monoclonal antibody moiety of human monoclonal antibody B11-hCG beta fusion protein CDX1307 binds to mannose receptors on antigen presenting cells (APCs), including human dendritic cells (DCs) and macrophages. Upon internalization and processing, APCs present the processed hCG beta antigen on their cell surfaces, which may initiate an antibody-dependent cell-mediated cytotoxicity (ADCC) response against hCG beta-expressing tumor cells.
CDX-1401 [180]	00948961	↓tumor cells expressing NY-ESO-1 antigen	A fusion protein consisting of a fully human monoclonal antibody directed against the endocytic dendritic cell (DC) receptor, DEC-205, linked to the tumor-associated antigen (TAA) NY-ESO-1 with potential immunostimulating and antineoplastic activities. The monoclonal antibody moiety of DEC-205/NY-ESO-1 fusion protein CDX-1401 binds to the endocytic DC receptor, which may result in DC endocytic internalization of this agent, specifically delivering the NY-ESO-1 moiety. DC processing of NY-ESO-1 may boost the immune system to mount a cytotoxic T-lymphocyte response (CTL) against cancer cells expressing NY-ESO-1.
CHP-HER2 [115]	00291473, 00228358	↓tumor cells expressing HER2	CHP-HER2 vaccine, comprising truncated 146HER2 protein complexed with nanogels of cholesteryl pullulan (CHP), is a novel protein antigen vaccine that elicits 146HER2-specific CD8(+) and CD4(+) T-cell immune responses in patients with HER2-expressing tumors.
CRS-207 [180]	00585845	↓tumor cells expressing mesothelin	A recombinant Listeria-based cancer vaccine containing a live-attenuated strain of the facultative intracellular bacterium Listeria monocytogenes (Lm) expressing human mesothelin with potential immunostimulatory and antineoplastic activities. Upon administration of this vaccine, Listeria invade professional phagocytes within the immune system and express mesothelin, which may activate a cytotoxic T-lymphocyte (CTL) response against mesothelin-expressing tumor cells, resulting in tumor cell lysis.
DC vaccination	00703105	↓tumor cells	Information unknown/not publicly unavailable.

Continued on next page

Table A.1 – continued from previous page

Ovarian Cancer Drugs	NCT ID	Drug Effect	Mechanism of Action
DC-Ova [180]	00478452	↓tumor cells expressing TAA	Produced in vitro by pulsing autologous dendritic cells with killed autologous primary ovarian tumors as a source of tumor-associated antigens (TAAs); the pulsed DCs are then matured using various cytokines. Upon administration, the vaccine may stimulate a cytotoxic T lymphocyte (CTL) response against ovarian cancer TAA-expressing ovarian cancer cells.
DCVax-L	00683241, 00603460	↓tumor cells	Information unknown/not publicly unavailable.
dendritic cell/tumor fusion vaccine [180]	00799110	↓tumor cells	A therapeutic cancer vaccine consisting of autologous dendritic cells (DCs) fused with autologous tumor cells with potential immunostimulatory and antineoplastic activities.
DPX-0907 [180]	01095848	↓tumor cells expressing TAA	Lyophilized liposomal proprietary preparation comprised of 7 tumor-specific HLA-A2-restricted epitopes (TAAs): topoisomerase II alpha, B-cell receptor-associated protein 31 (CDM protein), TNF-alpha-converting enzyme (TACE/ADAM17), Abelson homolog 2 (Abl2), gamma catenin (Junction plakoglobin), epithelial discoidin domain receptor 1 (EDDR1) and integrin beta 8 subunit. Upon vaccination, the lyophilized antigen/adjuvant/liposome complex is resuspended in Montanide 1SA51 VG to create a depot effect, thereby presenting the TAAs to the immune system for a prolonged period of time. This may stimulate a potent cytotoxic T-lymphocyte (CTL) immune response against cancer cells that express these 7 TAAs and share epitopes with the vaccine epitope peptides, resulting in tumor cell lysis.
falimarev [180]	00091000	↓tumor cells expressing CEA- and MUC-1	A cancer vaccine comprised of a recombinant fowlpox viral vector encoding the carcinoembryonic antigen (CEA), MUC-1, a transmembrane glycoprotein secreted by glandular epithelial tissues, and TRICOM. This agent may enhance CEA and MUC-1 presentation to antigen-presenting cells (APC) and may activate a cytotoxic T-cell response against CEA- and MUC-1-expressing tumor cells.
FBP peptides ovarian cancer vaccine [180]	00373217	↓tumor cells expressing MAGE-A1:161-169, FBP:191-199, Her-2/neu:369-377, MAGE-A1:96-104, and Her-2/neu:754-762	A cancer vaccine containing multiple synthetic antigen peptides derived from MAGE-A1, Her-2/neu, and folate binding protein (FBP) with potential immunostimulating and antineoplastic properties. MAGE-A1, Her-2/neu, FBP peptides cancer vaccine includes the antigen peptides MAGE-A1:161-169, FBP:191-199, Her-2/neu:369-377, MAGE-A1:96-104, and Her-2/neu:754-762. Upon administration, this cancer vaccine may stimulate the immune system to mount a cytotoxic T-cell (CTL) response against tumor cells expressing these antigen peptides, resulting in tumor cell lysis.
HER-2/neu peptide vaccine [180]	00194714, 00373217, 00003002, 00005023	↓tumor cells expressing HER-2/neu	May induce antibodies with anti-tumor activity and may also elicit a specific CD8 T-cell response against specific tumor cell types.
herceptin [180] [trastuzumab]	00189579, 00433407, 00194714, 00028535	↓tumor cells expressing HER-2/neu	After binding to HER-2 on the tumor cell surface, trastuzumab induces an antibody-dependent cell-mediated cytotoxicity against tumor cells that overexpress HER-2.
IMF-001 [180]	01234012	↓tumor cells expressing NY-ESO-1 antigen	May stimulate the host immune system to mount a humoral and cytotoxic T-cell response against tumor cells expressing NY-ESO-1 antigen, resulting in tumor cell lysis.
inalimarev [180]	00091000	↓tumor cells expressing CEA- and MUC-1 antigen	May enhance CEA and MUC-1 presentation to antigen presenting cells (APC) and may activate a cytotoxic T lymphocyte (CTL) response against CEA- and MUC-1-expressing tumor cells.
ING-1 ING-1(heMAb) [221]	00051675	↓tumor cells expressing EpCAM	A human-engineered monoclonal antibody (MAb) that specifically targets the epithelial cell adhesion molecule (EpCAM), kills adenocarcinoma cells in vitro and inhibits tumor growth in vivo.
LMB-9 immunotoxin [180]	00005858	↓tumor cells expressing Lewis Y antigen	A recombinant disulfide stabilized anti-Lewis Y IgG immunotoxin containing a 38KD toxic element. LMB-9 immunotoxin attaches to tumor cells, facilitating he entry of the exotoxin. The exotoxin moiety induces caspase-mediated apoptosis of tumor cells via a mechanism involving mitochondrial damage.
MAGE-12 peptide vaccine [253]	00020267	↓tumor cells expressing MAGE-A12	Vaccine targeted at cells expressing MAGE-A12.
MAGE-A1 [52]	00373217	↓tumor cells expressing MAGE-A1	Vaccine targeted at cells expressing MAGE-A1.
MFE23 scFv-expressing autologous anti-CEA MFEz T lymphocytes [38]	01212887	↓tumor cells expressing CEA-antigen	Vaccine targeted at cells expressing CEA antigen.
MGAH22 [180]	01148849, 01195935	↓tumor cells expressing HER2	anti-HER2 monoclonal antibody. After binding to HER2 on the tumor cell surface, MGAH22 may induce an antibody-dependent cell-mediated cytotoxicity (ADCC) against tumor cells overexpressing HER2.
monoclonal antibody Hu3S193 [180]	00006099, 00617773, 01137071, 00072410	↓tumor cells expressing Lewis Y antigen	A humanized monoclonal antibody directed against the Lewis Y antigen, a tumor-associated epithelial antigen, with potential antineoplastic activity. Following binding, monoclonal antibody Hu3S193 triggers an antibody-dependent cell-mediated cytotoxicity in cells expressing Lewis Y antigen.

Continued on next page

Table A.1 – continued from previous page

Ovarian Cancer Drugs	NCT ID	Drug Effect	Mechanism of Action
MORAb-003 [180] [farletuzumab]	00318370, 00428766, 01018563, 00738699, 00849667, 01004380	↓tumor cells expressing GP-3	A humanized, immunoglobulin G1 monoclonal antibody. Farletuzumab specifically targets at glycoprotein 3 (GP-3), a cell surface antigen that is overexpressed on many epithelial-derived cancer cells. Upon binding to the GP-3 antigen, farletuzumab triggers a host immune response against GP-3 expressing cells resulting in cell lysis.
MT110 [180]	00635596	↓tumor cells expressing EpCAM	Directed against both CD3 and epithelial cell adhesion molecule (EpCAM). MT110 attaches to both CD3-expressing T lymphocytes and EpCAM-expressing tumor cells, thereby selectively cross-linking tumor and T lymphocytes; this may result in the recruitment of cytotoxic T lymphocytes (CTL) to T lymphocyte/tumor cell aggregates and the CTL-mediated death of EpCAM-expressing tumor cells.
MUC1 dendritic cell vaccine [180]	01068509	↓tumor cells expressing MUC1	MUC1 vaccine may induce the host immune system to mount a cytotoxic T cell response against MUC1-expressing tumor cells.
MUC1-KLH conjugate vaccine [180]	00006041	↓tumor cells expressing MUC1	Human tumor-associated antigen epithelial mucin (MUC1 antigen) conjugated with keyhole limpet hemocyanin (KLH). Result in stimulation of a cytotoxic T-lymphocyte (CTL) response against tumor cells expressing the MUC1 antigen.
MVF-HER-2(628-647)-CRL 1005 vaccine [181]	00017537	↓tumor cells expressing HER-2	Consists of a mutated HER-2 B-cell epitope, HER-2(628-647), and a promiscuous T cell epitope (amino acid sequence 288-302) of the measles virus fusion protein (MVF). Vaccination with this immunogen may stimulate the host immune response to mount a cytotoxic T-lymphocyte response against tumor cells that overexpress the HER-2 protein, resulting in tumor cell lysis.
tucotuzumab celmoleukin [180] [EMD 273066]	00408967, 00132522	↓tumor cells expressing EpCAM	A recombinant fusion protein comprised of a human monoclonal antibody directed against the epithelial cell adhesion molecule (EpCAM or KS) linked to an active interleukin-2 (IL2) molecule with potential antineoplastic activity. The humanized monoclonal antibody moiety of tucotuzumab celmoleukin recognizes and binds to EpCAM, a cell surface epithelial protein that is expressed on a wide variety of cancer cells, thereby concentrating IL2 in EpCAM-expressing tumor tissue. Subsequently, the localized IL2 moiety of this fusion protein may stimulate a cytotoxic T-cell antitumor immune response.
wild-type reovirus [180]	00602277, 01199263	↓tumor cells with activated Ras pathway	A serotype 3 Dearing strain (T3D) of reovirus (Respiratory Enteric Orphan virus) with potential oncolytic activity. Reovirus, a dsRNA virus, is able to replicate specifically in cancer cells bearing an activated Ras pathway. In contrast to normal cells, two-thirds of human cancer cells are Ras-activated. Unlike normal cells, Ras-activated tumor cells are deficient in host cellular protein kinase R (PKR) activity and so are unable to mount an antiviral response. In Ras-activated tumor cells, reovirus freely replicates and induces apoptosis; tumor cell lysis frees progeny viral particles to infect surrounding tumor cells. A cycle of infection, replication and cell death may continue until Ras-activated tumor cells are eradicated.
yttrium Y 90 monoclonal antibody HMFG1 [181]	00004115	↓tumor cells expressing MUC1	A radioimmunoconjugate of humanized monoclonal antibody (MoAb) HMFG1 labeled with Yttrium 90 (Y-90). MoAb MFG1 was raised against Human Milk Fat Globules and reacts with an epitope (PDTR) in the protein core of MUC1 mucins, which are up-regulated in human breast and other carcinomas.Y-90 MoAb HMFG1 delivers beta particle emitting Y-90 radionuclide directly to tumor cells that express MUC1, thereby this agent may be used in radioimmunotherapy of cancers.
ZYC300 [180]	00381173	↓tumor cells expressing CYP1B1	Vaccination with ZYC300 may stimulate the immune system to elicit a cytotoxic T lymphocyte (CTL) response against the tumor-associated antigen (TAA) CYP1B1, which may result in the lysis of tumor cells expressing CYP1B1 overexpressed in many cancers with only restricted expression in normal tissues.
Ad5-delta24RGD [181]	00562003	↓cancer cell expressing RGD-4C antigen	Oncolytic adenovirus Ad5-Delta 24RGD contains an integrin binding RGD-4C motif, allowing Coxsackie adenovirus receptor-independent infection of tumor cells, which are often deficient for Coxsackie and adenovirus receptors (CARs).
EC145 [180]	00722592, 01170650, 00507741	↓tumor cells expressing folic acid receptors	Consist of folate and the vinca alkaloid desacetylvinblastine monohydrazide (DAVLBH). The folate moiety of EC145 binds to folic acid receptors on the tumor cell surface and the agent is internalized via folate receptor-mediated endocytosis, delivering the tubulin-binding DAVLBH moiety directly into the tumor cell; DAVLBH binding to tubulin results in the disruption of microtubule assembly-disassembly dynamics, cell cycle arrest, and tumor cell apoptosis.
EC20 [180]	00722592, 01170650	↓tumor cells expressing folic acid receptors	A folate receptor-targeting radiopharmaceutical consisting of a folate-containing tetrapeptide chelator to which technetium Tc 99m is linked. The folate component of folate receptor-targeted technetium Tc 99m EC20 binds to folic acid receptors, which are frequently upregulated in many types of tumor cells and activated macrophages.
EMD525797 [180]	00848510	↓active alphavbeta3 integrin	A chimeric antibody which includes the antigen binding sites of the anti-integrin mouse antibody 17E6, binds to and inhibits the activity of alphavbeta3 integrin (vitronectin receptor).

Continued on next page

Table A.1 – continued from previous page

Ovarian Cancer Drugs	NCT ID	Drug Effect	Mechanism of Action
NGR--hTNF [180]	00484432	↓cells expressing CD13	Consists of cytokine-peptide of cytokine tumor necrosis factor alpha (TNF-alpha) and peptide CNGRC. The peptide moiety CNGRC, a ligand for the membrane-bound metalloprotease CD13, binds to endothelial cells of the angiogenic vasculature that express CD13 (also known as aminopeptidase N); subsequently, the TNF-alpha moiety induces apoptosis in endothelial cells expressing CD13, thereby inhibiting tumor-associated angiogenesis.
OCPM immunotherapeutic vaccine [180] [IMT-1012]	00437502	↓cells expressing TAA	Contains twelve different synthetic peptides or tumor associated antigens (TAAs), including cyclin I (CCNI), cyclin-dependent kinase CDC2, EDDRI and TACE/ADAM17, each of which is involved in a different pathway associated with tumor growth, survival, and metastasis. Each antigen in the vaccine elicits a specific cytotoxic T-lymphocyte (CTL) immune response against tumor cells expressing that antigen.
oregovomab [180]	00004064, 00551265, 00003634, 00086632, 00050375, 00034372, 00034138	↓cells expressing CA125	A murine monoclonal antibody that attaches to the tumor-associated antigen CA125. Vaccination with monoclonal antibody B43.13 may stimulate a host cytotoxic immune response against tumor cells that express CA125.
ovarian cancer peptide vaccine [180]	00091273	↓cells expressing related ovarian cancer cell antigen	A cancer vaccine comprised of synthetic peptides corresponding to naturally-occurring peptides derived from ovarian cancer cell antigens. Ovarian cancer peptide vaccine may elicit a cytotoxic T-cell response against tumor cells expressing the related ovarian cancer cell antigens.
OVax [180]	00660101	↓cells expressing related ovarian cancer cell antigen	A cancer vaccine consisting of autologous ovarian cancer cell peptide antigens conjugated to the hapten 2,4-dinitrophenol (DNP) with potential immunostimulating and antineoplastic activities. Administration of autologous dinitrophenyl-modified ovarian cancer vaccine may induce a cytotoxic T-lymphocyte (CTL) response against ovarian cancer cells.
p53 synthetic long peptides vaccine [180] [Ad5CMV-p53, SCH-58500]	00003588, 00019084, 00001827, 00019916, 00844506, 00003880, 00002960	↓cells expressing p53	The host cytotoxic T lymphocytes (CTL) are directed against p53-positive tumor cells, which may result in tumor cell death and decreased tumor growth.
pNGVL3-hICD vaccine [180]	00436254	↓tumor cells expressing HER-2	Expresses the HER-2/neu protein, which, after intracellular processing, may elicit both antigen-specific cytotoxic T-lymphocyte (CTL) and humoral immune responses against tumor cells expressing HER-2.
PSMA/PRAME [180]	00423254	↓tumor cells expressing PRAME and PSMA	A cancer vaccine consisting of a DNA plasmid encoding epitopes of the human preferential antigen of melanoma (PRAME) and the prostate specific membrane antigen (PSMA) with potential immunostimulating activity. Upon direct administration of this vaccine into lymph nodes, peptides expressed by DNA plasmid vector pPRA-PSM may activate the immune system, resulting in a cytotoxic T-lymphocyte (CTL) response against PRAME- and PSMA-expressing cells.
indium In 111 folic acid [167]	00003763	↓tumor cells expressing folate receptor	Radiopharmaceutical for targeting tumor-associated folate receptors.
iodine I 131 monoclonal antibody 3F8 [180]	00445965	↓tumor cells expressing GD2	A radioimmunoconjugate consisting of 3F8, a murine anti-GD2 ganglioside monoclonal antibody labeled with iodine 131 (I-131), with radioimaging and radioimmunotherapeutic properties. Using monoclonal antibody 3F8 as a carrier for I-131 results in the targeted imaging and/or destruction of cells expressing GD2.
ras peptide cancer vaccine [180]	00019084	↓tumor cells expressing ras	Mutant ras oncogenes produce novel proteins that are processed and displayed through HLA molecules on tumor cells. Vaccine is targeted at tumour cells carrying the ras mutation.
recombinant fowlpox-CEA6D/TRICOM vaccine [180]	00028496, 00027534	↓tumor cells expressing CEA	A cancer vaccine comprised of a recombinant fowlpox virus vector encoding the carcinoembryonic antigen (CEA) and a TRIad of COstimulatory Molecules (B7-1, ICAM-1 and LFA-3) (TRICOM). This agent may enhance CEA presentation to antigen presenting cells (APC) and activate cytotoxic T-cells against CEA-expressing tumors.
SS1(dsFv)-PE38 [180] [SS1P]	00024674, 00024687, 00006981, 00066651	↓cells expressing mesothelin	The single chain anti-mesothelin monoclonal antibody SS1(dsFv) link to Pseudomonas exotoxin PE38. The antibody moiety binds to cells that express mesothelin, a cell surface glycoprotein which may be overexpressed in ovarian cancer, mesotheliomas, and some squamous cell carcinomas; after internalization, the exotoxin moiety inactivates eukaryotic translation elongation factor 2, thereby disrupting tumor cell protein synthesis.
AEZS-108 [180]	00569257	↓GnRH-1R, ↓DNA	Binds to GnRH-1Rs, which may be highly expressed on endometrial and ovarian tumor cell membrane surfaces, and is internalized. Once inside the cell, the doxorubicin moiety of this agent intercalates into DNA and inhibits the topoisomerase II activity, which may result in the inhibition of tumor cell DNA replication and tumor cell proliferation.
177Lu-J591 [20]	00967577	↓cells expressing PSMA	Made up of two compounds called J591 and 177Lutetium (177Lu) that are joined together. J591 is a monoclonal antibody, or a type of protein. 177Lu is a radioactive molecule J591 attaches to a protein called prostate specific membrane antigen (PSMA).

Continued on next page

Table A.1 – continued from previous page

Ovarian Cancer Drugs	NCT ID	Drug Effect	Mechanism of Action
abagovomab [180]	00058435, 00418574	↓tumor cells expressing CA-125	A murine IgG1 monoclonal anti-idiotype antibody. With a variable antigen-binding region that acts as a surrogate antigen for CA-125, abagovomab may stimulate the host immune system to elicit humoral and cellular immune responses against CA-125-positive tumor cells, resulting in inhibition of tumor cell proliferation.
AGS-8M4 [180]	01016054, 00816764	↓tumor cells expressing AGS-8	A humanized monoclonal antibody. Selectively binds to AGS-8 (the activator of g-proteins signaling (AGS) cell surface protein), triggering complement-dependent cell lysis and antibody-dependent cell-mediated cytotoxicity in tumor cells expressing AGS-8.
alemtuzumab [180]	00109993, 00410657, 00637390	↓cells expressing CD52	A recombinant DNA-derived humanized monoclonal antibody directed against the cell surface glycoprotein CD52. Selectively binds to CD52, thereby triggering a host immune response that results in lysis of CD52+ cells.
BB-10901 [180]	00346385	↓tumor cells expressing CD56 antigen, ↓microtubule	Consist of monoclonal antibody (huN-901) and DMI. the antibody moiety selectively attaches to CD56 antigen, a neural cell adhesion molecule (NCAM)) expressed on the surface of cells of small cell lung cancer (SCLC) and other neuroendocrine (NE) tumors. Thus, the DMI conjugate is targeted specifically to CD56-expressing tumor cells, where it inhibits tubulin polymerization and assembly, resulting in inhibition of mitosis and cell cycle arrest in the S phase.
CC49 [180]	00002734	↓carcinoma cell expressing TAG72	Based on the antibody B72.3 that is directed against tumor-associated glycoprotein 72 (TAG72), which is expressed by gastric, breast, pancreatic, colorectal, and ovarian carcinoma cells.
amatuximab [180] [MORAb-009]	00325494	↓tumor cells expressing mesothelin	Binds to mesothelin, triggering an antibody dependent cellular cytotoxicity (ADCC)-mediated host immune response against mesothelin-expressing tumor cells, which may result in tumor cell lysis.
recombinant fowlpox GM-CSF vaccine adjuvant [180]	00028496	↓tumor cells expressing GM-CSF	A cancer vaccine adjuvant consisting of a recombinant fowlpox virus encoding human granulocyte-macrophage colony-stimulating factor (GM-CSF). GM-CSF binds to specific cell surface receptors on various immuno-hematopoietic cell types, enhancing their proliferation and differentiation and stimulating macrophage and dendritic cell functions in antigen presentation and antitumor cell-mediated immunity. Administration of recombinant fowlpox GM-CSF vaccine adjuvant may induce an immune response against tumor cells.
mutant p53 peptide pulsed dendritic cell vaccine [180]	00019084	↓tumor cells expressing mutant p53	A cancer vaccine consisting of autologous dendritic cells which have been pulsed with a mutant p53 peptide. Vaccination with mutant p53 peptide pulsed dendritic cells may stimulate the host immune system to mount a cytotoxic T lymphocyte (CTL) response against tumor cells expressing mutant p53, resulting in tumor cell lysis.
autologous tumor cell vaccine [180]	00004021, 00003386	↓tumor cells expressing TAA	A therapeutic agent produced by isolating tumor cells from an individual and processing these tumor cells into a vaccine formulation in vitro; the vaccine is then administered to the individual from whom the tumor cells were isolated. Typically combined with an adjuvant immunostimulant, an autologous cell vaccine may elicit a cytotoxic T-lymphocytic immune response to cell surface-expressed tumor-associated antigens (TAAs), resulting in tumor cell death.
tumor vaccine ALVAC-hB7.1 [180]	00004032	↑HLA class I, ↑HLA class II, ↑CD54, ↑CD80	A vaccine comprise of a canarypox viral vector that carries the gene for human B7.1 (CD80 antigen), which stimulates increased expression of HLA class I and class II, CD54 (ICAM), and CD80. Increased expression of these proteins by this autologous cell line may activate an antitumor T-cell response.
polyvalent antigen-KLH conjugate vaccine [180]	00857545, 00693342, 01223235	↓tumor cells expressing globo H, GM2 ganglioside, Tn-MUC1, TF, or sTn	A multivalent cancer vaccine comprised of the five tumor-associated antigens (TAAs) globo H, GM2 ganglioside, Tn-MUC1, TF, and sTn conjugated with the immunoadjuvant keyhole limpet hemocyanin (KLH), with potential antineoplastic activity. Upon administration, polyvalent antigen-KLH conjugate vaccine may induce production of IgG and IgM antibodies and antibody-dependent cell-mediated cytotoxicity (ADCC) against tumor cells expressing these TAAs, resulting in tumor cell death and tumor growth inhibition.
General Immune Response			
keyhole limpet hemocyanin [180]	00023634	?	Immunogenic carrier protein that, in vivo, increases antigenic immune responses to haptens and other weak antigens such as idiotype proteins.
OPT-821 [180]	01223235, 00693342, 00857545	?	A purified, natural saponin isolated from the soapbark tree Quillaja saponaria Molina with potential immunoadjuvant activity. When co-administered with vaccine peptides, OPT-821 may increase the antibody and cytotoxic T-cell responses against the targeted antigen(s).
PV701 [196]	00055705	?	Highly purified, replication-competent naturally attenuated strain of Newcastle disease virus, an avian paramyxovirus. PV701 directly lyses diverse human cancer cells in vitro (oncolytic) while being significantly less toxic toward normal human cells. In addition to its direct oncolytic properties, PV701 is capable of stimulating T-cell-mediated specific antitumor immunity and nonspecific activation of immune function, including interferon release and activation of tumoricidal macrophages.

Continued on next page

Table A.1 – continued from previous page

Ovarian Cancer Drugs	NCT ID	Drug Effect	Mechanism of Action
QS21 [180]	00006041	?	A purified, natural saponin isolated from the soapbark tree Quillaja saponaria Molina with potential immunoadjuvant activity. When co-administered with vaccine peptides, QS21 may increase total antitumoral vaccine-specific antibody responses and cytotoxic T-cell responses.
tetanus toxoid helper peptide [180]	00027534, 00091273	?	Obtained by genetic engineering from the bacterial Clostridium tetani toxoid, tetanus toxoid helper peptide QYIKANSKFIGITEL (amino acids 830-844) binds to class II MHC molecules as a nonspecific vaccine helper epitope (adjuvant) and induces an increased (and long term) immune response by increasing the helper T-cell response.
therapeutic allogeneic lymphocytes [180]	00019136, 00060372, 00068718, 00096161	?	A population of lymphocytes isolated from an individual, altered in vitro, and returned to the same individual for therapeutic purposes.
therapeutic autologous lymphocytes [180]	00004021, 00562640, 00019084, 00004178	?	A population of lymphocytes isolated from an individual, altered in vitro, and returned to the same individual for therapeutic purposes.
AlloStim [180]	01065441	↑IFN-γ, ↑TNF-β, ↑IL2	Consist of allogeneic, differentiated Th1-like T cells and T cell-stimulating monoclonal antibodies. Stimulated by the microparticle-bound monoclonal antibodies, the infused T cells produce pro-inflammatory, anti-tumor cytokines such as like IFN-γ, TNF-β, and IL2, disabling tumor immune avoidance mechanisms and stimulating the host immune system to both reject the infused T cells and kill tumor cells.
incomplete Freund's adjuvant [31] [Montanide ISA-51]	00091273, 00066729, 00887796, 00020267	↑TNFα	Induces expression of cytokines, predominantly tumor necrosis factor α (TNFα) in regional lymph nodes, and causes opening of the blood-brain barrier.
therapeutic tumor infiltrating lymphocytes [180]	00019084	?	A preparation of cells, consisting of autologous tumor infiltrating lymphocytes, that are manipulated in vitro and, upon administration in vivo, re-infiltrate the tumor to initiate tumor cell lysis. In vitro, therapeutic tumor-infiltrating lymphocytes (TILs) are isolated from tumor tissue and cultured with lymphokines such as interleukin-2; the therapeutic TILs are then infused into the patient, where, after re-infiltration of the tumor, they may induce lysis of tumor cells and tumor regression.
MAPK-PI3K (Hatakeyama et. al)			
TLN-4601 [180][42] [diazepinomicin, ECO-4601]	00338026	↓Raf1	Degrades Raf-1 protein through a proteasomal-dependent mechanism
ISIS 5132 [61]	00003892	↓Raf1	Binds to Raf mRNA to downregulate Raf expression.
lapatinib [203] [GW572016]	00317434, 00888810, 00316407, 00436644, 00113373, 00313599, 00447226	↓phosphorylated EGFR, ↓phosphorylated ErbB2, ↓phosphorylated ErbB4	Bind to ATP-binding site of EGFR, ErbB2, ErbB4, preventing its autophosphorylation.
perifosine [133]	00431054	↓Akt:PIP, ↓Akt:PIPP, ↓Akt:PIP3	Bind to lipid binding PH domain of Akt.
PF-05212384 [261] [PKI-587]	00940498	↓active mTOR, ↓active PI3K	Inhibits both PI3K and mTOR kinases, which may result in apoptosis and growth inhibition of cancer cells overexpressing PI3K/mTOR.
PKI-179 [180]	00997360	↓active mTOR, ↓active PI3K	Small-molecule mimetic of ATP that targets the mammalian target of rapamycin (mTOR). PKI-179 selectively inhibits mTOR and phosphoinositide-3-kinase (PI3K) alpha.
selumetinib [285] [AZD6244]	00551070	↓MEKPP	Bind and lock MEK into inactive conformation.
sorafenib [276] [Nexavar, BAY43-9006]	00526799, 00096395, 01047891, 00436215, 00390611, 00791778, 00522301, 00096200, 00093626, 00245102, 00098592	↓active Raf	Bind to ATP-binding site of Raf, preventing activation of Raf.
XL147 [180]	00756847	↓active PI3K	Bind to ATP-binding site of PI3K, preventing activation of PI3K.
BKM120 [180]	01068483	↓active PI3K	PI3K inhibitor BKM120 specifically inhibits class I PI3K in the PI3K/AKT kinase (or protein kinase B) signaling pathway in an ATP-competitive manner, thereby inhibiting the production of the secondary messenger PIP3 and activation of the PI3K signaling pathway.
Other Signaling Pathways			
7-hydroxystaurosporine [159]	00072267, 00045175, 00031681, 00047242	↓active PKC	target PKC ATP binding sites.
852A [180]	00319748	↑active TLR7	Toll-like receptor 7 (TLR7) agonist. Binds to and activates TLR7, thereby stimulating plasmacytoid dendritic cells (pDC) through the TLR7-MyD88-dependent signaling pathway.
A6 [180] [urokinase-derived peptide]	00939809, 00083928	↓uPA:uPAR	Inhibits the interaction of uPA with its receptor uPAR.
ABT-263 [257]	00891605	↓Bcl-2/Bcl-xL:pro-death proteins (e.g., Bim)	Potent, orally bioavailable Bad-like BH3 mimetic. Disrupts Bcl-2/Bcl-xL interactions with pro-death proteins (e.g., Bim), leading to the initiation of apoptosis.
acetyl-L-carnitine [249] [ALC]	00751205	↑NGFR	Stimulates NGFR expression.

Continued on next page

Table A.1 – continued from previous page

Ovarian Cancer Drugs	NCT ID	Drug Effect	Mechanism of Action
ADH-1 [180] [Exherin]	00265057	↓N-cadherin	Selectively and competitively binds to and blocks N-cadherin, which may result in disruption of tumor vasculature, inhibition of tumor cell growth, and the induction of tumor cell and endothelial cell apoptosis.
aflibercept [180] [AVE0005, VEGF trap]	00327444, 00436501, 00327171, 00396591	↓VEGF:VEGFR	Functioning as a soluble decoy receptor, binds to pro-angiogenic vascular endothelial growth factors (VEGFs), thereby preventing VEGFs from binding to their cell receptors.
AFP464 [180]	00348699	↑aminoflavone	Rapidly converted to aminoflavone in plasma. Aminoflavone activates the aryl hydrocarbon receptor (AhR) signaling pathway leading to an increase in cytochrome expression. Subsequently, aminoflavone is metabolized to toxic metabolites by the cytochromome P450 enzymes that it induces; these toxic metabolites covalently bind to DNA, resulting in the phosphorylation of p53, the induction of the p53 downstream target p21Waf1/Cip1, and apoptosis.
aldesleukin [180] [interleukin 2]	00004021, 00652899, 00019916, 00019136, 01212887, 00003408, 00019084, 00020163, 00020267	↑active IL2 receptor	Binds to and activates the IL2 receptor.
alendronate [180]	00593580	↓active geranyltranstransferase	Binds to and inhibits the activity of geranyltranstransferase, an enzyme involved in terpenoid biosynthesis, leading to the inhibition of biosynthesis of isoprenoid lipids (FPP and GGPP) that are donor substrates of farnesylation and geranylgeranylation during the post-translational modification of small GTPase signalling proteins, which is important in the process of osteoclast turnover.
allopurinol [180]	00652899	↓active xanthine oxidase	Inhibits xanthine oxidase, an enzyme that converts oxypurines to uric acid.
alvespimycin hydrochloride [180]	00089362	↓active Hsp90	Binds to hsp90, a chaperone protein that aids in the assembly, maturation and folding of proteins. Subsequently, the function of Hsp90 is inhibited, leading to the degradation and depletion of its client proteins such as kinases and transcription factors involved with cell cycle regulation and signal transduction.
alvocidib [180]	00083122, 00957905	↓phosphorylated CDKs	As an inhibitor of cyclin-dependent kinase, alvocidib induces cell cycle arrest by preventing phosphorylation of cyclin-dependent kinases (CDKs) and by down-regulating cyclin D1 and D3 expression, resulting in G1 cell cycle arrest and apoptosis.
AMG 386 [180]	00770536, 01204749, 01253681, 00479817	↓angiopoietin 1/2:tie2 receptors	Targets and binds to angiopoietin1 and 2, thereby preventing the interaction of the angiopoietins with their target tie2 receptors, inhibiting angiogenesis and may eventually lead to an inhibition of tumor cell proliferation.
AMG 479 [180] [ganitumab]	00719212, 00819169, 00718523	↓IGF:IGFR	Binds to membrane-bound IGF-1R, preventing binding of the ligand IGF-1 and the subsequent triggering of the PI3K/AKT signaling pathway.
conatumumab [180] [AMG 655]	00819169	↑active TR-2	A fully human monoclonal agonist antibody. Conatumumab mimics the activity of native TRAIL, binding to and activating TR-2.
amifostine trihydrate [180]	00003136, 00003072, 00004166, 00003624, 00003425, 00078845, 00003657, 00003269, 00003926, 00003811	↓cisplatin platinum-containing metabolites	After dephosphorylation of amifostine by alkaline phosphatase to an active free sulfhydryl (thiol) metabolite, the thiol metabolite binds to and detoxifies cytotoxic platinum-containing metabolites of cisplatin and scavenges free radicals induced by cisplatin and ionizing radiation.
anastrozole [180] [arimidex]	00181688	↓active aromatase	Selectively binds to and reversibly inhibits aromatase, a cytochrome P-450 enzyme complex.
angiotensin 1-7 [224] [180]	00771810, 00974545	↑active Mas	A synthetic heptapeptide identical to endogenous angiotensin-(1-7) which binds and activates the angiotensin-(1-7) receptor Mas.
AMG 102 [216]	01039207	↓HGF/SF:cMet receptor	Novel, fully human monoclonal antibody that selectively targets hepatocyte growth factor/scatter factor (HGF/SF), the only ligand for the c-Met receptor, potentially inhibiting tumor cell proliferation, survival, and invasion.
antineoplaston AS2-1 [180]	00003532	↓tumor-cell proteins	Inhibits the incorporation of L-glutamine into tumor-cell proteins, leading to cell cycle arrest in the G1 phase and inhibition of mitosis.
aprepitant [180]	01012336, 01017809, 00293384	↓substance P:substance P/neurokinin 1 receptor	Crossing the blood brain barrier, aprepitant binds selectively to the human substance P/neurokinin 1 receptor in the central nervous system (CNS), thereby inhibiting receptor binding of endogenous substance P.
aromasin [180] [exemestane]	00261027	↓active aromatase	Binds irreversibly to and inhibits the enzyme aromatase, thereby blocking the conversion of cholesterol to pregnenolone and the peripheral aromatization of androgenic precursors into estrogens.
arsenic trioxide [292]	00024258	↓oligomerated PML	Binds directly to cysteine residues in zinc fingers located within the RBCC domain of PML-RARα and PML. Arsenic binding induces PML oligomerization, which increases its interaction with the small ubiquitin-like protein modifier (SUMO)Ű conjugating enzyme UBC9, resulting in enhanced SUMOylation and degradation.
arzoxifene hydrochloride [246]	00190697, 00003670, 00253539	↓estrogen: estrogen receptor	Potent estrogen antagonist in mammary and uterine tissue while it acts as an estrogen agonist to maintain bone density and to lower serum cholesterol.
atrasentan hydrochloride [180]	00653328	↓endothelin-A:endothelin-A receptor	As a selective antagonist of the endothelin-A (ETA) receptor, atrasentan binds selectively to the ETA receptor, which may result in inhibition of endothelin-induced angiogenesis and tumor cell proliferation.

Continued on next page

Table A.1 – continued from previous page

Ovarian Cancer Drugs	NCT ID	Drug Effect	Mechanism of Action
avastin [180] [bevacizumab]	00945139, 00127920, 00856180, 00545792, 00511992, 00652119, 00520013, 00583622, 00130520, 01091259, 00097019, 00748657, 01131039, 00483782, 00126542, 00343044, 00072566, 00407563, 00434642, 00698451, 00436215, 01031381, 00262847, 00565851, 00951496, 00079430, 01010126, 00989651, 00886691, 00022659, 00085358, 00504257, 01223235, 00792545, 00737243, 00098592, 00267696, 00846612, 00866723, 00976911, 01239732, 00937560, 01202890, 01081262, 00744718, 00129727, 01146795, 01219777, 01097746, 00408070, 00523809, 00959647, 00588237, 00418093, 00868192, 00296816, 01132014	↓VEGF:VEGFR	A recombinant humanized monoclonal antibody directed against, binds to VEGF and inhibits VEGF receptor binding, thereby preventing the growth and maintenance of tumor blood vessels.
saracatinib [90] [AZD0530]	01000896, 00475956, 01196741	↓active Src kinase	ATP-competitive inhibitor of Src kinase
cediranib maleate [180] [AZD2171]	00275028, 00475956, 00532194, 01116648, 01065662, 00544973, 00278343, 01115829, 01131234, 00354848	↓VEGF:VEGFR	Competing with adenosine triphosphate, cediranib binds to and inhibits all three vascular endothelial growth factor receptor (VEGF-1,-2,-3) tyrosine kinases, thereby blocking VEGF-signaling, angiogenesis, and tumor cell growth.
BCG vaccine [50]	00003386	↓fibronectin: tumor proteases	By binding near the carboxyl terminal region and adjacent to the heparin-binding domain of the fibronectin molecule, BCG may protect this region of the molecule from tumor proteases, and may thus allow the antitumor activity of the host immune cells to take place.
beclomethasone dipropionate [282]	00010283	↑active glucocorticord receptor	Binds to the glucocorticoid receptor activating it.
BI 2536 [180]	00526149	↓active Polo-like kinase 1 (Plk1)	Binds to and inhibits Polo-like kinase 1 (Plk1).
BI 6727 [180]	01121406	↓active Polo-like kinase 1 (Plk1)	Selectively inhibits Polo-like kinase 1(PIk1).
BIBF 1120 [101]	01015118, 00710762	↓active VEGFR, ↓active FGFR, ↓active PDGFR	Inhibitor of VEGFR, FGFR and PDGFR kinase. Binds to the ATP-binding site in the cleft between the NH2 and COOH terminal lobes of the kinase domain.
bicalutamide [180]	00012090	↓androgen: androgen receptor	Competitively binds to cytosolic androgen receptors in target tissues, thereby inhibiting the receptor binding of androgens.
bryostatin 1 [134]	00006942, 00004008	↑active PKC (short term), ↓PKC (long term)	Bryostatin-1 is a macrocyclic lactone derived from a marine invertebrate that binds to the regulatory domain of protein kinase C. Short-term exposure to bryostatin-1 promotes activation of PKC, whereas prolonged exposure promotes significant downregulation of PKC.
carboxyamidotriazole [180]	00019461, 00019019	↓intracellular Ca^{2+}	Binds to and inhibits non-voltage-operated Ca^{2+} channels, blocking both Ca^{2+} influx into cells and Ca^{2+} release from intracellular stores.
carfilzomib [180]	00531284	↓active 20S proteasome	Irreversibly binds to and inhibits the chymotrypsin-like activity of the 20S proteasome, an enzyme responsible for degrading a large variety of cellular proteins.
CBT-1 [180]	00972205	↓active MDR efflux pump P-glycoprotein	Binds to and inhibits the MDR efflux pump P-glycoprotein (P-gp), which may inhibit the efflux of various chemotherapeutic agents from tumor cells and reverse P-gp-mediated tumor cell MDR.
temsirolimus [209] [CCI-779]	00523432, 00926107, 01196429, 01010126, 00429793, 00408655, 01065662, 01155258, 00982631	↓active mTOR	Inhibition of mTOR by temsirolimus requires a specific binding complex. Temsirolimus forms this complex with the FK506-binding protein and prohibits the activation of mTOR.
celecoxib [180]	01124435, 01175772, 00084370, 00084448, 00093678, 00538031	↓active COX-2	Selectively inhibits cyclo-oxygenase-2 activity (COX-2).
cetuximab [21]	00082212, 00063401, 00086892	↓dimerized EGFR	EGFR inhibitor. Cetuximab is a human:mouse chimeric monoclonal antibody that binds with high specificity to the extracellular domain of EGFR and prevents receptor dimerization and signalling.
cholecalciferol [180]	00593580	↑active vitamin D receptor	The active form of cholecalciferol, calcitriol plays an important role in maintaining blood calcium and phosphorus levels and mineralization of bone, which binds to vitamin D receptors and modulates gene expression, leading to an increase in serum calcium concentrations by increasing intestinal absorption of phosphorus and calcium, promoting distal renal tubular reabsorption of calcium and increasing osteoclastic resorption.
siltuximab [291] [CNTO 328, CCLB8]	00841191	↑IL6:IL6R	A human-mouse chimeric MAb to IL6 (K(d) approx. 10(-12) M) that inhibits IL6 function.
CP-547,632 [25]	00096239, 00074867	↓active VEGFR-2	An ATP competitive kinase inhibitor that blocks VEGFR-2-2 kinase autophosphorylation and VEGF-induced VEGFR-2 phosphorylation.
CS-1008 [180]	00945191	↑active TRAIL-R2	Mimicking the natural receptor ligand TRAIL, CS-1008 binds to TRAIL-R2(human tumor necrosis factor-related apoptosis-inducing ligand receptor 2), activating signal transduction pathways that may result in tumor cell apoptosis and a reduction in tumor growth.
custirsen sodium [51] [OGX-011]	00471432	↓clusterin	A 2′-methoxyethyl modified phosphorothioate antisense oligonucleotide that is complementary to clusterin mRNA.

Continued on next page

Table A.1 – continued from previous page

Ovarian Cancer Drugs	NCT ID	Drug Effect	Mechanism of Action
cyclosporine [153] [cyclosphorin A]	01105650, 00096161	↓active calcineurin	Complexes cyclophilin-CsA and FKBP-FK506 competitively bind to and inhibit the Ca^{2+}- and calmodulin-dependent phosphatase calcineurin, although the binding and inhibition of calcineurin do not require calmodulin.
dalteparin [180] [104]	00239980	↓thrombin	A synthetic heparin, dalteparin binds to antithrombin and enhances the inhibition of Factor Xa (thrombin).
dasatinib [227] [BMS-354825]	00672295, 00671788, 00792545, 00788125	↓active SRC, ↓active ABL	A small-molecule, ATP-competitive inhibitor of SRC and ABL tyrosine kinases with potency in the low nanomolar range.
deferasirox [180]	00602446, 01159067	↓Fe^{2+}	A synthetic, orally bioavailable, achiral, tridentate triazole derived from salicylic acid with iron-chelating activity.
denileukin diftitox [180] [ontak]	00703105, 00880360, 00357448, 00228358	↓active EF-2	Consists of interleukin-2 (IL-2) protein sequences fused to diphtheria toxin. The IL-2 protein sequence moiety directs the cytocidal action of diphtheria toxin to cells that express IL-2 receptors; After the toxin moiety is internalized into target IL-2 receptor-expressing cells, its catalytic domain catalyzes the transfer of the ADP-ribose moiety of NAD to a posttranslationally modified histidine residue of elongation factor 2 (EF-2), called diphthamine. This covalent modification inactivates EF-2 and disrupts polypeptide chain elongation, resulting in cell death.
dexamethasone [234]	00817479, 01012336, 00003449, 00293384, 01110135, 00016380	↑active glucocorticoid receptor	Binds and activate glucocorticoid receptors.
dimesna [85]	00003569	↓acrolein	Converted into reactive thiol form (Mesna) which binds and detoxify acrolein.
dipyridamole [180]	00002487	↓adenosine	Inhibits adenosine uptake by platelets and endothelial cells, triggering an accumulation of cyclic adenosine monophosphate (cAMP), and inhibiting the stimulation of platelet aggregation by agents such as platelet activating factor and collagen.
DTA-H19 [180]	00826150	↓active EF-2	A plasmid DNA encoding the A chain of the diphtheria toxin (DT-A) which catalyzes ADP-ribosylation of translation elongation factor 2 (EF-2). This covalent modification inactivates EF-2 and disrupts polypeptide chain elongation, resulting in cell death.
E7080 [180]	01133756	↓VEGF:VEGFR2	Blocks VEGFR2 activation by VEGF, resulting in inhibition of the VEGF receptor signal transduction pathway, decreased vascular endothelial cell migration and proliferation, and vascular endothelial cell apoptosis.
EGEN-001 [180] [phIL-12-005/PPC]	00473954, 01118052, 00137865	↑IL12	Consist of a plasmid DNA encoding the human gene for interleukin 12 (IL12) and is designed to increase the local concentration of IL12 in the tumor microenvironment.
EGFR antisense DNA [180]	00023634	↓EGFR	A synthetic sequence of DNA constructed in the antisense orientation to a sequence of DNA in epidermal growth factor receptor (EGFR), a member of the erbB gene family. EGFR antisense DNA suppresses the expression of EGFR by tumor cells, thereby inhibiting tumor cell proliferation and decreasing tumor growth.
elesclomol sodium [281]	00888615	↓Cu^{2+}, ↓Ni^{2+}	Cu^{2+} and Ni^{2+} to a lesser degree favor the formation of chelating complexes with elesclomol.
matuzumab [180] [EMD 72000]	00073541	↓EGF:EGFR	Binds to the epithelial growth factor receptor (EGFR) on tumor cells and blocks growth signals.
ENMD-2076 [142]	01104675, 00658671	↓active aurora A, ↓active aurora B, ↓active SRC kinase, ↓active KIT kinase, ↓active PTK2 kinase, ↓active VEGFR2 kinase	Selectively binds to and inhibits non-specified tyrosine kinases (SRC, KIT, PTK2, VEGFR2) and Aurora kinases (AKs) A and B.
enzastaurin hydrochloride [180]	00391118, 00420381, 00407758	↓active PKCβ	Binding to the ATP-binding site, enzastaurin selectively inhibits protein kinase C β.
EPO [180] [epoetin α]	00517621, 00270166, 00189371	↑EPO:EPO receptor	Produced primarily by cells of the peritubular capillary endothelium of the kidney in response to hypoxia, circulating EPO binds to EPO receptors on the surface of committed erythroid progenitors in the bone marrow resulting in their replication and maturation into functional erythrocytes.
erlotinib hydrochloride [180]	01003938, 00130520, 00520013, 00603356, 00737243, 00063895, 00263822, 00030446, 00126542, 00217529, 00059787, 00030498	↓EGF:EGFR	Competing with adenosine triphosphate, erlotinib reversibly binds to the intracellular catalytic domain of epidermal growth factor receptor (EGFR) tyrosine kinase, thereby reversibly inhibiting EGFR phosphorylation and blocking the signal transduction events and tumorigenic effects associated with EGFR activation.
everolimus [180] [RAD001]	01149434, 00886691, 01031381	↓active mTOR	In cells, everolimus binds to the immunophilin FK Binding Protein-12 (FKBP-12) to generate an immunosuppressive complex that binds to and inhibits the activation of the mammalian Target of Rapamycin (mTOR), a key regulatory kinase.
letrozole [180] [femara]	00505661, 00673335, 00634894	↓active aromatase	Selectively and reversibly inhibits aromatase.
fenretinide [180]	00098800, 00017134, 00026091	↑active retinoic acid receptors	Binds to and activates retinoic acid receptors (RARs), thereby inducing cell differentiation and apoptosis in some tumor cell types.
fentanyl [180]	00295945, 00538850	↑active mu-opioid receptor	Selectively binding to the mu-opioid receptor in the central nervous system (CNS), thereby mimicking the effects of endogenous opiates.
floxuridine [180]	00005049	↓active thymidylate synthetase	As an antimetabolite, floxuridine inhibits thymidylate synthetase, resulting in disruption of DNA synthesis and cytotoxicity.

Continued on next page

Table A.1 – continued from previous page

Ovarian Cancer Drugs	NCT ID	Drug Effect	Mechanism of Action
flutamide [180]	00699907	↓ dihydrotestosterone: androgen receptor	Competitively block dihydrotestosterone binding at androgen receptors, forming inactive complexes which cannot translocate into the cell nucleus.
fondaparinux sodium [180]	00659399, 00381888	↓thrombin	Selectively binds to antithrombin III, thereby potentiating the innate neutralization of activated factor X (Factor Xa) by antithrombin.
forodesine hydrochloride [180]	00073944	↓active purine nucleotide phosphorylase	Binds to and inhibits purine nucleotide phosphorylase (PNP), resulting in the accumulation of deoxyguanosine triphosphate and the subsequent inhibition of the enzyme ribonucleoside diphosphate reductase and DNA synthesis.
fulvestrant [180] [ZD9238]	00617188	↓estrogen: estrogen receptor	Binds competitively to estrogen receptors in breast cancer cells, resulting in estrogen receptor deformation and decreased estrogen binding.
RO4929097 [180]	01131234, 01154452, 01175343	↓active γ secretase	γ secretase (GS) is a multi-subunit protease complex that cleaves single-pass transmembrane proteins, such as Notch receptors, at residues within their transmembrane domains inhibitor. RO4929097 binds to GS and blocks activation of Notch receptors, which may inhibit tumor cell proliferation.
gefitinib [180]	00049556, 00317772, 00023699	↓active EGFR	Inhibits the catalytic activity of numerous tyrosine kinases including EGFR, which may result in inhibition of tyrosine kinase-dependent tumor growth.
imatinib [64] [gleevec]	00510653, 00928642, 00039585, 00042952, 00036751, 00041041, 00006357, 00154388, 00216112, 00840450	↓active Abl tyrosine kinase	Competitive inhibition of ATP binding of the Abelson (Abl) tyrosine kinase.
glutathione [180]	00979082	↑active glutathione peroxidase	A tripeptide which acts as an antioxidant, a free radical scavenger and a detoxifying agent. Glutathione is also important as a cofactor for the enzyme glutathione peroxidase, in the uptake of amino acids, and in the synthesis of leukotrienes.
GM-CSF [186] [sargramostim, lenograstim, leukine]	00799110, 00501644, 00157573, 00023634, 00466960, 00091273, 00436254, 00003002, 00803569, 00887796, 00003269, 00003408, 00091000, 00019084, 00005023, 00028496, 00551122	↑active GM-CSF receptor	Binds to GM-CSF receptor which consists of 2 glycoprotein subunits, GMRα and GMRβ. GMRα in isolation binds to GM-CSF with low affinity. GMRβ does not bind GM-CSF by itself, but forms a high-affinity receptor in association with GMRα.
goserelin acetate [163]	00012090	↑active GnRH receptor	Bind to the GnRH receptor and adopt a U-shape conformation. GnRH agonists, such as leuprolide, bruserelin, and goserelin, are similar in structure and function to natural GnRH, but are as much as 60 times more potent than the natural hormone.
granisetron hydrochloride [180]	00293384	↓serotonin-5:5-HT3 receptor	Competitively blocks the action of serotonin at 5-hydroxytryptamine3 (5-HT3) receptors.
GDC-0449 [180]	01154452, 00739661, 00959647	↓active PTCH receptor, ↓active SMO receptor	Hedgehog antagonist GDC-0449 targets the Hedgehog signaling pathway, blocking the activities of the Hedgehog-ligand cell surface receptors PTCH and/or SMO and suppressing Hedgehog signaling.
hydromorphone hydrochloride [180]	00295945	↑active mu-opioid receptor	Selectively binds the mu-opioid receptor, a G protein-coupled receptor, stimulating the exchange of GTP for GDP on the G-protein complex, resulting in inhibition of plasma membrane-associated adenylate cyclase (AC) and a reduction in intracellular cAMP levels.
idronoxil [175] [phenoxodiol]	00091377, 00303888, 00382811	↓active NOX	Binds with high affinity to purified recombinant NADH-oxidase, compromising its ability to oxidize both NADH and ubiquinol and to catalyze protein disulfide-thiol interchange activity. This protein is a truncated form of tumor-specific cell surface NADH-oxidase, tNOX, thought to be involved in the transfer of electrons from intracellular NADH to extracellular acceptor via plasma membrane ubiquinone.
ILX-295501 [180] [36]	00005645	↑intracellular K^+	A novel sulfonylurea compound that has demonstrated in-vivo antitumor activity against a broad spectrum of solid tumors. sulfonylureas block cardiac ATP-sensitive K^+ (KATP) channels. Potassium flux through KATP channels is regulated by intracellular nucleotides and synthetic sulfonylureas, which bind to channel subunits.
IMC-3G3 [180]	00913835	↓PDGF:PDGFR	Selectively binds to PDGFR α, blocking the binding of its ligand, PDGF.
imiquimod [270]	00799110	↑active TLR7	Binds and activate Toll-like receptor 7 (TLR7).
interferon γ-1b [33]	00004032, 00501644, 00047632	↑IFNγ	Natural ligand of interferon γ receptor.
tgDCC-E1A [263]	00102622	↑E1A	The anti-cancer gene, E1A, can be complexed to a lipid carrier, DC-Cholesterol:DOPE, to form tgDCC-E1A, which can be injected directly into tumors.
ipilimumab [272]	00039091, 00060372	↓active CTLA4	Binds and inhibit CTLA4.
iressa [180] [ZD1839]	00181688, 00189358	↓active EGFR	Competes with the binding of ATP to the tyrosine kinase domain of EGFR, thereby inhibiting receptor autophosphorylation and resulting in inhibition of signal transduction.
ispinesib [141]	00097409	↑KSP:ADP	Binds and inhibits the mitotic motor protein, kinesin spindle protein (KSP). ispinesib alters the ability of KSP to bind to microtubules and inhibits its movement by preventing the release of ADP without preventing the release of the KSP-ADP complex from the microtubule.
JI-101 [180]	01149434	↓active VEGFR2, ↓active PDGFRb, ↓active EphB4	Binds to and inhibits VEGFR2, PDGFRb and EphB4.

Continued on next page

Table A.1 – continued from previous page

Ovarian Cancer Drugs	NCT ID	Drug Effect	Mechanism of Action
levonorgestrel [180]	00445887	↑active progesterone receptor	Binds to the progesterone receptor in the nucleus of target cells, thereby stimulating the resulting hormone-receptor complex, initiating transcription, and increasing the synthesis of certain proteins.
lithium carbonate [180]	00408681	↓active Na^+, K^+-ATPase	Interferes with transmembrane sodium exchange in nerve cells by affecting sodium, potassium-stimulated adenosine triphosphatase (Na^+, K^+-ATPase).
lonafarnib [180]	00281515, 00539968	↓active farnesyl transferase	Binds to and inhibits farnesyl transferase, an enzyme involved in the post-translational modification and activation of Ras proteins.
lovastatin [248]	00585052	↓active HMG-CoA reductase	Binds and inhibits HMG-CoA reductase.
litronesib [180] [LY2523355]	01059643	↓active Eg5	Selectively inhibits the activity of Eg5, which may result in mitotic disruption, apoptosis and consequently cell death in tumor cells that are actively dividing.
LY2606368 [180]	01115790	↓active chk1	Selectively binds to checkpoint kinase 1 (chk1), thereby preventing activity of chk1 and abrogating the repair of damaged DNA.
volociximab [180] [M200]	00635193, 00516841	↓active $\alpha5\beta1$ integrin	Binds to and inhibits the activity of $\alpha5\beta1$ integrin, thereby inhibiting endothelial cell-cell interactions, endothelial cell-matrix interactions, and angiogenesis.
MDX-1105 [180]	00729664	↓PD-L1:PD-1	Binds to Programmed Death-1 Ligand 1 (PD-L1), blocking its binding to and activation of its receptor, Programmed Death 1 (PD-1).
mesna [180]	00432094, 00002854	↓acrolein	Converted to a free thiol compound in the kidney, where it binds to and inactivates acrolein and other urotoxic metabolites of ifosfamide and cyclophosphamide, thereby reducing their toxic effects on the urinary tract during urinary excretion.
methotrexate [180]	00002487, 01175772, 00002489, 00357084	↓active dihydrofolate reductase	Binds to and inhibits the enzyme dihydrofolate reductase, resulting in inhibition of purine nucleotide and thymidylate synthesis and, subsequently, inhibition of DNA and RNA syntheses.
methylprednisolone [204]	00109993, 00410657, 00357084	↑active glucocorticoid receptor	Binds to and activates gluococorticoid receptor.
midazolam hydrochloride [190]	00436735	↑active GABAA receptor	Benzodiazepines agonist which bind to a specific site that is distinct from that of GABA binding on the GABAA receptors.
mifepristone [180]	00459290	↓ progesterone: progestrone receptor	Competitively binds to the progesterone receptor, resulting in inhibition of the effects of endogenous or exogenous progesterone.
MK-1775 [181]	01164995	↓active WEE1	Selectively targets and inhibits WEE1, a tyrosine kinase that phosphorylates cyclin-dependent kinase 1 (CDC2) to inactivate the CDC2/cyclin B complex.
MLN8237 [180]	01091428, 00853307	↓active Aurora A kinase	Binds to and inhibits Aurora A kinase, which may result in disruption of the assembly of the mitotic spindle apparatus, disruption of chromosome segregation, and inhibition of cell proliferation.
MM-121 [180]	01209195	↓active ErbB3	Binds to and inhibits human epidermal growth factor receptor ErbB3 activation.
motesanib diphosphate [180]	00574951	↓active VEGFR, ↓active PDGFR, ↓active Kit receptor, ↓active Ret receptor	Selectively targets and inhibits vascular endothelial growth factor (VEGFR), platelet-derived growth factor (PDGFR), kit, and Ret receptors, thereby inhibiting angiogenesis and cellular proliferation.
motexafin gadolinium [92] [180] [MGd]	00120939, 00080041	↓active TrxR	Acts as a substrate of the cytosolic selenocysteine-dependent mammalian TrxR, generating ROS from NADPH in the presence of oxygen. MGd acts as a non-competitive inhibitor of TrxR and inhibits the protein-disulfide reduction activity of the Trx system.
motexafin lutetium [180]	00087191	↑singlet oxygen	Preferentially accumulates in tumor cells due to their increased rates of metabolism and absorbs light, forming an extended high energy conformational state that produces high quantum yields of singlet oxygen, resulting in local cytotoxic effects.
muromonab-CD3 [27] [OKT3]	00004021	↓active CD3 receptor	Binds to and inhibits CD3 on the surface of circulating T-lymphocytes.
mycophenolate mofetil [280]	00096161, 00089141	↓active IMP dehydrogenase	Mycophenolate mofetil is the morpholinoethyl ester of mycophenolic acid (MPA). Immunosuppressive activity of MPA results from the potent reversible inhibition of IMP dehydrogenase (IMPDH). Kinetics of inhibition by MPA are uncompetitive with respect to both substrates IMP and NAD. Uncompetitive inhibition indicates that MPA preferentially binds to the enzyme after substrates, perhaps to an enzyme-IMP-NAD ternary complex or to an enzyme-XMP binary complex in the product side of the reaction.
N-acetylcysteine [180]	01138137	↑glutathione	N-acetylcysteine acetylcysteine regenerates liver stores of glutathione and also reduces disulfide bonds in mucoproteins, resulting in liquification of mucus.
nadroparin calcium [180]	00951574	↓thrombin	Binds to antithrombin III (ATIII) and inhibits the activity of activated factor X (factor Xa), thereby inhibiting the final common pathway of the coagulation cascade and preventing the formation of a cross-linked fibrin clot.
brivudine phosphoramidate [180] [textscnb1011]	00248404	↓ deoxyuridine monophosphate:TS	Converted intracellularly by thymidylate synthase (TS) to BVdUMP which competes with the natural substrate, deoxyuridine monophosphate, for binding to TS.
nelfinavir mesylate [180]	00436735	↓active HIV protease	Selectively inhibits human immunodeficiency virus (HIV) protease, thereby preventing cleavage of the gag-pol viral polyprotein and resulting in the release of immature, noninfectious virions.

Continued on next page

Table A.1 – continued from previous page

Ovarian Cancer Drugs	NCT ID	Drug Effect	Mechanism of Action
filgrastim [180] [neulasta, pegfilgrastim]	00277160, 00217568, 00217529, 00352300, 00569673, 00470366, 00551122, 00575952, 00437047, 00117442, 00004221, 00002913, 00004921, 00003382, 00003413, 00004177, 00005612, 00002600, 00562640, 00550784, 00003944, 00002559, 00003425, 00004157, 00014456, 00002931, 00467051, 00003657, 00003173, 00002489, 00003926, 00423852, 00007813, 00002515, 00432094, 00005952, 00025441, 00003852, 00002558, 00020514, 00004066, 00002641, 00002764, 00002526, 00638898, 01110135, 00002854, 00003597	↑active G-CSF receptor	Chemically identical to or similar to the endogenous cytokine human granulocyte colony-stimulating factor (G-CSF).
NOV-002 [255]	00345540	↑active GGT	Binds and activates gamma-glutamyl transpeptidase (GGT).
daclizumab [264]	01132014	↓active interleukin-2 receptor	A genetically engineered human IgG1 monoclonal antibody that binds specifically to the α chain of the interleukin-2 receptor and block the receptor.
octreotide acetate [87]	00004895, 00033605	↑active somatostatin receptor	Binds and activates somatostatin receptor.
oglufanide disodium [180]	00003773, 00017303	↓active VEGF	Consists of L-glutamic acid and L-tryptophan. Oglufanide inhibits vascular endothelial growth factor (VEGF), which may inhibit angiogenesis.
OGX-427 [180]	00487786	↓Hsp27	OGX-427, an antisense oligonucleotide, suppresses tumor cell expression of Hsp27, which may induce tumor cell apoptosis and enhance tumor cell sensitivity to cytotoxic agents.
ON 01910.Na [181]	00856791	↓active Plk1	Inhibits polo-like kinase1 (Plk1), inducing selective G2/M arrest followed by apoptosis in a variety of tumor cells.
ondansetron [180]	00795769, 00016380	↓serotonin: 5HT3 receptor	As a selective serotonin receptor antagonist, ondansetron competitively blocks the action of serotonin at 5HT3 receptors, resulting in suppression of chemotherapy- and radiotherapy-induced nausea and vomiting.
linsitinib [180] [OSI-906]	00889382, 00514007, 00514306	↓active IGF-1R	Selectively inhibits insulin-like growth factor 1 receptor (IGF-1R), which may result in the inhibition of tumor cell proliferation and the induction of tumor cell apoptosis.
palifermin [32] [kepivance]	00728585	↑active FGFR2b	Mimics the actions of endogenous KGF, binding specifically to a tyrosine kinase receptor fibroblast growth factor receptor (FGFR2b).
panitumumab [284]	00861120	↓EGF:EGFR	Binds EGFR with high affinity and inhibits ligand-dependent receptor activation.
pazopanib [139] [GW786034]	01035658, 01227928, 00866697, 01238770, 00561795, 00794521, 00281632	↓active VEGFR, ↓active PDGFR, ↓active c-Kit tyrosine kinase	ATP-competitive, multitargeted kinase inhibitor which inhibits VEGFR, PDGFR, and c-Kit tyrosine kinases at low nanomolar.
PD-0332991 [66]	01037790	↓active CDK4, ↓active CDK6	A highly reversible specific inhibitor of CDK4 (IC50, 0.011/L) and CDK6 (IC50, 0.016 μmol/L), having no activity against a panel of 36 additional protein kinases. It is a potent antiproliferative agent against Rb-positive tumor cells in vitro, inducing an exclusive G1 arrest.
pentostatin [129]	00074035, 00096161	↓active adenosine deaminase	Tight-binding inhibitor of adenosine deaminase (ADA).
pertuzumab [180] [rhuMAb 2C4]	00058552, 00096993	↓dimerized Her2 receptor	Binding of the antibody to the dimerization domain of the HER-2 tyrosine kinase receptor protein directly inhibits the ability of HER-2 to dimerize with other HER tyrosine kinase receptor proteins, preventing the activation of HER signaling pathways, resulting in tumor cell apoptosis.
poly-ICLC [295]	00553683, 00948961	↑active TLR3	Binds and activate TLR3.
pralatrexate [180]	01188876	↓active DHFR	Selectively enters cells expressing RFC-1 and competes for the folate binding site of DHFR, blocking tetrahydrofolate synthesis.
prednisone [215]	00410657, 00357084	↑active glucocorticoid receptor	Binds and activates glucocorticoid receptor.
bortezomib [180] [PS-341, velcade]	00059618, 00923247, 00610792, 00028912, 00620295, 01074411, 00023712, 00237627, 00667641, 00923247	↓active 26S proteasome	Reversibly inhibits the 26S proteasome, a large protease complex that degrades ubiquinated proteins.
valspodar [86] [PSC 833]	00001302, 00001383	↓active p-glycoprotein	Binds and inhibits p-glycoprotein, the multidrug resistance efflux pump, thereby restoring the retention and activity of some drugs in some drug-resistant tumor cells.
vatalanib [180] [PTK787]	00268918	↓active VEGFR1/2	Binds to and inhibits the protein kinase domain of vascular endothelial growth factor receptors 1 and 2.
ramosetron [180]	01012336	↓active 5-HT3 receptor	Selectively binds to and blocks the activity of 5-HT subtype 3 (5-HT3) receptors located in the vagus nerve terminal and in the vomiting center in the central nervous system (CNS), suppressing chemotherapy-induced nausea and vomiting.
ramucirumab [180]	00721162	↓active VEGFR-2	Specifically binds to and inhibits VEGFR-2, which may result in an in inhibition of tumor angiogenesis and a decrease in tumor nutrient supply.
ravuconazole [180] [BMS-207147]	00064311	↓active 14a demethylase	Inhibits 14a demethylase, an enzyme involved in sterol synthesis, resulting in lysis of the fungal cell wall and fungal cell death.
recombinant interferon α [283]	00178802, 00085384, 00003408	↑active interferon α receptor	Binds and activate interferon α receptor.

Continued on next page

Table A.1 – continued from previous page

Ovarian Cancer Drugs	NCT ID	Drug Effect	Mechanism of Action
recombinant interleukin-11 [181]	00004157	↑activate interleukin 11 receptor	A recombinant therapeutic agent which is chemically identical to or similar to the endogenous cytokine interleukin 11 (IL-11). IL-11 binds to and activates its cell-surface receptor.
recombinant interleukin-12 [181]	00016289, 00003107, 00020163, 00028535	↑active interleukin 12 receptor	A recombinant form of the endogenous heterodimeric cytokine interleukin-12. Recombinant interleukin-12 binds to and activates its cell-surface receptor, stimulating the production of interferon-γ (IFN) which, in turn, induces IFN-γ-inducible protein-10 (IP-10) and so inhibits tumor angiogenesis.
recombinant interleukin-21 [180]	00523380	↑active interleukin 21 receptor	Binds to and activates IL-21 receptors, expressed on T-cells, B-cells, dendritic cells (DC), and natural killer (NK) cells, modulating the proliferation and/or differentiation of T and B cells, promoting T cell survival, and increasing the cytolytic activity of cytotoxic T lymphocytes (CTLs) and NK cells.
resiquimod [110]	00948961	↑active TLR7, ↑active TLR8	Binds and activates Toll-like receptor (TLR) 7 and 8.
ridaforolimus [180]	01256268	↓active mTOR	Binds to and inhibits the mammalian target of rapamycin (mTOR), which may result in cell cycle arrest and,consequently, the inhibition of tumor cell growth and proliferation.
RO5323441 [180]	01148758	↓PGF1/2:VEGFR1	Binds to both PGF-1 and -2, thereby inhibiting the binding of PGF-1 and -2 to the vascular endothelial growth factor receptor-1 (VEGFR1) and subsequent VEGFR1 phosphorylation.
ropivacaine hydrochloride [180]	00295945	↓intracellular Na^+	Binds to voltage-gated sodium ion channels in the neuronal membrane, thereby preventing the permeability of sodium ions and resulting in a stabilization of the neuronal membrane and inhibition of depolarization.
SB-485232 [210]	00659178	↑active interleukin 18 receptor	Binds and activates interleukin 18 receptor.
sodium thiosulfate [180]	00716976	↓cyanide	Likely provides an exogenous source of sulfur, thereby hastening the detoxification of cyanide through the enzyme rhodanese (thiosulfate cyanide sulfurtransferase) which converts cyanide to the relatively nontoxic, excretable thiocyanate ion.
squalamine lactate [91]	00021385	↓active NHE-3	May alter cellular responses to growth stimuli that increase intracellular calcium by binding to and inhibiting NHE-3 and redistributing calmodulin, a calcium transducer within endothelial cells.
SU5416 [180]	00006155	↓active VEGFR2	Reversibly inhibits ATP binding to the tyrosine kinase domain of vascular endothelial growth factor receptor 2 (VEGFR2), which may inhibit VEGF-stimulated endothelial cell migration and proliferation and reduce the tumor microvasculature.
sunitinib malate [217] [SU-11248]	00543049, 00768144, 00979992, 00003887, 00474994, 00813423, 00388037	↓active VEGFR1, ↓active VEGFR2, ↓active VEGFR3, ↓active PDGFRa, ↓active PDGFRb, ↓active Kit, ↓active Flt-3, ↓active CSF-1R	Binds reversibly to the ATP binding site of their target kinases and thereby inhibit their catalytic activity. Inhibits at least eight receptor protein-tyrosine kinases including vascular endothelial growth factor receptors 1Ű3 (VEGFR1Ű VEGFR3), platelet-derived growth factor receptors (PDGFRa and PDGFRb), stem cell factor receptor (Kit), Flt-3, and colony-stimulating factor-1 receptor (CSF-1R).
tacrolimus [22]	00109993	↓active calcineurin	Binds FKBP, an immunophilin. Binding of tacrolimusŰFKBP complex to calcineurinŰcalmodulin inhibited the phosphatase activity of calcineurin.
TAK-165 [179]	00034281	↓active HER2 receptor	HER2 selective tyrosine kinase inhibitor.
talabostat mesylate [4] [PT-100]	00303940	↓active FAP, ↓active CD26/DPP-IV	Competitively inhibits the dipeptidyl peptidase (DPP) activity of fibroblast activation protein (FAP) and CD26/DPP-IV.
tamoxifen citrate [180]	00189358, 00305838, 00003080, 00041080, 00253539	↓estradiol: estrogen receptor	Competitively inhibits the binding of estradiol to estrogen receptors, thereby preventing the receptor from binding to the estrogen-response element on DNA. The result is a reduction in DNA synthesis and cellular response to estrogen.
tanespimycin [180]	00093496, 00004065, 00004241	↓active HSP90	Binds to and inhibits the cytosolic chaperone functions of heat shock protein 90 (HSP90).
tariquidar [180] [XR9576]	00069160, 00020514, 00001944	↓active p-glycoprotein	Non-competitively binds to the p-glycoprotein transporter, thereby inhibiting transmembrane transport of anticancer drugs.
taurolidine [277]	00021034	↓active endotoxin	An amino acid derivative. Methylol group reacts with cell wall of bacteria and the primary groups of endotoxin.
toremifene [180]	00003865	↓estrogen: estrogen receptor	A selective estrogen receptor modulator (SERM). This agent binds competitively to estrogen receptors, thereby interfering with estrogen activity.
tranexamic acid [180]	00740116	↓plasmin: plasminogen	With strong affinity for the five lysine-binding sites of plasminogen, transexamic acid competitively inhibits the activation of plasminogen to plasmin, resulting in inhibition of fibrinolysis; at higher concentrations, this agent non-competitively inhibits plasmin.
triapine [229]	00081276, 00335998	↓active ribonucleotide reductase	Behaves by two mechanisms: chelating protein-bound iron and affecting tyrosyl radical stability as an iron chelator; and forming a redox species with iron and strongly quenching the tyrosyl radical in the form of Triapine/Fe complex. The strongest inhibitory activity of Triapine/Fe^{2+} complex may relate with its low redox potential, reducing the di-ferric iron/tyrosyl radical center of the small subunits and hence inhibiting ribonucleotide reductase (RR) activity.

Continued on next page

Table A.1 – continued from previous page

Ovarian Cancer Drugs	NCT ID	Drug Effect	Mechanism of Action
XL184 [180]	00940225	↓active VEGFR2	Strongly binds to and inhibits several tyrosine receptor kinases, especially VEGFR2, which may result in inhibition of tumor growth and angiogenesis, and tumor regression.
XL999 [60]	00277290	↓active VEGFR2, ↓active PDGFR, ↓active FGFR1, ↓active FLT-3, ↓active SRC	A small molecule inhibitor of multiple kinases involved in tumor cell growth, angiogenesis, and metastasis, including VEGFR2 (KDR), PDGFR, FGFR1, FLT-3, and SRC.
vandetanib [265] [zactima, ZD6474]	00862836, 00872989, 00923247, 00445549	↓active VEGFR, ↓active RET, ↓active EGFR	An ATP-competitive inhibitor of RET, epidermal growth factor receptor (EGFR), and vascular endothelial growth factor receptors kinases.
zibotentan [180] [ZD4054]	00929162, 00610714	↓active ET-A receptor	Binds selectively to the ET-A receptor, thereby inhibiting endothelin-mediated mechanisms that promote tumor cell proliferation.
zoledronic acid [68]	00305695, 00321932	↓active farnesyl pyrophosphate synthase	A bisphosphonate having nitrogen-containing R2 side chains. Nitrogen-containing bisphosphonates bind to and inhibit the activity of farnesyl pyrophosphate synthase, a key regulatory enzyme in the mevalonic acid pathway critical to the production of cholesterol, other sterols, and isoprenoid lipids.
Information Unavailable/Mechanism Unknown			
D4064A	00753480	?	?
leucovorin calcium [180]	00004206, 00002489, 00957905, 00959647	?	An active metabolite of folic acid, the molecular target of folate antagonist-type chemotherapeutic drugs. Leucovorin calcium counteracts the toxic effects of these medications, 'rescuing' the patient while permitting the antitumor activity of the folate antagonist. This agent also potentiates the effects of fluorouracil and its derivatives by stabilizing the binding of the drug's metabolite to its target enzyme, thus prolonging drug activity.
tasisulam [180] [LY573636]	00428610, 01214668	?	Activates the intrinsic mitochondrial-mediated cell death pathway as manifested by decreased ATP, cytochrome C release, activation of caspases, loss of mitochondrial membrane potential, production of reactive oxygen species (ROS) and eventually apoptosis.
essiac [180]	00287482	?	An herbal formula containing burdock root (Arctium lappa), Turkey rhubarb root (Rheum palmatum), sheep sorrel (Rumex acetosella), and slippery elm bark (Ulmus fulva) with potential immunostimulating, anti-inflammatory and anti-tumor activities. The exact chemical profile, their respective concentrations and the mechanism of action of Essiac are largely unknown due to the proprietary nature of the formula and product inconsistency.

Table A.1: Ovarian cancer drugs found in [184]. ? indicates that information is either unavailable or mechanism is unknown.

B. ATRIAL FIBRILLATION DRUGS

Atrial Fibrillation Drugs	NCT ID	Drug Effect	Mechanism of Action
DNA/RNA			
moxifloxacin [180]	00437242	↓active topoisomerase II, ↓active topoisomerase IV	Binds to and inhibits the bacterial enzymes DNA gyrase (topoisomerase II) and topoisomerase IV, resulting in inhibition of DNA replication and repair and cell death in sensitive bacterial species.
Ion Channels			
vernakalant [75] [RSD1235-SR]	00267930, 00989001, 00526136, 01174160, 00468767, 00668759, 00125320, 00281554, 00115791	↓intracellular K^+, ↑intracellular Na^+	Predominantly blocks K^+ channel (inward K^+ channel) and partially blocks Na^+ channel block at antiarrhythmic concentrations.
tedisamil sesquifumarate [70]	00126074, 00126061, 00126022	↑intracellular K^+	Primarily suppresses the transient outward K^+ current.
Strychnos Nux vomica [120]	00861237	↑intracellular K^+, ↑intracellular Na^+	Blocks primarily K_V which causes K^+ efflux, and in addition the Na^+ channels.
quinidine [7]	00578617, 00000556, 00589303, 00911508	↑intracellular Na^+, ↓intracellular K^+	Binds and inhibits Na^+/K^+ ATPase.
propafenone [194]	00578617, 00933634, 00000556, 00392106, 00408200, 00589303, 00911508, 00523978	↓intracellular Na^+	Binds and inhibits sodium channel, thereby slowing influx of sodium ions.
moricizine [5]	00000556	↓intracellular Na^+	Binds and inhibits sodium channel.
lidocaine [28]	00840918	↓intracellular Na^+	Binds and inhibits voltage-gated Na^+ channel.
ibutilide fumarate [197]	00589992, 01014741	↑intracellular K^+	Binds and inhibits human ether-a-go-go related gene (hERG) channel, inhibiting the rapidly activating delayed rectifier K current (I_{Kr})
flecainide [205]	00863213, 00189319, 00000556, 00408473, 00945867, 00702117, 00392106, 00340314, 00578617, 00408200, 00589303, 00911508, 00523978, 00215774	↓intracellular Na^+, ↑intracellular K^+	Rapidly gains access to its binding site when the channel is open and inhibits Na^+ current by a pore blocking mechanism. Closing of either the activation or the inactivation gate traps flecainide within the pore resulting in the slow recovery of the drug-modified channels at hyperpolarized voltages.
dofetilide [147]	00578617, 00392106, 00408200, 00589303, 00911508	↑intracellular K^+	Binds and inhibits human ether-a-go-go related gene (hERG) channel, inhibiting the rapidly activating delayed rectifier K current (I_{Kr}).

Continued on next page

Table B.1 – continued from previous page

Atrial Fibrillation Drugs	NCT ID	Drug Effect	Mechanism of Action
disopyramide [135]	00000556, 00589303	↓intracellular Na^+	Binds and inhibits the fast sodium channels.
digoxin [119]	01181414, 00878384, 00578617, 00712465, 00000556, 00940056, 01047566, 00911508	↑intracellular Na^+, ↓intracellular K^+	Binds and inhibits Na^+/K^+ ATPase.
celivarone [83] [SSR149744C]	00233441, 00232310	↓intracellular Na^+, ↓intracellular Ca^{2+}	Multi-channel blocker. Blocks Na^+ inward current and l-type Ca^{2+} current.
azimilide dihydrochloride [267] [71]	00035477, 00035464, 00035451	↑intracellular K^+	Binds and inhibits human ether-a-go-go related gene (hERG) channels, inhibiting the rapidly activating delayed rectifier K current (I_{Kr}). Inhibit slow activating potassium currrent (I_{Ks}) via a binding site on the KCNQ1 protein.
AZD7009 [198]	00255281	↑intracellular K^+, ↓intracellular Na^+	Binds and inhibits human ether-a-go-go related gene (hERG) channel, inhibiting the rapidly activating delayed rectifier K current (I_{Kr}). Binds and inhibits human voltage-gated Na+ channel (hNav1.5) channel, inhibiting sodium influx.
AZD1305 [44]	00643448, 00915356, 00712465	↑intracellular K^+, ↓intracellular Na^+, ↓intracellular Ca^{2+}	A combined ion channel blocker. AZD1305 predominantly blocked the human ether-a-go-go related gene (hERG), the L-type calcium and the human voltage-gated Na^+ channel (hNav1.5) channels in a concentration-dependent manner.
verapamil [146]	00911508, 00313157, 00000556, 00578617, 00589303	↓intracellular Ca^{2+}	Competes with external Ca^{2+} for binding on Ca^{2+} channel.
spironolactone [173]	00141778, 00689598	↓intracellular Ca^{2+}	Interacts at a binding site of the calcium entry blocker receptor complex in vascular membranes and allosterically modulates the binding of calcium entry blockers to this complex.
magnesium sulphate [73]	01049464, 00965874	↓intracellular Ca^{2+}	Competes with calcium for binding sites, in this case for voltage-operated calcium channels (VOCC). Decreased calcium channel activity lowers intracellular calcium, causing relaxation and vasodilation.
K201 [117]	00626652, 01259622, 01067833	↓intracellular Na^+, ↓intracellular Ca^{2+}, ↑intracellular K^+	Non-specific blocker of sodium (I_{Na}), potassium (I_{Ki}) and calcium (I_{Ca}) channels, inhibiting sodium influx, K^+ efflux and Ca^{2+} influx.
diltiazem [146]	00578617, 00911508, 00863213, 01211808, 00834925, 00313157, 00000556, 00589303	↓intracellular Ca^{2+}	Competes with external Ca^{2+} for binding on Ca^{2+} channel.
calcium antagonist [77]	01047566	↓intracellular Ca^{2+}	Calcium channel antagonist blocks entry of Ca^{2+} into cells. Consists of drugs, such as verapamil, nifedipine, which inhibit the myocardial trans-sarcolemmal Ca^{2+} carrier system (slow Ca^{2+} channels) with extremely high selectivity and drugs, such as terodiine, caroverine, which are less specific and also interfere with Na^+- or Mg^{2+}-dependent myocardial membrane phenomena.
Myosin Phosphorylation Signaling Network (Maeda et. al)			
celivarone [83] [SSR149744C]	00233441, 00232310	↓intracellular Na^+, ↓intracellular Ca^{2+}	Multi-channel blocker. Blocks Na^+ inward current and l-type Ca^{2+} current.
AZD1305 [44]	00643448, 00915356, 00712465	↑intracellular K^+, ↓intracellular Na^+, ↓intracellular Ca^{2+}	A combined ion channel blocker. AZD1305 predominantly blocked the human ether-a-go-go related gene (hERG), the L-type calcium and the human voltage-gated Na^+ channel (hNav1.5) channels in a concentration-dependent manner.
ximelagatran [168] [exanta]	00206063	↓active thrombin	Inhibits fluid-phase and clot-bound thrombin with similar high potency. Binding to the active site of thrombin is direct and competitive and does not require the presence of co-factors.
simvastatin [76] [202]	00321802	↓thrombin, ↓Rho.GTP.Rho-kinase	Inhibits rate of thrombin generation by directly interfering with tissue factor (TF). Inhibits Rho geranylgeranylation (Rho-kinase activation).
edoxaban [273] [DU-176b]	00504556, 00806624, 00829933, 00781391	↓active thrombin	Reversibly blocks the active site of thrombin.
dabigatran etexilate [241] [BIBR 1048]	01136408, 00262600, 00157248, 01227629, 00808067	↓thrombin: thrombin receptor	Binds to thrombin and blocks interaction with substrate.
apixaban [273]	00787150, 00412984, 00496769	↓active thrombin	Reversibly blocks the active site of thrombin.
verapamil [146]	00911508, 00313157, 00000556, 00578617, 00589303	↓intracellular Ca^{2+}	Competes with external Ca^{2+} for binding on Ca^{2+} channel.
spironolactone [173]	00141778, 00689598	↓intracellular Ca^{2+}	Interacts at a binding site of the calcium entry blocker receptor complex in vascular membranes and allosterically modulates the binding of calcium entry blockers to this complex.
magnesium sulphate [73]	01049464, 00965874	↓intracellular Ca^{2+}	Competes with calcium for binding sites, in this case for voltage-operated calcium channels (VOCC). Decreased calcium channel activity lowers intracellular calcium, causing relaxation and vasodilation.

Continued on next page

Table B.1 – continued from previous page

Atrial Fibrillation Drugs	NCT ID	Drug Effect	Mechanism of Action
K201 [117]	00626652, 01259622, 01067833	↓intracellular Na^+, ↓intracellular Ca^{2+}, ↑intracellular K^+	Non-specific blocker of sodium (I_{Na}), potassium (I_{Ki}) and calcium (I_{Ca}) channels, inhibiting sodium influx, K^+ efflux and Ca^{2+} influx.
diltiazem [146]	00578617, 00911508, 00863213, 01211808, 00834925, 00313157, 00000556, 00589303	↓intracellular Ca^{2+}	Competes with external Ca^{2+} for binding on Ca^{2+} channel.
calcium antagonist [77]	01047566	↓intracellular Ca^{2+}	Calcium channel antagonist blocks entry of Ca^{2+} into cells. Consists of drugs, such as verapamil, nifedipine, which inhibit the myocardial trans-sarcolemmal Ca^{2+} carrier system (slow Ca^{2+} channels) with extremely high selectivity and drugs, such as terodiine, caroverine, which are less specific and also interfere with Na^+- or Mg^{2+}-dependent myocardial membrane phenomena.
AZD0837 [241]	00645853, 00623779, 00684307	↓thrombin: thrombin receptor	An anticoagulant that binds selectively to thrombin and blocks its interaction with its substrates. AZD0837 is the prodrug of ARH06737, a potent, competitive, reversible inhibitor of free and fibrin-bound thrombin.
budiodarone [225] [187] [ATI-2042]	00389792	↓MLCK.Ca^{2+}.CaM, ↓MLCK.2Ca^{2+}.CaM, ↓MLCK.3Ca^{2+}.CaM, ↓MLCK.4Ca^{2+}.CaM	An oral, rapidly metabolized chemical analogue of amiodarone with a half-life of 7h, which is expected to have a similar efficacy profile to amiodarone but without the side effects attributable to long-term dosing and tissue accumulation. Amiodarone binds to Ca^{2+}-calmodulin complex to prevent binding of enzyme substrate.
amiodarone [187]	01198275, 01199081, 01140581, 00233441, 00272636, 00215761, 00668759, 00578617, 00251706, 00392431, 00784316, 01173809, 00300495, 00654290, 00000556, 00127712, 00287209, 00845780, 00313443, 00489736, 00420017, 00724581, 01266681, 01229254, 00953212, 00007605, 01181414, 00392106, 00826826, 00821353, 00340314, 00589303, 00911508, 00863213	↓MLCK.Ca^{2+}.CaM, ↓MLCK.2Ca^{2+}.CaM, ↓MLCK.3Ca^{2+}.CaM, ↓MLCK.4Ca^{2+}.CaM	Binds to Ca^{2+}-calmodulin complex to prevent binding of enzyme substrate.
Reactive Oxygen Species (ROS)			
vitamin C [233] [ascorbic acid]	00953212, 01107730	↓free radicals	Antioxidant.
General Drug Categories			
renin-angiotensin-aldosterone system (RAAS) inhibitors [79] [176]	01198275	↓active ACE or ↓angiotensin II: angiontensin II receptor	Could be angiotension converting enzyme (ACE) inhibitor or angiotensin II type 1 receptor blocking agent (ARB).
calcium antagonist [77]	01047566	↓intracellular Ca^{2+}	Calcium channel antagonist blocks entry of Ca^{2+} into cells. Consists of drugs, such as verapamil, nifedipine, which inhibit the myocardial trans-sarcolemmal Ca^{2+} carrier system (slow Ca^{2+} channels) with extremely high selectivity and drugs, such as terodiine, caroverine, which are less specific and also interfere with Na^+- or Mg^{2+}-dependent myocardial membrane phenomena.
anti-arrhythmic drugs [212]	00741611, 00392054, 00227344, 00137540, 00940056	?	Antiarrhythmic drugs consists of a variety of drugs such as propafenone and procainamide which are sodium channel blockers, potassium channel blockers and verapamil which are calcium channel blockers.
angiotensin receptor blockers [23] [ARB]	00321945	↓angiotensin II: angiontensin II receptor	Interacts selectively at angiotensin II receptor to prevent binding of angiotensin II to its receptor.
aldosterone receptor antagonists [201]	00877643	↓aldosterone: aldosterone receptor	Decreases potassium excretion by preventing aldosterone from binding to its receptor.
β adrenergic antagonists [80] [β blocker]	00000556, 00863213, 00170274, 00940056, 01047566, 01181414	↓catecholamines: β adrenergic receptors	Blocks the access of catecholamines to β adrenergic receptors.
ACE inhibitors [232]	00321945	↓active ACE	Binds to zinc ions located in the active site of the angiotensin-converting enzyme (ACE) molecule to inhibit ACE.
statins [242]	00877643, 00201552	↓HMG-CoA: HMGCR	Competitively inhibits the hepatic enzyme hydroxymethylglutaryl-coenzyme A reductase (HMGCR).
oral anticoagulation [105]	00776633	↓active vitamin K oxide reductase	Vitamin K antagonist.
Other Signaling Pathways			
fluindione [34]	00911300	↓active vitamin K oxide reductase	Vitamin K antagonist.
valsartan [164]	00376272, 00343499	↓angiotensin II: AT1 receptor	Competitively and selectively inhibits the actions of angiotensin II at the AT1 receptor subtype which is responsible for most of the known effects of angiotensin II.
thiazolidinediones [116]	00321204	↓active PPARγ	Binds and inhibits PPARγ.
tecadenoson [178]	00713401	↑active A1 adenosine receptor	Selectively targets A1 adenosine receptor (A1 adenosine receptor agonist) activation of a potassium outward current ($I_{KAdo,Ach}$), as well as the suppression of inward calcium current (I_{Ca}) and the hyperpolarization-activated current ("funny" current) (I_f).

Continued on next page

Table B.1 – continued from previous page

Atrial Fibrillation Drugs	NCT ID	Drug Effect	Mechanism of Action
idraparinux [273] [SSR126517E, SR34006]	00580216, 00070655	↑active antithrombin	Binds antithrombin and enhance its inhibition of thrombin.
YM150 [262] [darexaban]	00938730, 00448214	↓active Factor X	Directly and selectively inhibits activated Factor X in the cascade of blood coagulation and, thus, is expected to prevent VTE by suppressing the thrombin production.
warfarin [11]	00769938, 00721136, 00787150, 00806624, 00829933, 00781391, 00603317, 00511173, 00622102, 00244725, 01178034, 01081327, 01042067, 00927862, 00904293, 00559988, 00334464, 00206063, 00356759, 00839657, 00925028, 00000517, 00905177, 00580216, 00938730, 00448214, 00973323, 00973245, 01119274, 00162435, 01182441, 00403767, 00129545, 00970892, 00494871, 00904982, 01119261, 01119300, 00742859, 00872079, 01118299, 00814177, 00401414, 01227629, 00412984, 01136408, 00262600, 01104337, 00504556, 00911300, 00645853, 00684307, 00070655, 00691470, 00484640	↓active vitamin K oxide reductase	Inhibits factors II, VII, IX, and X by blocking vitamin KŰmediated carboxylation of their precursors. The vitamin K oxide reductase is inhibited by the S enantiomer of warfarin.
triiodothyronine [174] [T3]	00289367	↑active thyroid hormone receptors	Binds nuclear receptor proteins, thyroid hormone receptors (TRs) that in turn, bind to thyroid hormone response elements in the promoter region of thyroid hormone responsive genes. In the presence of T3, TRs activate transcription by recruiting coactivator complexes and in the absence of T3, TRs repress transcription by recruiting corepressor complexes. Genes regulated by T3 includes SERCA2, phospholamban, alpha and beta myosin heavy chains.
rivaroxaban [2] [xarelto, BAY59-7939]	00403767, 00779064, 00973323, 00973245, 00494871	↓active Factor X	Produces its anticoagulant effects by directly, selectively, and reversibly inhibiting free and clot-bound factor Xa without binding to antithrombin. Inhibition of factor Xa prevents the conversion of factor II to factor IIa, resulting in decreased generation of thrombin.
sotalol [162]	00392106, 00340314, 00578617, 00000556, 00007605, 00035451, 00408200, 00589303, 00911508, 00523978	↓active β adrenoceptor, ↑cAMP	Competitive β adrenoceptor antagonist that prolongs myocardial action potential duration (APD) and effective refractory period (ERP) and increases cAMP which in turn decreases excess intracellular Ca^{2+}.
sevoflurane [289] [89]	00484575	↓active LFA-1, ↓active NADH: ubiquinone oxidoreductase	Binds and allosterically blocks integrin lymphocyte function-associated antigen 1. Binds weakly to "hydrophobic inhibitory site" of NADH:ubiquinone oxidoreductase (complex 1).
SB-207266 [30]	0041496	↓active 5-HT4 receptors	Acts as a 5-HT4 antagonist with great binding affinity for 5-HT4 receptors which are important and involved in the regulation of cisapride stimulated orocaecal transit.
ramipril [172]	00141778, 00736294, 00215761	↓active ACE	Binds to and inhibit angiotensin converting enzyme (ACE).
propranolol [14]	00578617, 00911508, 00654290	↓catecholamines: β adrenergic receptors	Binds to and inhibit interaction between β adrenergic ligand and β adrenergic receptor preventing activation of the receptor.
propofol [19]	00484575	↑active GABA-A receptor	Binds to and activates GABA-A receptors.
procainamide [145]	00000556, 00702117, 01205529, 00589303	↓DNMT1: hemimethylated DNA, ↓DNMT1: S-adenosyl-L-methionine	Partial competitive inhibitor of DNA methyltransferase 1 (DNMT1), reducing the affinity of the enzyme for its two substrates hemimethylated DNA and S-adenosyl-L-methionine.
prednisone [279] [35] [solumedrol]	01206452, 00807586	↑active glucocorticoid receptor	Metabolized into active form, prednisolone which binds and activate glucocorticoid receptor.
phenprocoumon [279] [218] [marcoumar]	00586287, 01119274, 01119261, 01119300, 00911300	↓active VKORC1	Inhibits vitamin K reductase, by targeting the vitamin K epoxide reductase complex subunit 1 (VKORC1).
paracetamol [48] [acetaminophen]	01104337	↓active COX-3	Binds to and inhibits COX-3.
odiparcil [273] [SB424323]	00244725, 00437242, 00240643	↑active heparin cofactor II	Indirectly inhibits thrombin by catalyzing heparin cofactor II.
nebivolol [195]	00878384	↓active β1 adrenergic receptor	Binds to and inhibits β 1 adrenergic receptor.
metoprolol [237]	00953212, 00783900, 01211821, 00313157, 00784316, 00198614, 00578617, 00589303, 00911508	↓active β1 adrenergic receptors	Binds and inhibits β1 adrenergic receptors.
mangosteen juice [53]	00951301	↓active IKK, ↓active histamine H1 receptor	γ-mangostin directly inhibits IKK activity preventing COX-2 gene transcription. α-mangostin is a competitive histamine H1 receptor antagonist.

Continued on next page

Table B.1 – continued from previous page

Atrial Fibrillation Drugs	NCT ID	Drug Effect	Mechanism of Action
omega 3-acid ethyl esters [183] [lovaza, omegaven, N-3 polyunsaturated fatty acids (n-3 PUFAs), fish oil]	00791089, 00841451, 01175330, 01235130, 00446966, 00970489, 00597220, 00402363, 01198275, 00232232, 00232245, 00232219, 00552084	↑active PPARα	Polyunsaturated omega-3 fatty acids such as DHA (docosahexaenoic acid) and EPA (eicosapentaenoic acid) are natural ligands of PPARα which binds and activates PPARα.
losartan [74] [cozaar]	00647257, 01233635	↓active AT1-receptor	Binds and inhibits angiotensin II type 1 receptor.
atorvastatin [242] [lipitor]	00579098, 00449410, 00252967	↓HMG-CoA: HMGCR	Competitively inhibits the hepatic enzyme hydroxymethylglutaryl-coenzyme A reductase (HMGCR).
irbesartan [74]	00215761, 00225667, 00613496, 00352560, 00249795	↓active AT1-receptor	Binds and inhibits angiotensin II type 1 receptor.
indobufen [29]	00244426	↓active platelet cyclooxygenase	Inhibits platelet aggregation by reversibly inhibiting the platelet cyclooxygenase enzyme thereby suppressing thromboxane synthesis.
hydrocortisone [180]	00442494	↑active glucocorticoid receptor	A synthetic or semisynthetic analog of natural hydrocortisone hormone produced by the adrenal glands with primary glucocorticoid and minor mineralocorticoid effects. As a glucocorticoid receptor agonist, hydrocortisone promotes protein catabolism, gluconeogenesis, capillary wall stability, renal excretion of calcium, and suppresses immune and inflammatory responses.
heparin [2]	00721136, 00911300	↑active antithrombin	Indirectly inhibits factors IIa, IXa, Xa, XIa, and XIIa by forming a complex with antithrombin and initiating its activity.
fondaparinux [2]	00911300	↑active antithrombin	Selectively inhibits factor Xa, antithrombin is required as a cofactor to produce its effect.
ezetimibe [82]	00449410	↓active NPC1L1	Binds specifically to a single site in brush border membranes and to human embryonic kidney cells expressing Niemann-Pick C1-Like 1 (NPC1L1), inhibiting activity of NPC1L1.
eplerenone [109]	00647192	↓aldosterone: mineralocorticoid receptor	Selectively binds to mineralocorticoid receptor (MR) and blocks aldosterone-mediated activation.
enoxaparin [152]	00354796, 00289042	↑active antithrombin	Binds to and enhances activity of antithrombin which binds thrombin.
selodenoson [124] [DTI-0009]	00040001	↑active A1 adenosine receptor	Binds and activates A1 adenosine receptor.
dronedarone [259] [SR33589]	00697086, 00174785, 01151137, 01198873, 01213368, 00489736, 00259428, 00259376, 01070667, 01182376, 01199081, 01140581, 01026090, 01135017, 01266681, 01047566	↓T3: TRα1	Dronedarone via its metabolite DBDron, is a TRα1-selective inhibitor of T3 binding to its receptor.
dexamethasone [236]	01143129	↑active glucocorticoid receptor	Binds and activates glucocorticoid receptor.
dalteparin [180]	00786474	↑active antithrombin	A low molecular weight, synthetic heparin. As an anticoagulant/antithrombotic agent, dalteparin binds to antithrombin and enhances the inhibition of Factor Xa.
perindopril [69] [coversyl]	00461903	↓active ACE	Binds principally to the C-terminal site of ACE, inhibiting it.
clopidogrel [273] [SR25990C]	00243178, 00249873, 00769938, 01141153, 00776633	↓active P2Y12 receptor	Irreversibly inhibits the P2Y12 receptor.
certoparin [132]	00171769	↑active antithrombin	Indirectly inhibits factors IIa, IXa, Xa, XIa, and XIIa by forming a complex with antithrombin and initiating its activity.
carvedilol [126]	00878384, 00198614, 00578617, 00911508, 00313157, 00589303	↓active β adrenoreceptor	Persistent β-blockade by to an allosteric site of β-adrenergic receptors (β-ARs).
capadenoson [182] [BAY68-4986]	00568945	↑active adenosine A1 receptor	Binds and activated adenosine A1 receptor.
candesartan [113]	00130975, 00294775	↓angiotensin II:AT1 receptor	Competes with angiotensin II for binding at the angiotensin II (AT1) receptor.
bisoprolol [131]	00878384	↓catecholamine: β adrenergic receptors	Competes with catecholamine for binding at β-adrenergic receptors.
betrixaban [208] [MK-4448, PRT054021]	01229254, 00742859	↓active factor Xa	Binds an inhibit factor Xa (FXa) which is required for thrombin generation.
esmolol [114] [CAS 103598-03-4, ASL-8052, brevibloc]	00713401	↓active β1 adrenoceptors	Binds and inhibits β1 adrenoceptors.
tecarfarin [54] [ATI-5923]	00691470, 00431782	↓active vitamin K oxide reductase	Inhibits vitamin K epoxide reductase and is metabolized by esterase (mainly human carboxylesterase 2) to a single major metabolite ATI-5900.
atenolol [18]	00911508, 00578617, 00589303	↓catecholamine: β adrenergic receptors	Competes with catecholamine for binding at β-adrenergic receptors.
acetylsalicylic acid [260] [aspirin]	00769938, 00243178, 00623779, 00244426, 00776633, 01141153, 00157248, 00496769, 01227629, 00249873	↓active COX	Selectively acetylates the hydroxyl group of one serine residue (Ser 530) located 70 amino acids from the C terminus of cyclooxygenase (COX). Acetylation leads to irreversible COX inhibition.
olmesartan [188]	00098137	↓angiotensin II: AT1 receptor	Selectively blocking angiotensin IIŰAT1 receptor sites in the vascular smooth muscle, thus inhibiting the vasoconstrictor effects of angiotensin II.

Continued on next page

Table B.1 – continued from previous page

Atrial Fibrillation Drugs	NCT ID	Drug Effect	Mechanism of Action
amoxicillin-clavulanic acid [191]	00603317	↓active β-lactamase	Amoxicillin has antimicrobial activity against many gram-positive aerobic and anaerobic bacteria and gram-negative aerobic bacteria. Clavulanic acid binds and inhibit β-lactamase enzymes.
ajmaline [123]	00702117	↑intracellular K^+, ↓intracellular Na^+	Aromatic residues Tyr-652 and Phe-656 are essential for ajmaline binding to and inhibition of human ether-a-go-go related gene (hERG) channels. Ajmaline blocks hERG channels in the open but not in the closed states. Binds and inhibits the sodium channel.
adenosine [57]	01058980	↑adenosine	Endogenous ligand of adenosine receptor.
acenocoumarol [165]	01119274, 01119261, 01119300, 01141153, 00070655	↓active VKORC1	Binds and inhibits vitamin K epoxide reductase (VKORC1).
acebutolol [171]	00578617, 00911508	↓active β1 adrenergic receptor	Binds and inhibits β1 adrenergic receptor.
Information Unavailable/Mechanism Unknown			
intralipid [fat emulsion]	01175330	?	?
BMS-914832	01211808	?	?
BMS-914392	01211821	?	?

Table B.1: Atrial fibrillation drugs found in [184]. ? indicates that information is either unavailable or mechanism is unknown.